Report No. FRA-OR&D-75-92

INVESTIGATION OF STEEL TUNNEL SUPPORTS

AUGUST 1975

FINAL REPORT

Prepared for

Department of Transportation
FEDERAL RAILROAD ADMINISTRATION
Washington, D.C. 20590

Technical Report Documentation Page

1. Report No.	2. Government Accession No.	3. Recipient's Catalog No.
FRA OR&D 75-92		

4. Title and Subtitle	5. Report Date
INVESTIGATION OF STEEL TUNNEL SUPPORTS	August 1975
	6. Performing Organization Code
7. Author(s)	8. Performing Organization Report No.
E. H. Gaylord, S. L. Paul, G. K. Sinnamon	UILU-ENG-75-2012
9. Performing Organization Name and Address	10. Work Unit No. (TRAIS)
Department of Civil Engineering University of Illinois at Urbana-Champaign Urbana, Illinois 61801	11. Contract or Grant No. DOT FR 30022
	13. Type of Report and Period Covered
12. Sponsoring Agency Name and Address	August 1974 - August 1975 Final Report
Federal Railroad Administration Department of Transportation Washington, D. C. 20590	14. Sponsoring Agency Code

15. Supplementary Notes

16. Abstract

A series of 18 steel ribs with 10 ft-radius arches and 7-ft straight legs were tested to investigate the effect of loading geometry, eccentricity of load, and various section shapes used for making the ribs. It was found that symmetrical loading about the rib center line gives higher rib capacity and that closed section shapes resist eccentrically applied loads much more effectively. Square structural-tube ribs filled with concrete and one square structural tube rib with sleeve connections were tested.

The practicality of using ribs made of closed-section telescoping segments is discussed. It is found that the greatest problem with ribs of this type is the tolerances required in the manufacture of sections that must slide within one another. Sleeve connections are evaluated and it is found that tolerances in section sizes are also a problem in making this type of connector practical.

A study of steel rib behavior with variation of blocking stiffness and connection stiffness is described, using a computer analysis. These parameters were constant in the test series described above. Finally, results of the tests on ribs are compared with the analysis commonly used for design and is found to predict their behavior with reasonable consistency.

17. Key Words	18. Distribution Statement
Tunnel Supports; Steel Ribs; Rib Analysis	Document is available to the public through the National Technical Information Service, Springfield, Virginia 22151

19. Security Classif. (of this report)	20. Security Classif. (of this page)	21. No. of Pages	22. Price
Unclassified	Unclassified		

Form DOT F 1700.7 (8-72) Reproduction of completed page authorized

PREFACE

Research described in this report was performed by the Department of Civil Engineering at the University of Illinois at Urbana-Champaign, Urbana, Illinois from August 1974 to August 1975. The project was sponsored by the Federal Railroad Administration, Department of Transportation, through contract No. DOT FR 30022. Mr. William N. Lucke was the technical representative for the Federal Railroad Administration. He helped to formulate the research goals and made many helpful suggestions during the work. His help is greatly appreciated.

Assistance was provided by Professors R. B. Peck, D. U. Deere, E. J. Cording and Mr. H. W. Parker. These men provided geotechnical input into the planning of the test programs by defining the major problems and giving advice in techniques for approaching the solution to those problems.

Much of the research was carried out by research assistants in the Department of Civil Engineering. Mr. H. Nikooyeh planned and supervised the testing of steel ribs described in Chapter 2. The analytic studies and connection tests were performed by Mr. M. Karshenas and T. VonAschwege. Student employees D. Coultas, D. Guse and B. Newman helped greatly in preparing the large-scale rib specimens and testing them.

TABLE OF CONTENTS

LIST OF TABLES

LIST OF FIGURES

LIST OF SYMBOLS

CHAPTER 1

E	modulus of elasticity
I	moment of inertia
K	passive force-displacement relationship
R	radius of circular portion of the rib

CHAPTER 2

E	modulus of elasticity
M_x	moment about the axis perpendicular to the rib
S	symmetrical load geometry
S_x	section modulus
T	axial thrust in straight leg
U	unsymmetrical load geometry
ε	strain

CHAPTER 6

A	cross sectional area of rib
f	maximum stress in rib

f_y	yield stress
F	radial component of W
F_p	passive force of rock on rib
F_r	active force of rib on the opening
F_t	tangential component of W
h	arch-segment rise
M	moment
R_v	vertical reaction at base of rib
S	section modulus
T	thrust
W	weight of rock acting at a blocking point

CHAPTER 1

INTRODUCTION

This report describes an investigation of steel tunnel supports. Load tests and analyses of conventional ribs are discussed and certain types of unconventional ribs and connections are evaluated. The loading conditions used in the tests are representative of steel ribs used in jointed-rock tunnels, in which the object is to support loosening rock blocks or wedges at the top or upper sides of the opening.

The overbreak in jointed-rock tunnels is irregular and may be large. Wood blocking is placed between the rib and the rock as close to the face as possible to prevent movement of the rock blocks along joints, fracture planes, or bedding planes. Wood wedges are driven between the wood blocking and rib from the side. Ideally, they are driven from both sides of the rib. However, this is not always done, and the blocking load acts on the rib eccentrically. As tunneling progresses the rock is further disturbed and the weight of the loosening rock acts increasingly on the rib through the blocking points. Generally, the rock loosens in only part of the opening and moves in directions parallel to the joints or bedding planes, thus exerting active forces on the rib. Deformation of the rib tends to displace it toward the rock in the regions of undisturbed rock; this interaction results in passive forces on the rib. Deformation occurs at the blocking points due to crushing at highly stressed regions such as contact points on the rock or rib, crushing of the wood wedges, or deformation of the wood blocking. Dampness of the wood influences its deformability

considerably. In this investigation an effort has been made to simulate these conditions.

Steel ribs are ordinarily used to support the ground only until the excavation is completed and a final concrete liner can be installed. The temporary nature of the structure influences the philosophy used in the design. The required factor of safety is not as large as for final long-term support and detailed analyses are not usually made. Certainly a new analysis is not justified for each change in geology, and the nature of the work does not usually allow sudden changes in support unless catastrophic difficulties are encountered. In many cases all the supports are purchased before the tunnel excavation begins, and the economics and contractural requirement do not allow a substantial variation. However, despite these uncertainties and constraints a better understanding of structural behavior can help the designer make a better selection of steel ribs before hand and evaluate alternatives during the excavation to counteract difficulties that might be encountered.

In the test program 18 ribs were loaded to failure under conditions that simulated reasonable loading in a tunnel. The ribs consisted of a circular arch of 5 ft (1.52 m) radius with 7 ft (2.13 m) straight legs and connections at the crown and the top of the straight legs. They were constructed of M4x13, TS 4x4x0.250 and TS 4 ODx0.226 sections. The M4x13 were standard supports manufactured by the Commercial Shearing Co., Inc. with the butt-plate connection recommended by that company. Ribs made of the other sections were made as similar to the standard ones as possible.

Two loading geometries were used in the tests. Loads were applied

by rams at 30 degree intervals around the arch in both cases. Thus there were 7 load points symmetrically placed about the centerline of the rib. Passive loads were controlled so that the load-deformation relationship was linear, with a slope of 20 kips/in. The crown load and one on each side were active in one case; this loading represents the case of loosening rock near the crown of the tunnel. The second loading was unsymmetrical, with the two loads between the springline and crown on one side active. Loosening rock in the upper side of the tunnel with inclined joints or bedding planes at an angle of about 45 degrees is represented by this loading. In a previous series of tests the horizontal load at the springline was also active in the unsymmetrical loading. This case is considered in Chapter 5 in a computer analysis study of blocking stiffness. Later it was decided that this was not representative because the springline active load controlled the failure and deflected a great deal more than the other active loads. If this were to occur due to rock movement at that point it would result from movement along very flat joints, and this is not likely. Furthermore, if the designer expected lateral loads at the springline he would specify curved-leg ribs. Therefore, the springline load was made passive in this study. These tests are described in Chapter 2 and comparisons made of the behavior and ultimate load for the variables considered.

Because of the large overhead costs in maintaining work at the heading during tunnel excavation, the rate of advance controls the overall tunnel cost. Therefore, any device or system that can increase the rate of advance becomes attractive. For this reason ribs that can be erected

more quickly may be cost effective even if their initial cost is higher. A system of telescoping box or pipe sections has been suggested as a means for reducing erection time. These sections would nest during transportation into the tunnel, reducing the space required for storage and transport, and be erected by expanding them into position. The practicality of this idea is discussed in Chapter 3. Another possibility for decreasing rib erection time is the use of simpler connections. Sleeves that would slide over the joint between rib segments are discussed in Chapter 4. Both split sleeve and solid sleeve connections were tested under eccentric load and their behavior is compared with that of the standard butt-plate connection. In addition, one rib was tested with solid sleeve connections.

All the variables that influence rib strength and behavior could not be investigated in the test program, so a study of two major variables was undertaken with a nonlinear computer analysis. These are blocking stiffness and connection stiffness, both of which were constant in the large-scale tests. The study was made with NASTRAN, which is a general-purpose structural-analysis program in which the structural section is composed of rods and shear panels to obtain a nonlinear beam element. This model was developed during the previous year of research and is described by Paul, et al. (1974). The unsymmetrical loading case is considered, with the springline load and the two above it assumed to be active. This differs from the unsymmetrical loading used in the tests described in this report, as noted earlier, but is the same as that used in tests described by Paul, et al. (1974). The results provide an indication of the influence

on rib strength of these two variables. The accuracy of the analysis was checked by comparison with a test from the previously reported series.

Application of the test results to the design of supports is considered in Chapter 6, where the working loads obtained by the approximate analysis described by Proctor and White (1968) are compared with the maximum active test loads. The resulting factors of safety are compared for in-plane loading, out-of-plane loading, and other load geometries.

CHAPTER 2

TESTS OF STEEL RIBS

2.1 TEST DESCRIPTION

2.1.1 SPECIMENS

The steel ribs tested were about half scale for the type usually used in running transportation-type tunnels. They were horseshoe shaped with a semicircular arch 5 ft (1.52 m) in radius and 7 ft (2.13 m) straight legs. Two-bolt butt-plate connections, which are the standard connections furnished by the manufacturer for ribs of the size tested, were used at the crown and springlines, except for one specimen in which sleeve connectors were used. The bolts in the butt-plate connections were 3/4 in. (19 mm) A307 fit-up type, 2.75 in. (70 mm) long with coarse threads. Bolts were tightened to a torque of 50 ft-lbs (67.8 N·m) for all tests except one in which they were intentionally loose. Rib dimensions and the test arrangement are shown in Fig. 2.1, and the connections in Fig. 2.2(a).

The sections used for the ribs and their section properties are shown below:

Shape	Section	Area, $in.^2(cm^2)$	I, $in.^4(cm^4)$	S, $in.^3(cm^3)$
Wide-flange, M	M4x13	3.81 (24.6)	10.5 (437)	5.24 (85.9)
Square structural tube	TS4x0.25	3.54 (22.8)	8.0 (333)	4.00 (65.6)
Circular structural tube	TS4OD0.25	2.68 (17.3)	4.8 (199)	2.39 (39.2)

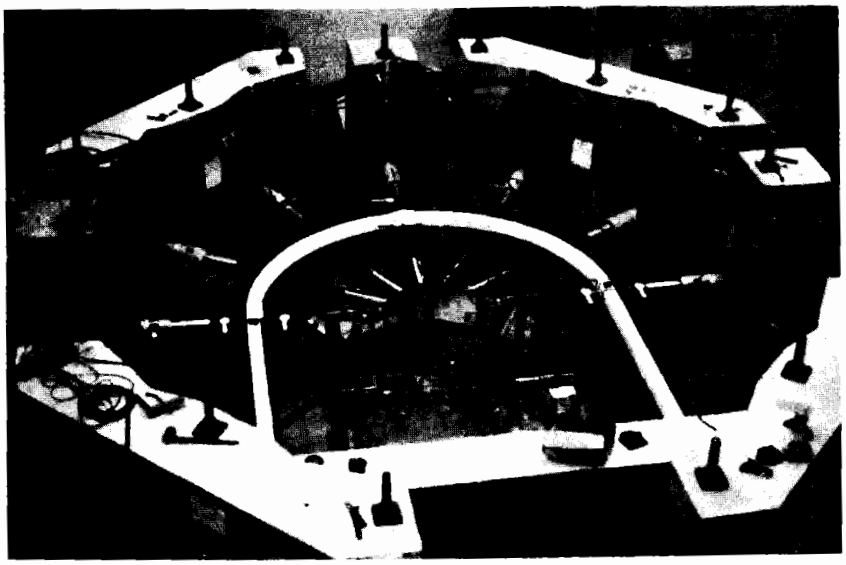

a) Photograph of test arrangement

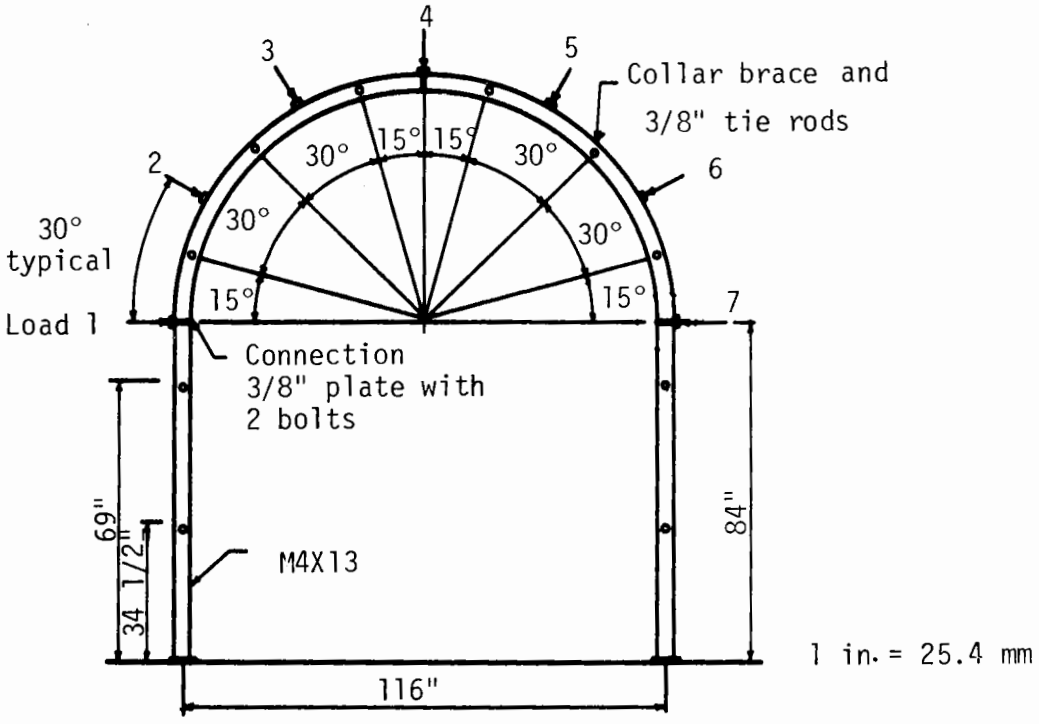

b) Location of load points, tie rods, and collar bracing

FIG. 2.1 TEST ARRANGEMENT

Properties of the steel in the ribs varied somewhat as they were obtained from different suppliers at different times. Coupons from each group were tested from straight pieces. For all the coupons except those from the circular TS section the yield stress varied from 37.7 to 43.7 ksi (260 to 301 MPa). This is within the range of variation that may be expected in a given lot of steel. Also, the arch material properties are different from the straight sections by at least an equivalent amount. Thus, it was decided not to correct the rib capacities for steel strength except in the case of the circular TS section ribs. The average yield stress for these was 34.2 ksi (236 MPa), so an additional factor to scale the circular TS ribs is included in the tables of comparison that appear later. This scaling is proportional to yield stress, using the above value for the circular tubes and an average of 41.0 ksi (283 MPa) for the other specimens.

2.1.2 LOADING

Loads were applied on the arch section at seven points equally spaced at 30 degrees as shown in Fig. 2.1. In order to simulate partial loading of a rib because of local loosening of rock, each of the seven rams was programmed to deliver either an active load or a passive reaction, as discussed in Chapter 1. One symmetrical load configuration, in which the three rams at the crown (rams 3, 4, and 5) were active, and one unsymmetrical configuration, in which rams 5 and 6 were active, were used. In each of these cases the remaining rams developed passive reactions due to the active loads, each of which bore a linear relationship to the radial displacement at its location. The unsymmetrical loading differed from that

used in a previous series of tests (Paul, et al., 1974), in which ram 7 was also active, for reasons discussed in Chapter 1.

Active loads were applied in the plane of the rib in 14 tests and in a plane 2 in. (50 mm) from the plane of the rib in 4 tests. Such an eccentric loading may result from wood blocking or lagging resting near the edge of the rib flange, or from wedges driven from one side between the rib and the blocking. An eccentric load can also result from forces acting on the flange of the rib but inclined to the plane of the rib. In tests reported previously (Paul, et al., 1974) an inclined loading that passed initially through the center of gravity of the rib section was used.

Passive-load rams were controlled to obtain a linear load-deflection relationship of 20 kips/in. (3.5 kN/mm). Tests on wood blocking are reported by Paul et al. (1974). The measured stiffness of a 10-1/2-in. (267 mm) high crib of dry hardwood was 80 kips/in. (14.0 kN/mm), which was a linear approximation of the load-deflection curve that was obtained. The linear relationship was considered acceptable in view of the somewhat uncertain and variable blocking stiffnesses encountered in a tunnel. Since wet blocking would be less stiff, this value was reduced to 40 kips/in. (7.0 kN/mm) to model the blocking in the previous series of tests. A computer analysis, discussed in Chapter 5, showed that the strength of a rib was relatively insensitive to variations in blocking stiffness for values larger than about 40 kips/in. (7.0 kN/mm), but smaller stiffnesses were reflected in noticeable reductions in strength. A blocking stiffness of 20 kips/in. (3.5 kN/mm) was used in the present series of tests to represent below average conditions in a tunnel.

2.1.3 TEST SET-UP

Each load was applied with a 60-ton ram. The seven rams were attached to concrete abutments that were themselves attached to the test floor as shown in Fig. 2.1(a). A double-cylindrical seat allowed vertical and horizontal rotation of the ram base relative to the abutments. At the other end of each ram, load was applied to the rib section through a 1-in. (25 mm) sphere to assure a point load on the rib. This sphere rested in spherical seats in steel plates; one plate distributed the load to a load cell connected to the ram and the other plate was attached to the steel rib as shown in Fig. 2.2(b). The steel block was attached to the rib to prevent it from slipping laterally when the section twisted. This was a safety precaution.

In the first four tests the lower end of the straight leg rested flat on a steel plate as shown in Fig. 2.3(a). In the remaining tests a semicircular bar was placed at the center of the leg end-plate to concentrate the load and inhibit the development of moment. This arrangement is shown in Fig. 2.3(b). The horizontal component of load was resisted in both types of support by steel bars confining the bottom of the leg.

Ribs in a tunnel are supported laterally by bracing between ribs. To simulate this type of support the test rib was placed in a plane parallel to the test floor and supported laterally through ties and collar bracing to another steel rib that was bolted to the test floor but separated from it by wood blocks, as shown in Fig. 2.4. The locations of the points of lateral support are shown in Fig. 2.1. Each tie was a 3/8 in. (10 mm) rod inside a 1.5 in. OD (30 mm) black pipe.

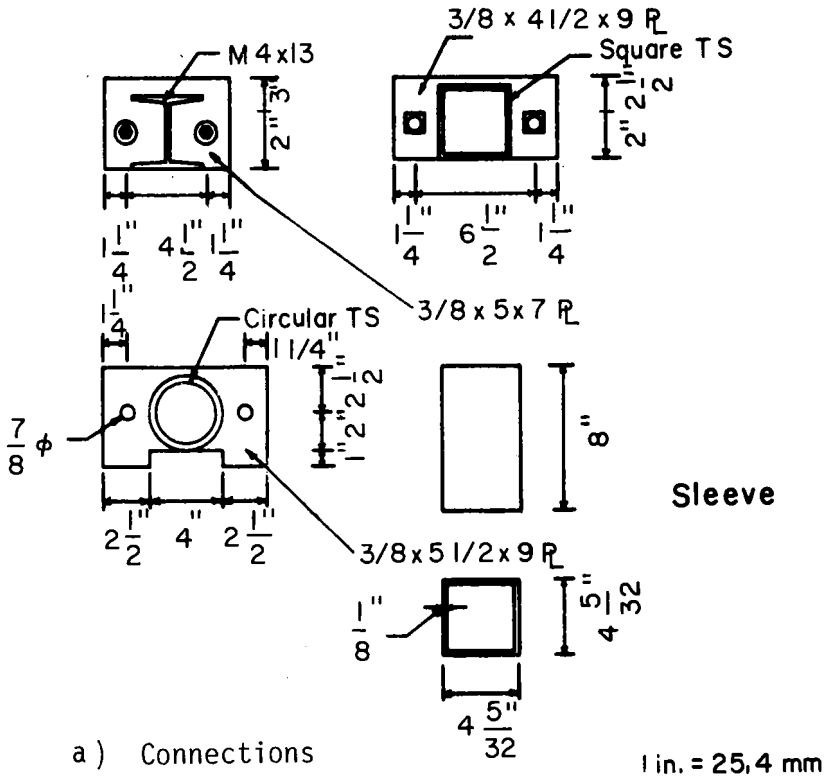

a) Connections

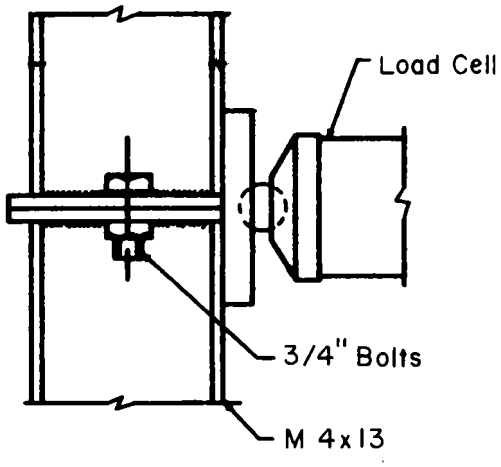

b) Load bearing assembly

FIG. 2.2 LOADING ASSEMBLY AND JOINT CONNECTIONS

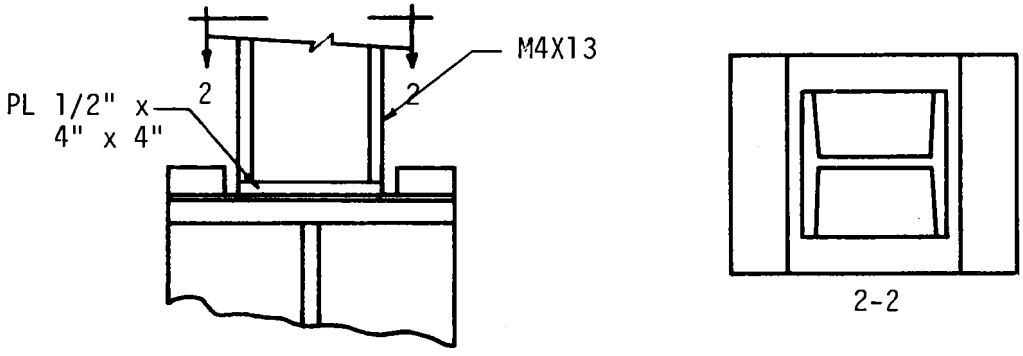

a) Support used in tests M1, B2, M3, and B4

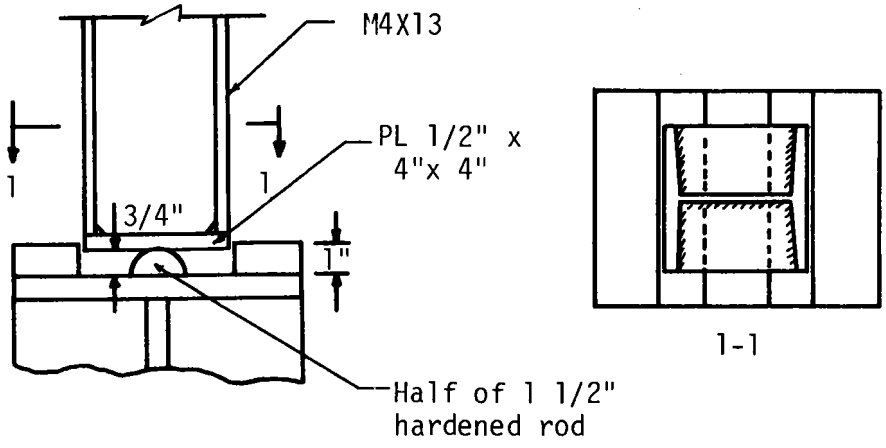

b) Support used for the remaining tests

FIG. 2.3 BASE SUPPORT FOR STRAIGHT LEGS OF RIBS

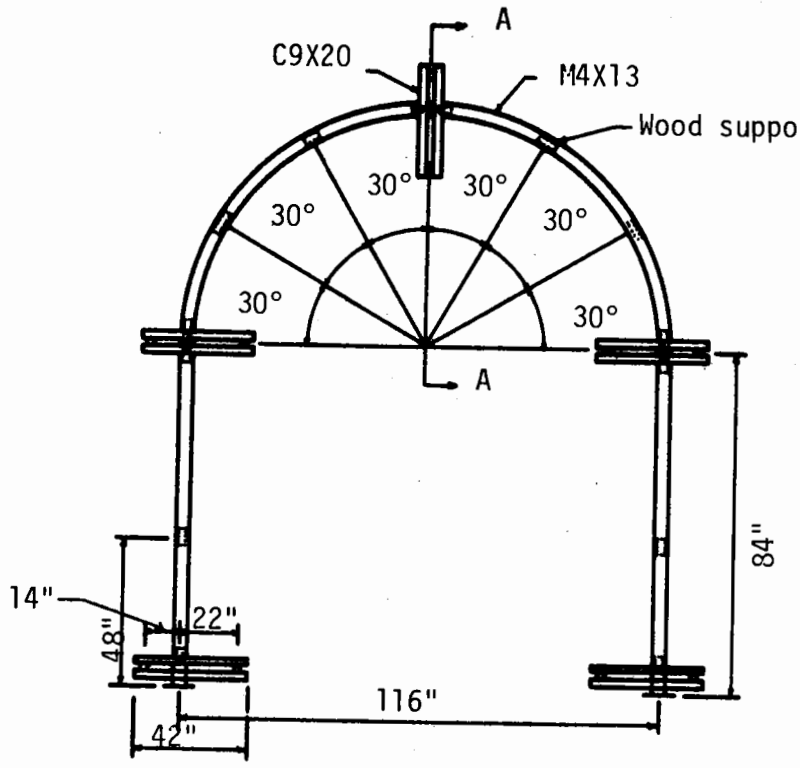

a) Plan view

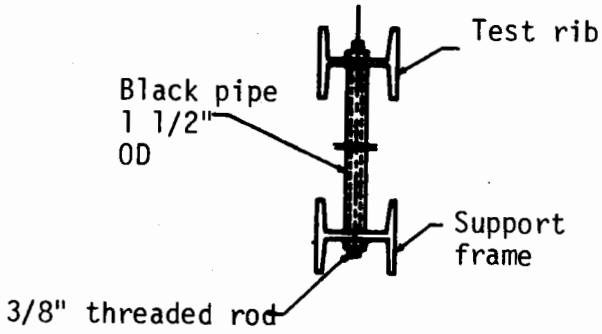

b) Lateral support

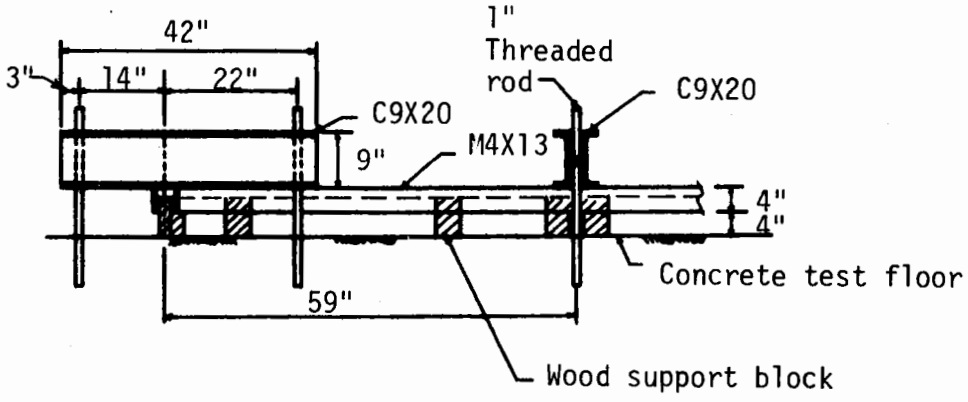

c) Section A-A

1 in = 25.4 mm

FIG. 2.4 SUPPORT FRAME FOR STEEL RIBS

2.1.4 INSTRUMENTATION

Radial displacements at the seven blocking points and lateral deflections of the straight legs were measured by linear variable differential transformers (LVDT's) with a range of ±3 in. (76 mm). Figure 2.5 shows their location.

Two sets of four strain gages were installed on the legs at about 18 in. (457 mm) from the base. This dimension varied somewhat from test to test. Figure 2.5 shows the position of the gages. Moment and thrusts at the gaged sections can be calculated from the formulas:

$$M_x = \frac{E\,S_x}{2}\,(\varepsilon_1 - \varepsilon_2)$$

$$P = \frac{E(\varepsilon_1 \pm \varepsilon_2 \pm \varepsilon_3 \pm \varepsilon_4)}{4}$$

where:

M_x = moment about the axis perpendicular to the plane of the rib

S_x = elastic section modulus

E = modulus of elasticity

ε = measured strain

With the moment and thrust calculated, it is possible to compute the reactions at the base of the straight legs, or the moment and thrust at any other location in the rib in the plane of the rib.

The relative rotation of two sections of the rib 6 in. (152 mm)

apart and symmetrically located about the strain-gaged sections was measured by clamping steel bars perpendicular to the rib 3 in. (76 mm) on each side of the gages and measuring the relative movement of each end of these bars with 0.0001 in. (0.00254 mm) dial gages. This measuring device is shown in Fig. 2.5. This measurement allowed the approximate calculation of thrust and moment at the strain-gaged section and served as a check on the calculations made from the gage readings. The joint rotations were measured to allow correlation of the moment-rotation relationship in the test with that obtained in connection tests, in which a rotation device similar to that described above was used, except that the dial gages were 0.001 in. (0.0254 mm).

Twist of the section at the active load points when those loads were applied eccentrically was measured with a device consisting of a large protractor connected rigidly to the section and a weight on a string hanging in front of the protractor. This allowed the reading on the protractor of the rotation of the section relative to the vertical.

Load cells were used to measure all loads. At passive loads points they were also used to control the prescribed load-deflection relationship during application of active load.

The specimens were coated with a waterbase paint made with hydrated lime. This coating flakes off when the strain of the base material reaches a certain value. Experience has shown that this is approximately the yield strain of the steel. While it is not exact, it shows where yielding occurs first and the sequence of yielding in the specimens.

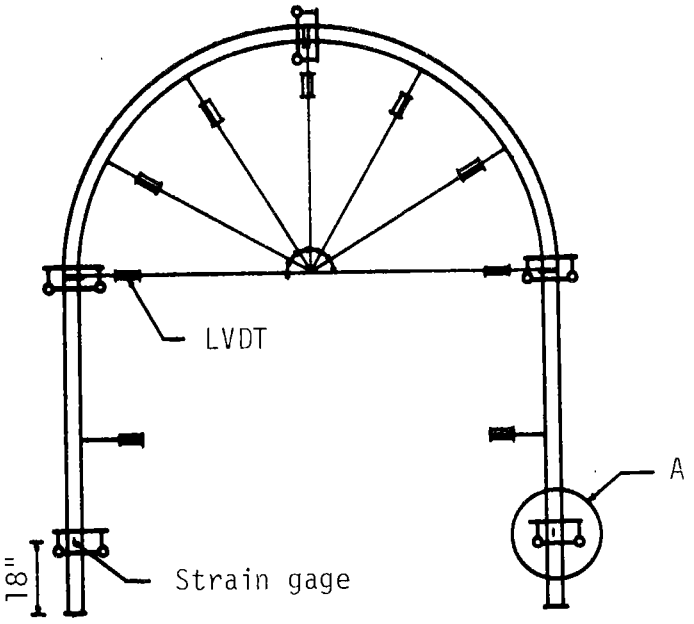

(a) Plan View

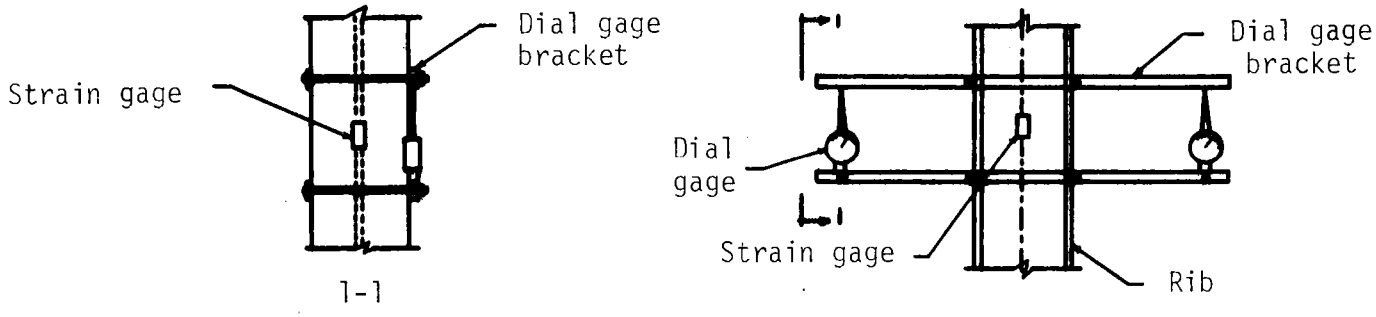

(b) Detail of A (Rotation measuring device)

Fig. 2.5 LOCATION OF INSTRUMENTATION

The sequences of yielding mentioned in the descriptions of the tests were detected in this way.

All of the above mentioned measurements were taken at each load increment. The output of LVDT's, strain gages and load cells were connected to automatic switching equipment. The sequence of reading consisted of first the load cells, then the LVDT's and strain gages, and finally the load cells again. The changes in voltage read by the balancing and reading equipment were automatically recorded by a teletype which produced a punched paper tape and typed copy. The data was then transmitted to a computer where the raw data was converted to more usable information and transmitted back to the test site immediately. In this way the information obtained for one loading increment was used to plan the next. The returned information consisted of the deformations measured by the LVDT's, ram loads at the start of reading and at the end of each increment. The program also automatically calculated the reactions and moments at various points along the rib.

2.2 RESULTS

Eighteen large-scale steel ribs were tested as described in the previous section. Table 2.1 summarizes the loading conditions and results. The wide-flange-section (M) rib behavior is the standard with which the other ribs are compared. No special precautions were taken in making the test specimens, so they have some out-of-plane deformation, twist and mismatch at the connections as would occur in a tunnel installation. Of the ribs tested, 8 were wide-flange (M) section, 7 were square structural tubes (TS), of which two were filled with concrete, 2 were circular structural

TABLE 2.1

SUMMARY OF STEEL RIB TESTS

Test	Section	Loading			Total active load, kips (kN)	Average active load per ram kips (kN)	Total vertical load, kips (kN)	Maximum Displacement at peak loading, in. (mm)
		Configuration	Eccentricity in. (mm)	Load omitted				
M1	M4	S	0	none	119.3 (530.7)	39.8 (177.0)	142.8 (635.2)	5.03 (127.7)
B2	TS	S	0	none	109.7 (488.0)	36.6 (162.8)	129.0 (573.8)	4.07 (103.4)
M3	M4	S	0	#2	66.6 (296.3)	22.2 (98.7)	64.4 (286.5)	2.80 (71.1)
B4	TS	S	0	#2	68.4 (304.3)	22.8 (101.4)	65.4 (290.9)	2.62 (66.5)
B5	TS	U	0	none	80.1 (356.3)	40.1 (178.4)	134.5 (598.3)	3.83 (97.3)
M6	M4	U	0	none	71.8 (319.4)	35.9 (159.7)	105.5 (469.3	2.57 (65.3)
M7	M4	U	2 (51)	none	42.8 (190.4)	21.4 (95.2)	59.1 (262.9)	1.22 (31.0)
M8	M4	U	0	#2	55.9 (248.7)	27.9 (124.1)	80.8 (359.4)	2.98 (75.7)
B9	TS	U	2 (51)	none	77.4 (344.3)	38.7 (172.1)	130.9 (582.3)	4.14 (104.8)
M10	M4	S	2 (51)	none	56.4 (250.7)	18.8 (83.6)	60.2 (268.0)	1.19 (30.2)
M11	M4	U	0	none	75.7 (336.7)	37.9 (168.6)	123.6 (549.8)	2.98 (75.7)
BC12	TS/w concrete	U	0	none	93.1 (414.1)	46.5 (206.8)	155.5 (691.7)	4.27 (108.5)
B13	TS	S	2 (51)	none	106.5 (473.7)	35.5 (157.9)	123.6 (549.8)	3.86 (90.4)
P14	TS	S	0	none	71.6 (318.5)	23.9 (106.3)	89.0 (395.9)	3.69 (93.7)
BS15	TS/w sleeve	S	0	none	88.2 (392.3)	29.4 (130.8)	107.3 (477.3)	3.83 (97.3)
BC16	TS/w concrete	S	0	none	129.9 (577.8)	43.3 (192.6)	149.8 (666.3)	4.42 (112.3)
M17	M4	S	0	none	121.9 542.2	40.63 (180.7)	139.1 (618.7)	4.07 (103.4)
P18	TS	U	0	none	48.2 (214.4)	24.1 (107.2)	79.2 (352.2)	2.48 (63.0)

tubes (TS), and one was a square structural tube rib with a sleeve connection.

The results of the tests will be presented in the following groups.

Group	Load geometry	Eccentricity of load	Note	Specimen designation
A	S	No	--	M1, M17, B2, P14, BC16
B	U	No	--	B5, M6, P18, BC12
C	S	Yes	--	M10, B13
	U	Yes	--	M7, B9
D	S	No	a	M3, B4
	U	No	a	M8
E	U	No	b	M11
	S	No	c	BS15

[a]Load #2 omitted
[b]Loose bolts at one springline connection
[c]Sleeve connections

The load-deflection diagrams are presented for all the tests; they are compared in Section 2.3. The load-deflection diagram for each active load is shown as well as for the total active load. Total active load is plotted against deflection of a single point, which is generally the active-load point whose deflection was largest. Those events that marked a change in behavior are shown on the individual active-load deflection diagrams. A notation is used to describe these events in order to conserve space. The

letter Y indicates initiation of yielding. Its location is shown by the angle, in degrees, measured from the springline joint upward for each arch segment. The letter W indicates the west arch and E the east. The letter I indicates that the event described occurred on the inside of the rib while O indicates that it occurred on the outside.

2.2.1 GROUP A

Tests M1, M17, B2, P14, and BC16 were loaded symmetrically in the plane of the rib. Test M17, which is a repeat of test M1, was performed toward the end of the test series to determine the effect on the test results of certain changes which had been made in the course of the tests. The major change is that of the support at the base of the straight legs as discussed in Section 2.1. Also, the later ribs were made from a different shipment of steel, and the joint configuration was changed slightly.

The load-deformation curves for this group of tests are shown in Figs. 2.6 to 2.11. In all these tests the crown moved inward and the crown joint began to open on the inside at a load on the order of 6 kips (26.7 kN), increasing throughout the test. The section about 15 deg from the side joint began to yield at a load of 28 to 35 kips (11.6 to 151.23 kN), except for test P14 which was somewhat lower. Up to this load, the springline joints rotated so that they were opening on the outside, but when yielding began the direction reversed. Shortly after initiation of yielding between the lower two load points, yielding began at a section between 35 and 45 deg. This yielding continued as the crown moved inward, although

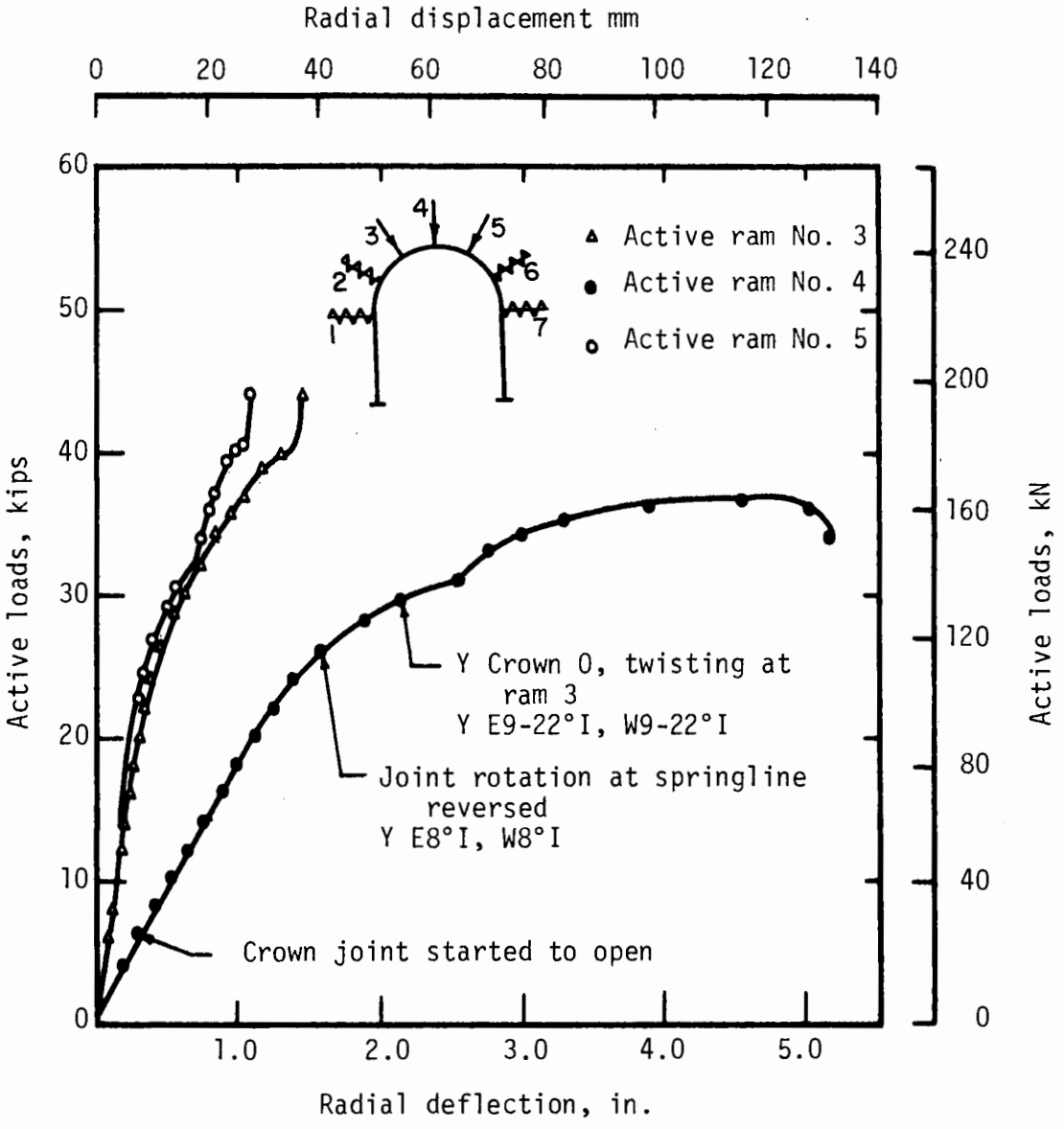

FIG. 2.6 ACTIVE LOAD-DISPLACEMENT IN TEST M1

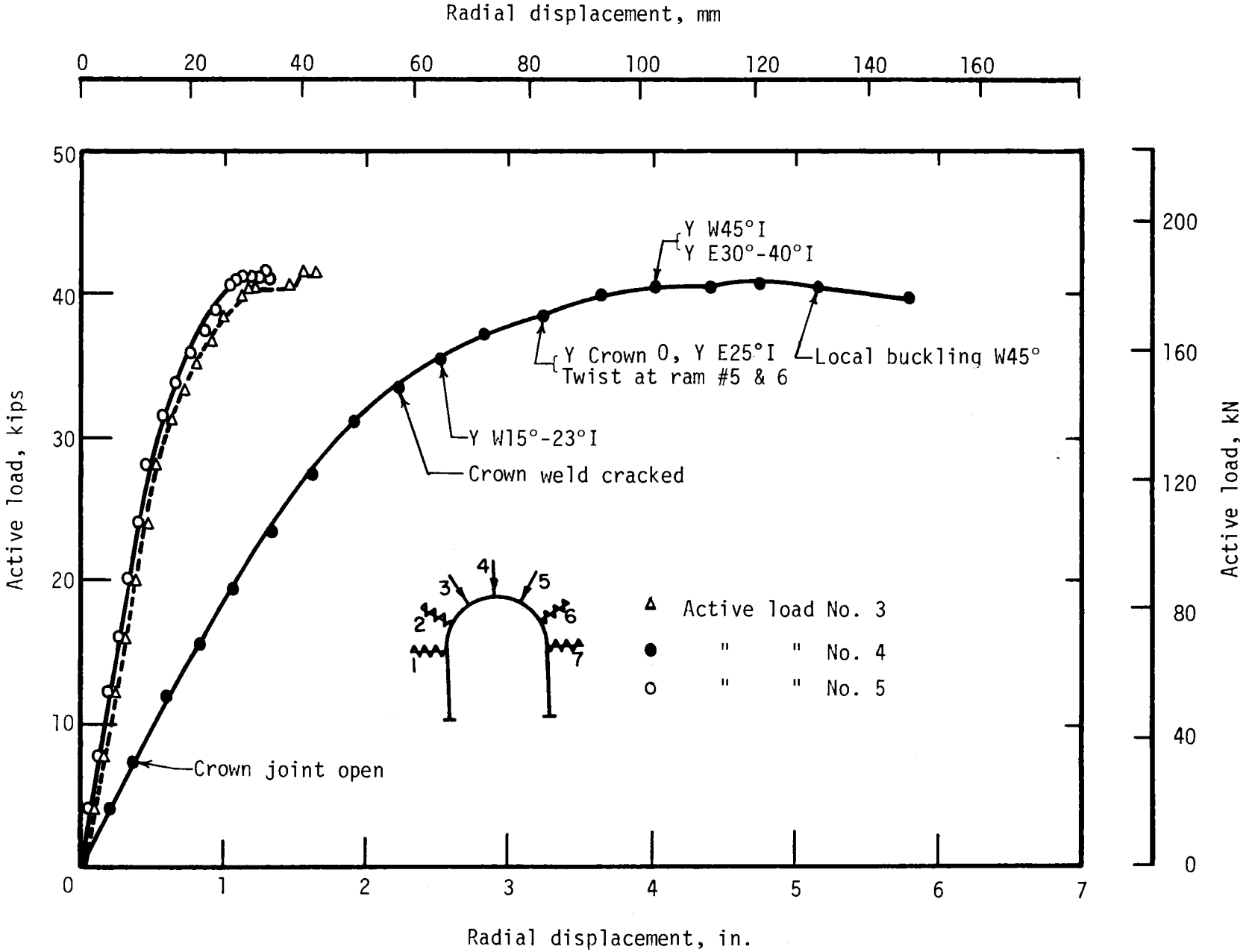

FIG. 2.7 ACTIVE LOAD-DISPLACEMENT IN TEST M17

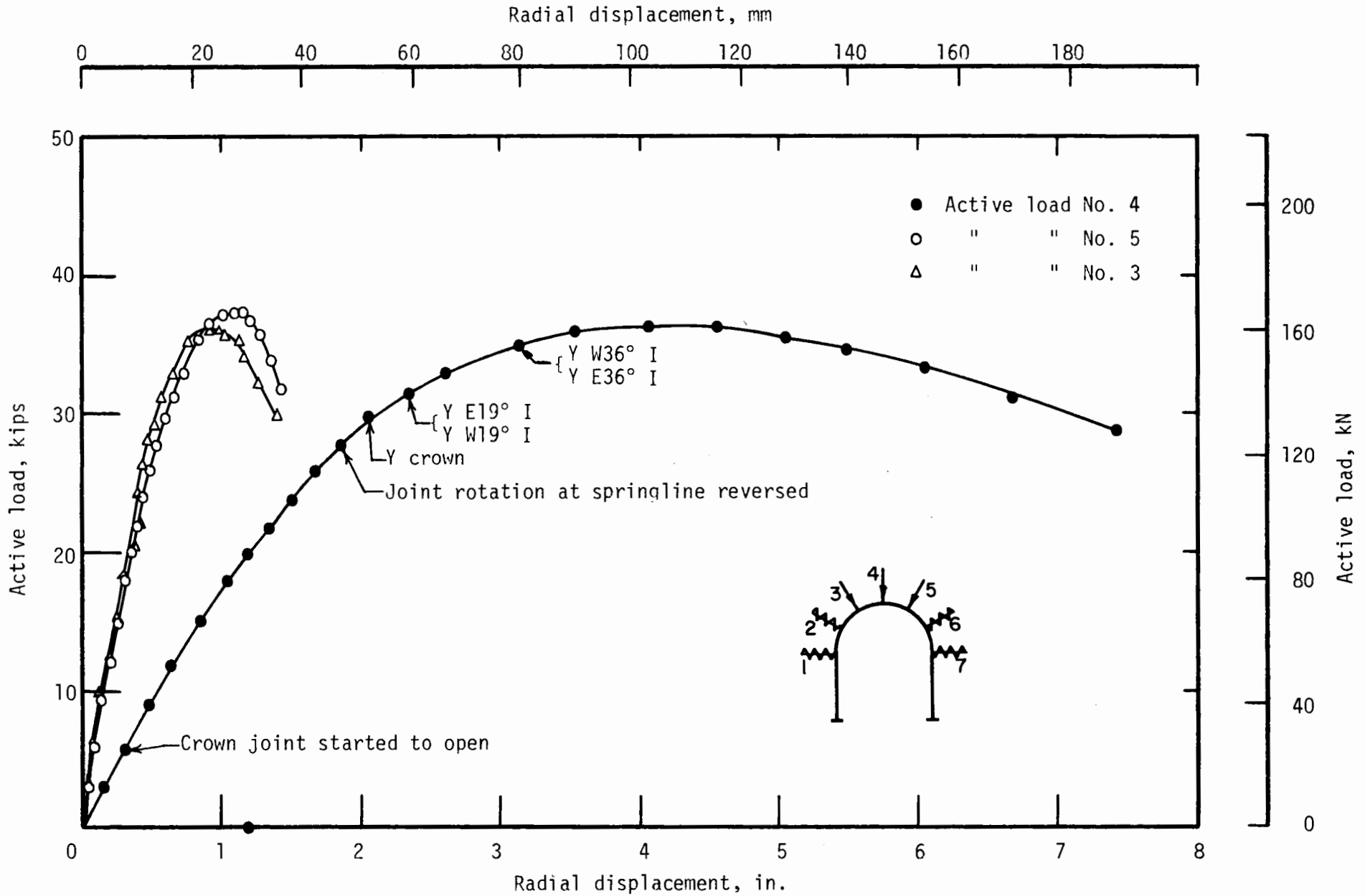

FIG. 2.8 ACTIVE LOAD-DISPLACEMENT IN TEST B2

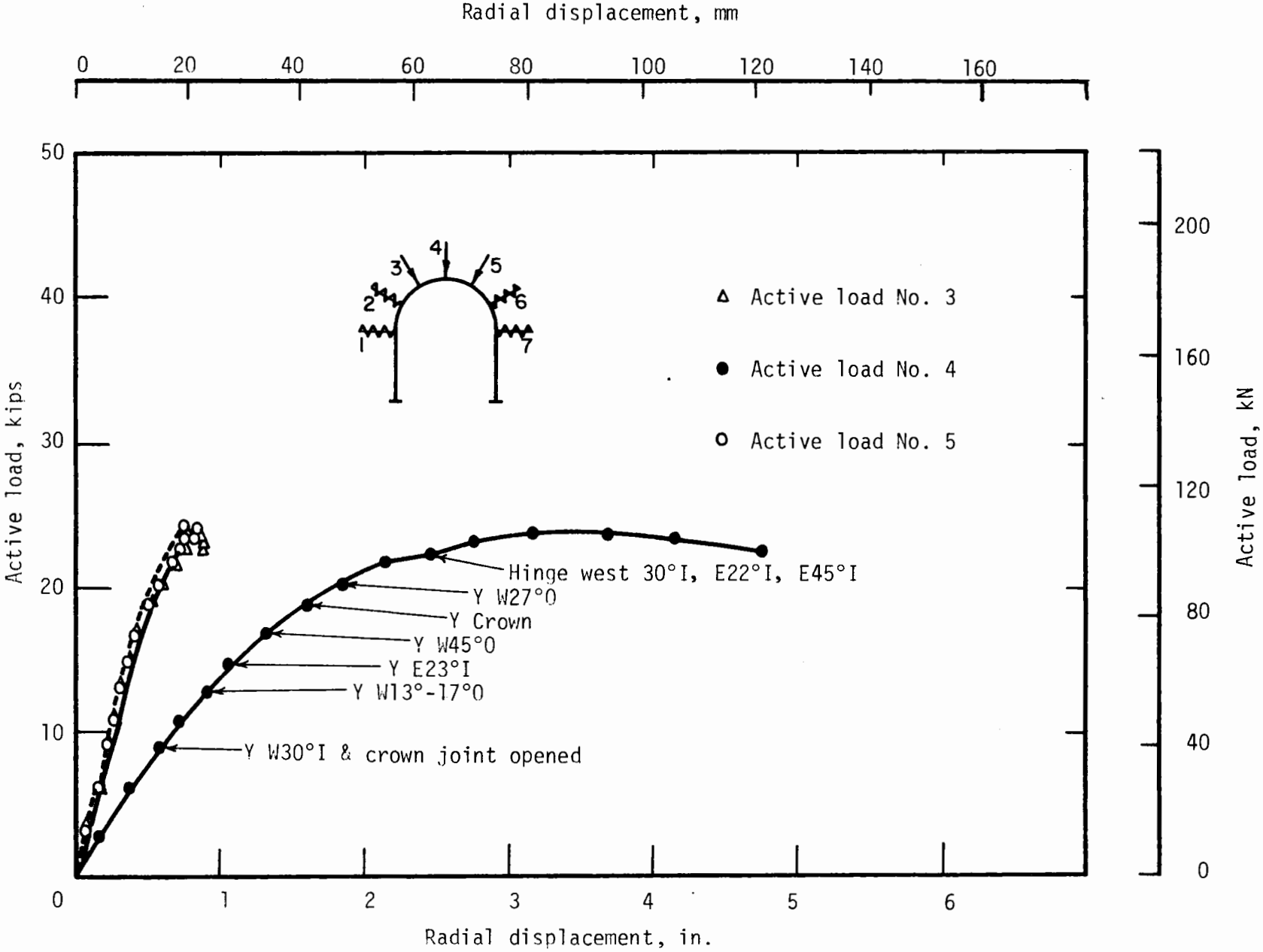

FIG. 2.9 ACTIVE LOAD-DISPLACEMENT IN TEST P14

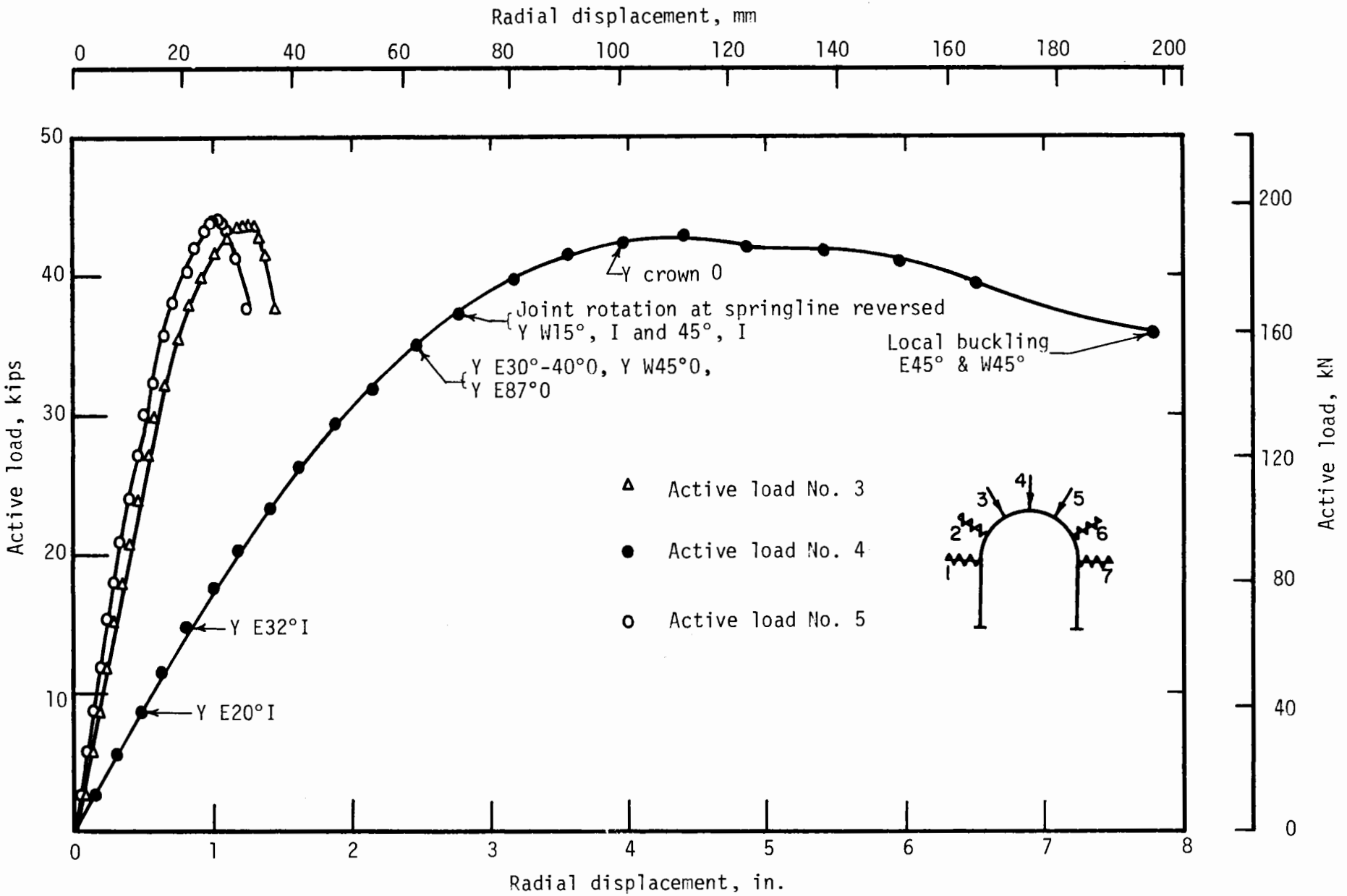

FIG. 2.10 ACTIVE LOAD-DISPLACEMENT
IN TEST BC16

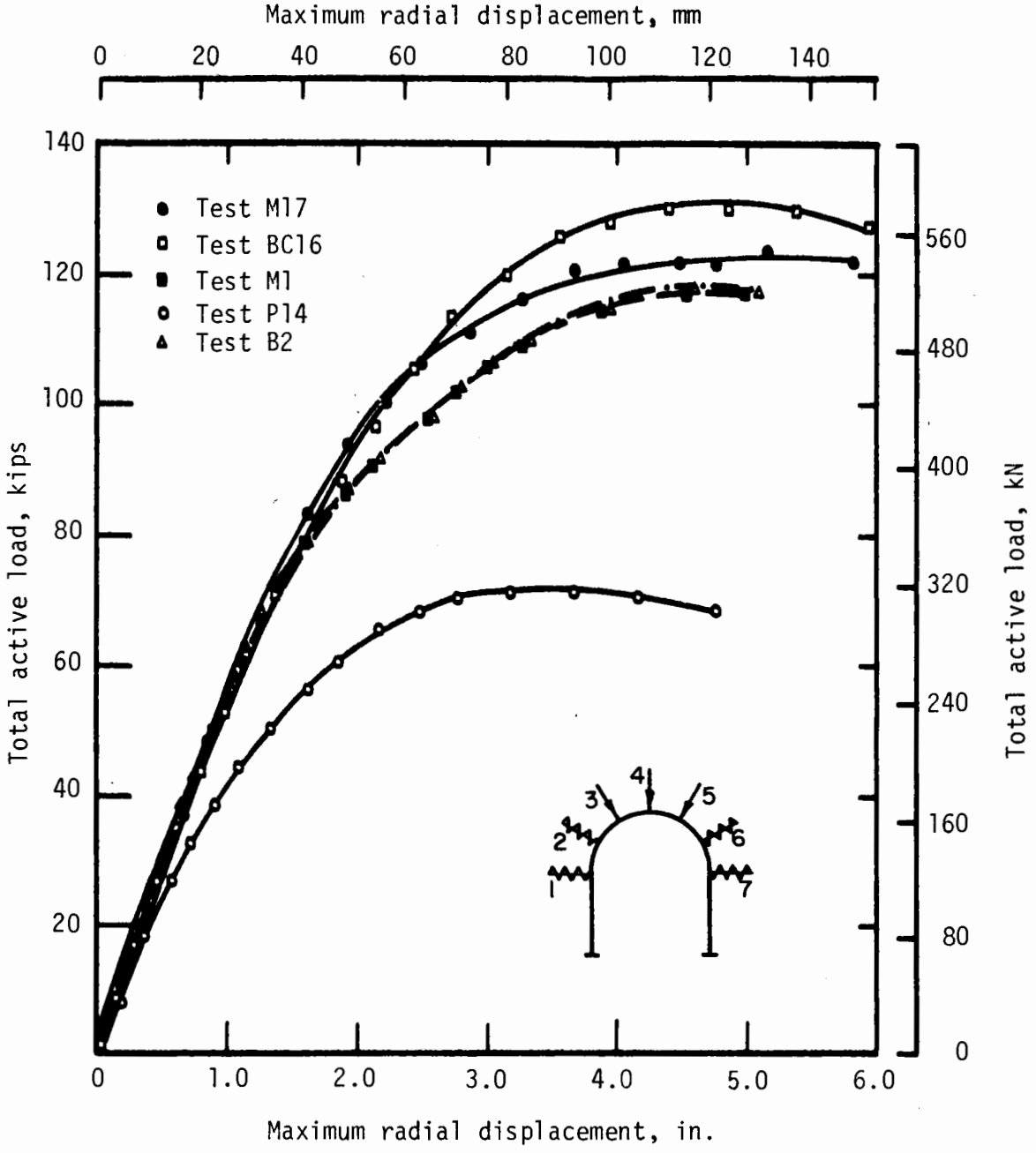

FIG. 2.11 TOTAL ACTIVE LOAD-MAXIMUM DISPLACEMENT IN TESTS M1, M17, B2, P14, AND BC16

active load points 3 and 5 did not deflect as much as the crown. These events are shown on the individual load-deflection curves.

Reversal of rotation of the springline joints indicates a change in the relative amounts of moment and thrust at the joint. The thrust continued to increase while the plastic section above the joint reduced the rate at which moment increased. Before the reversal, the resultant force, equivalent to the moment and thrust at the joint, was outside the center of the joint, and when reversals occurred it had moved inside. At the crown, the moment increased continually throughout the test. This behavior is shown by the total load-joint rotation curves for the crown and west springline in Fig. 2.12.

Photographs are shown in Figs. 2.13(a) and 2.13(b) for tests M1 and B2. In both tests the crown joint opened to the depth of the bolts but no further, and a kink or sudden change in slope is clearly seen there. In addition, severe regions of yielding can be seen between 30 and 45 deg in both specimens, indicating that yield hinges had developed. Thus, a mechanism was formed by these two hinges and the crown joint when the load reached its peak. Though yielding occurred at other locations in the arch and legs, only the regions noted above continued to deform significantly after the peak load was reached. The rib consisting of a concrete-filled structural tube (BC16) had major yielding at the same locations, as shown in Fig. 2.13(c), but the crown joint opened a great deal more. Yield hinges were centered around the 45-deg sections in the arches of test P14 and the crown joint opened a great deal less.

Local twisting of the M section, shown in the bottom photograph

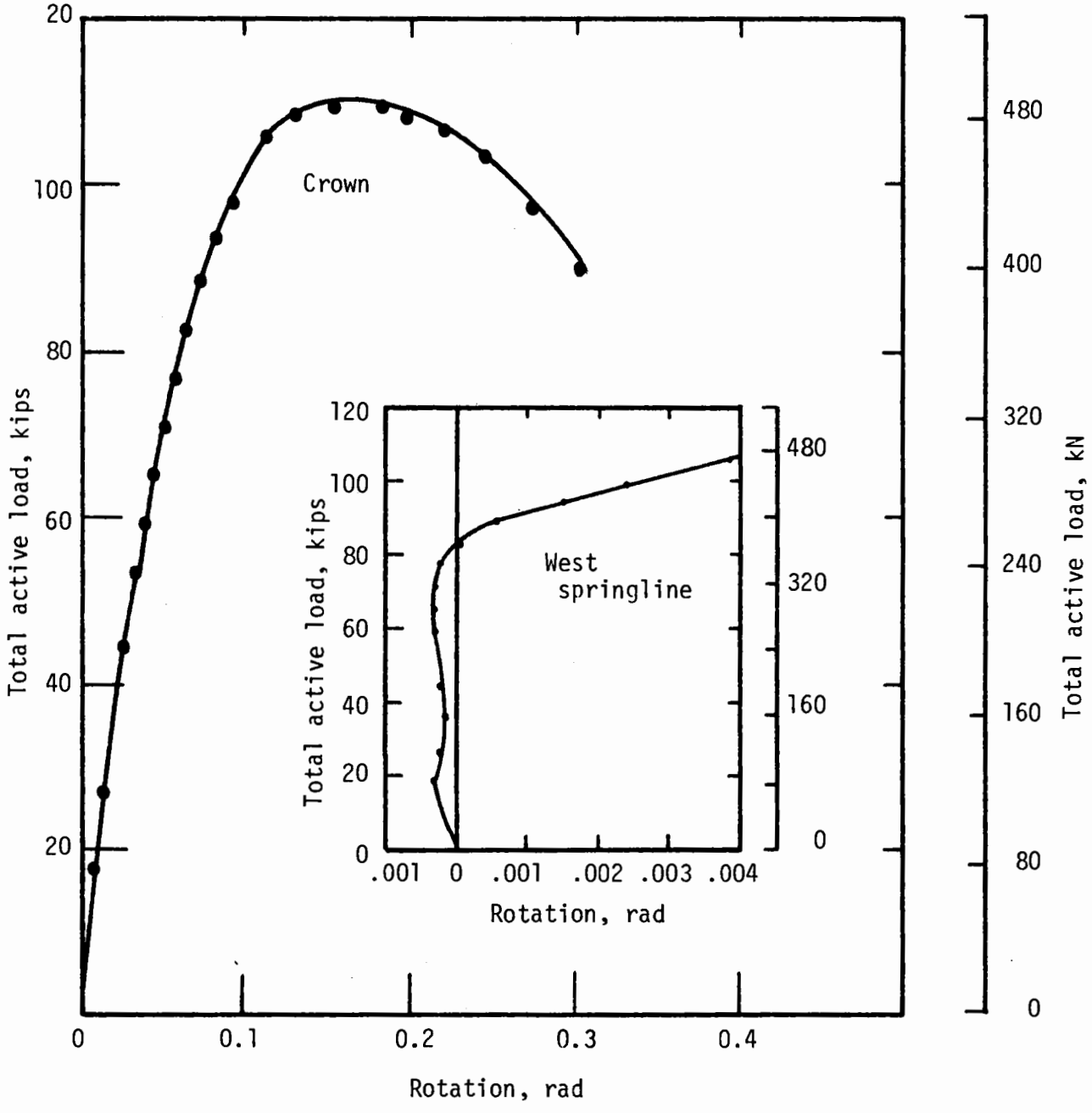

FIG. 2.12 TOTAL ACTIVE LOAD - JOINT ROTATION AT THE CROWN AND WEST SPRINGLINE IN TEST B2

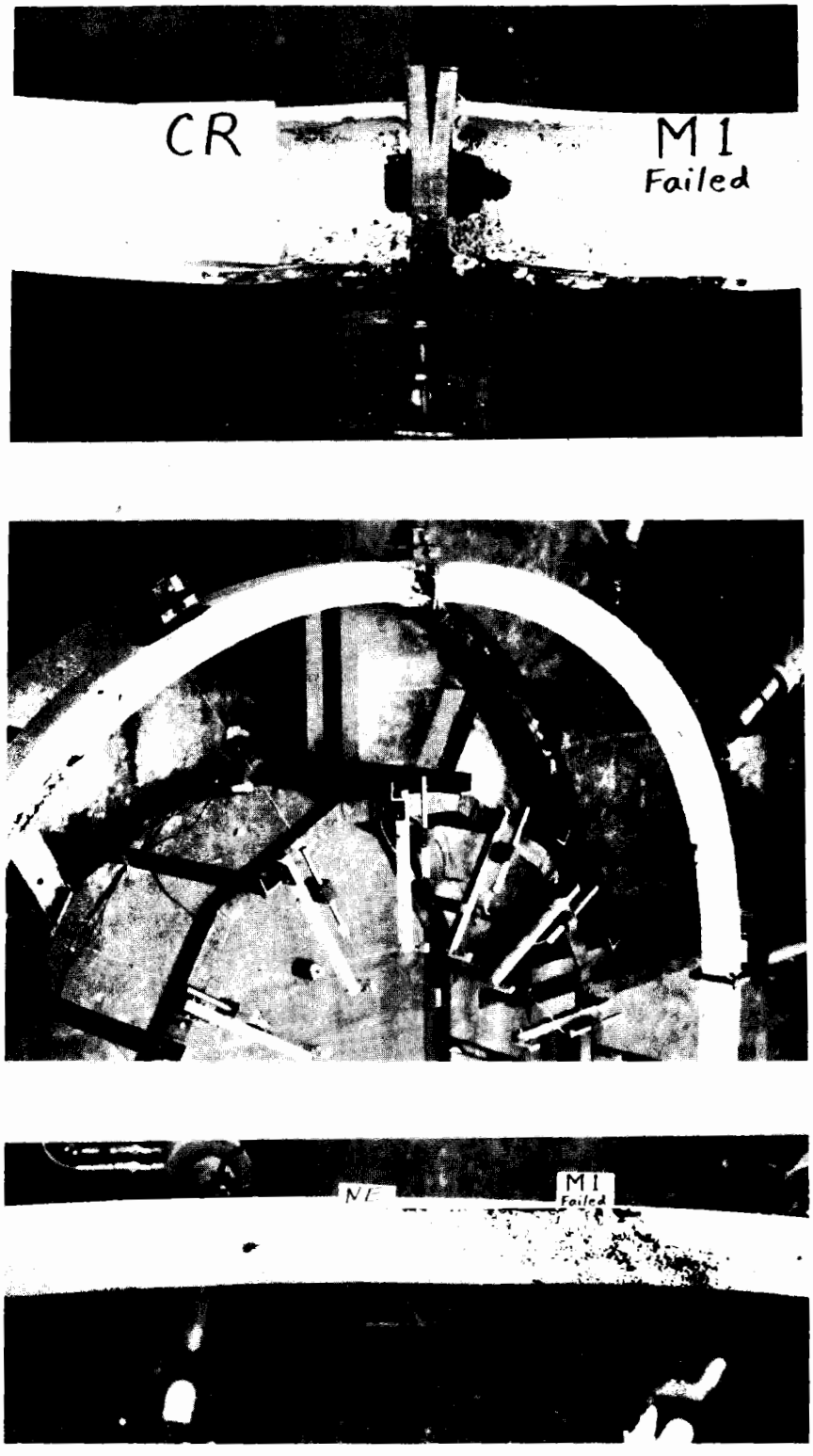

(a) Specimen M1

FIGURE 2.13 PHOTOGRAPHS OF SPECIMENS M1, B2 AND BC16 AFTER TESTING

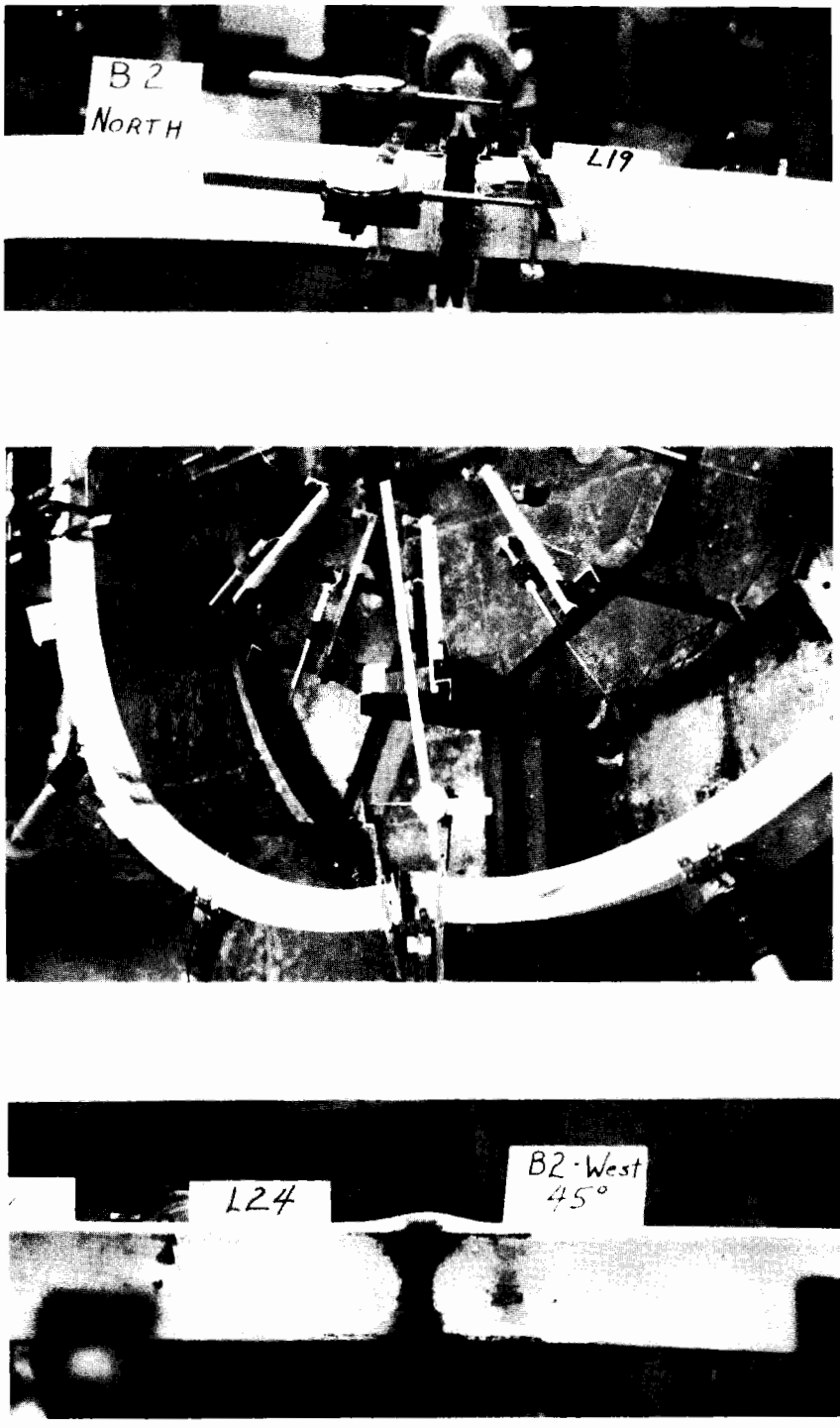

(b) Specimen B2

FIGURE 2.13 PHOTOGRAPHS OF SPECIMENS M1, B2 AND BC16 AFTER TESTING

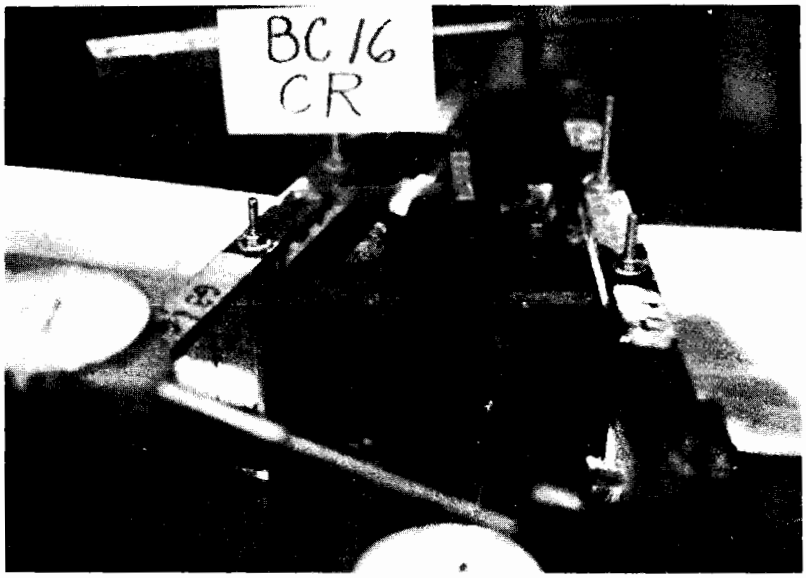

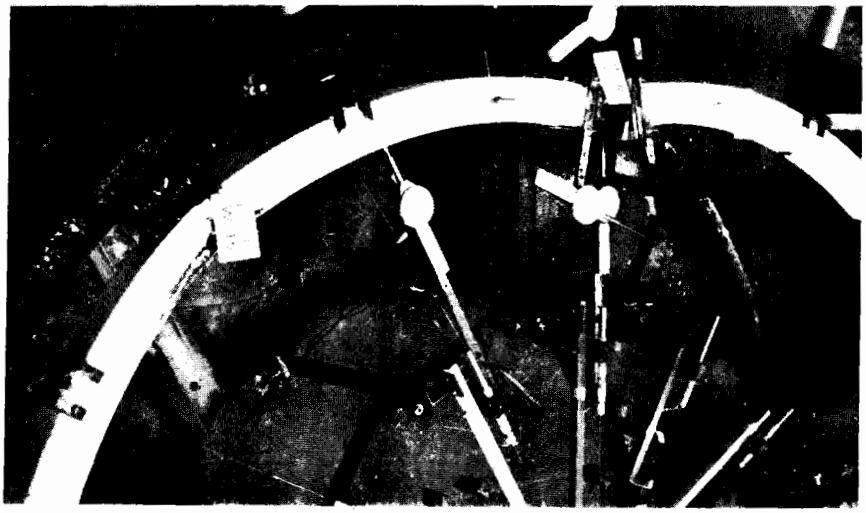

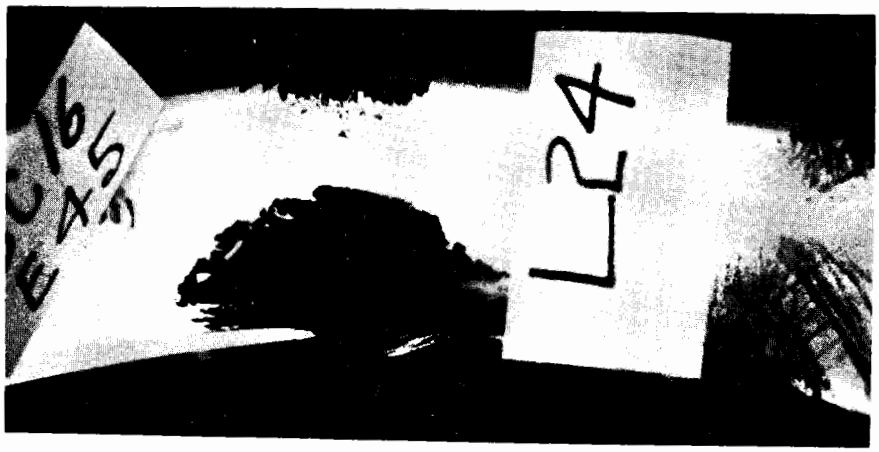

(c) Specimen BC16

FIGURE 2.13 PHOTOGRAPHS OF SPECIMENS M1, B2, AND BC16 AFTER TESTING

of Fig. 2.13(a), started before the peak load was reached and became quite pronounced at the peak. There was also some deformation of the compression flange, approximating a sine wave about its original curved shape, but this deformation never produced local failure. In almost all the M section tests there was considerable twist of the section even when the load was concentrically applied (within 1/8 in. (3.18 mm) of the web centerline).

At the regions of severe yielding in the structural tube sections local inward buckling of the walls on the compression face and outward buckling on the sides occurred as shown in Fig. 2.13(b), but this developed after the peak load was reached. Outward local buckling of the compression face also occurred in the concrete filled structural tube as shown in Fig. 2.13(c), but there was no significant buckling of the sides. No significant local deformation could be observed in test P14.

2.2.2 GROUP B

Tests B5, M6, P18 and BC12 were performed with unsymmetrical loading in the plane of the rib. Load-deflection curves are shown in Figs. 2.14 to 2.18. The rib behavior was quite different from that with symmetrical loading. The crown joint began to open on the outside at a low level of load, and the east springline joint began to move inward from the start of the test (the active loads were applied on the east side). In most cases the east side joint began to open on the inside at about the same load at which the crown joint opened. The first indication of a major change in behavior occurred when the movement of the east springline reversed its direction, while at the same load, or slightly higher, yielding was

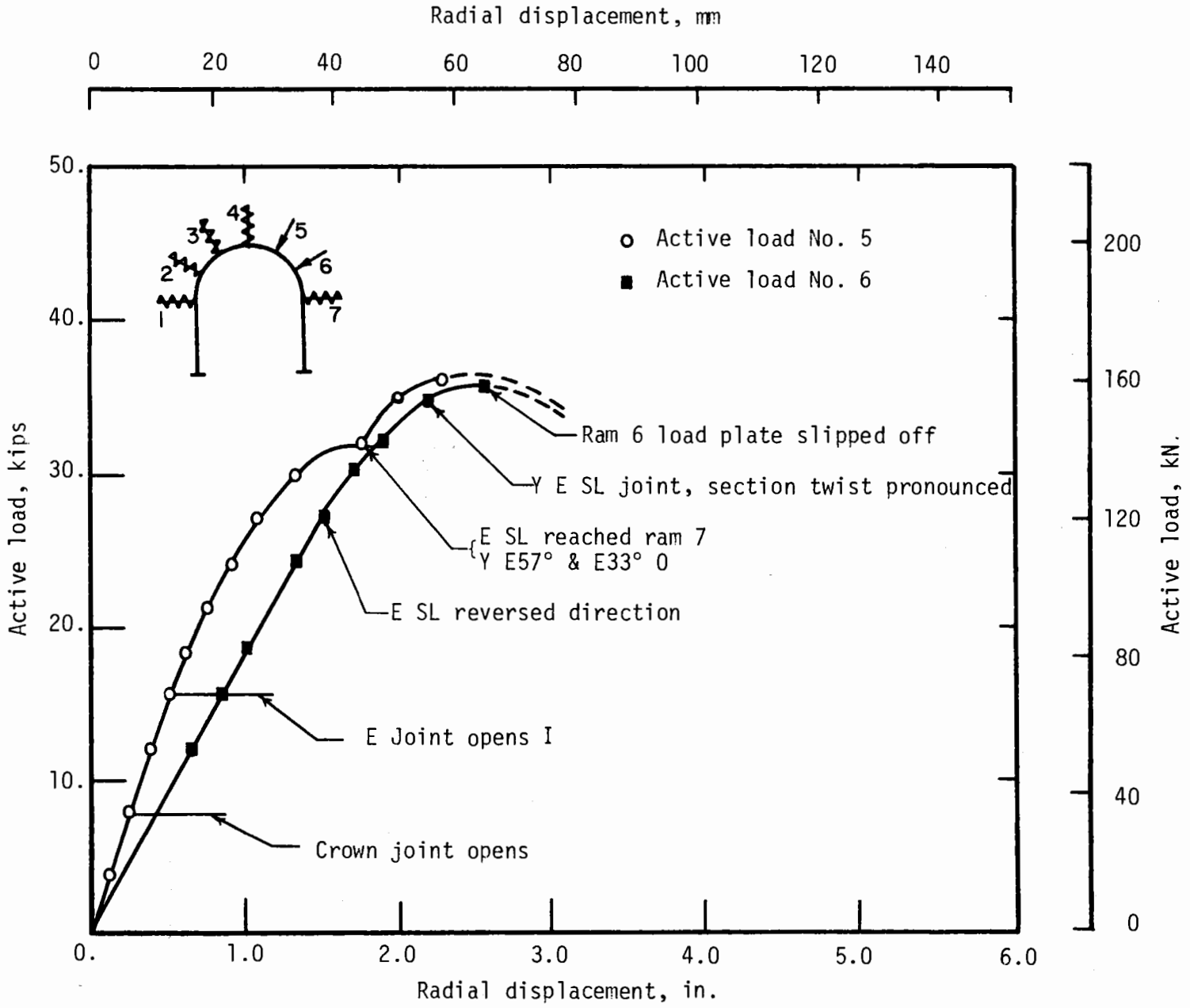

FIG. 2.14 ACTIVE LOAD-DISPLACEMENT IN TEST M6

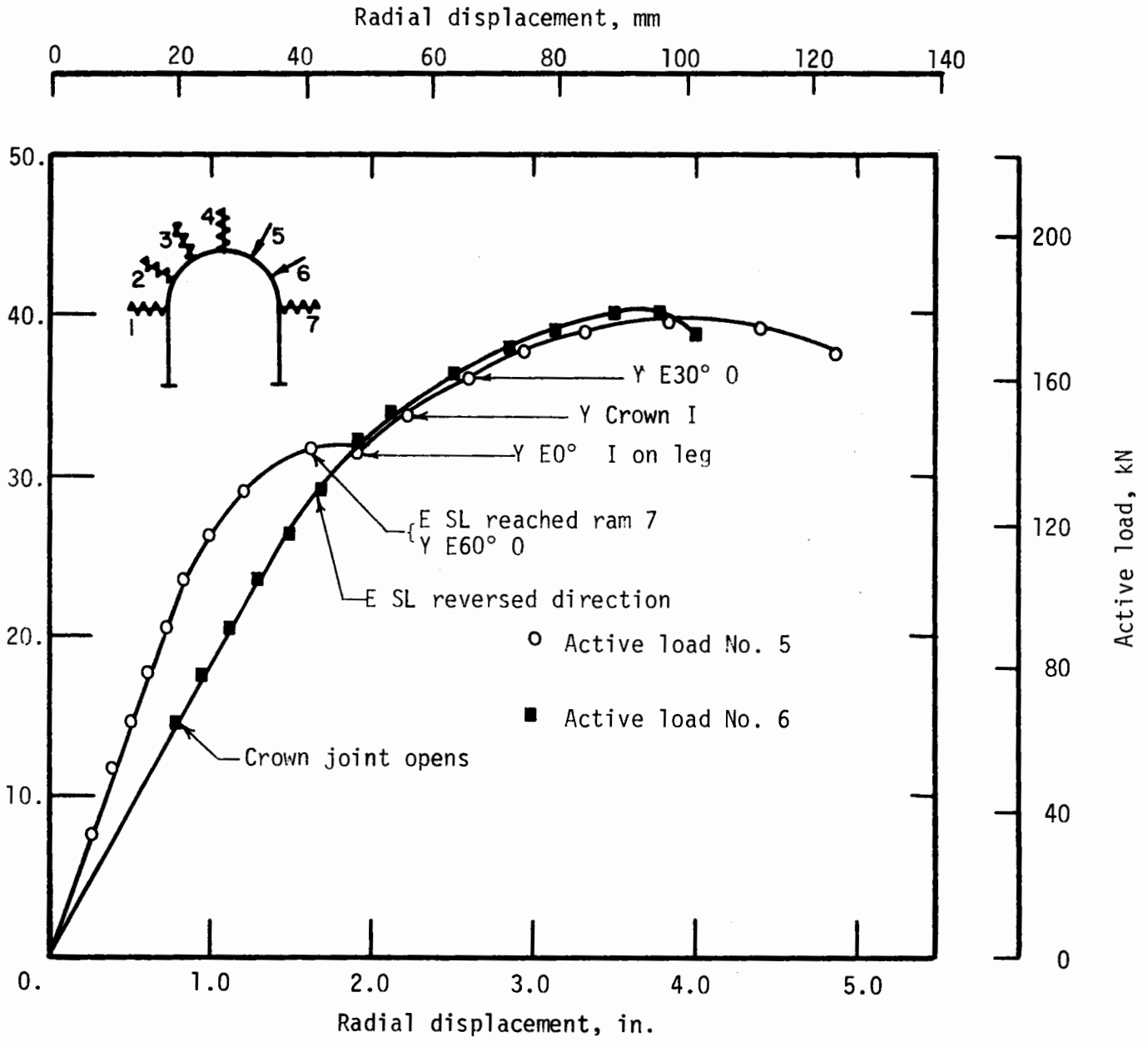

FIG. 2.15 ACTIVE LOAD-DISPLACEMENT IN TEST B5

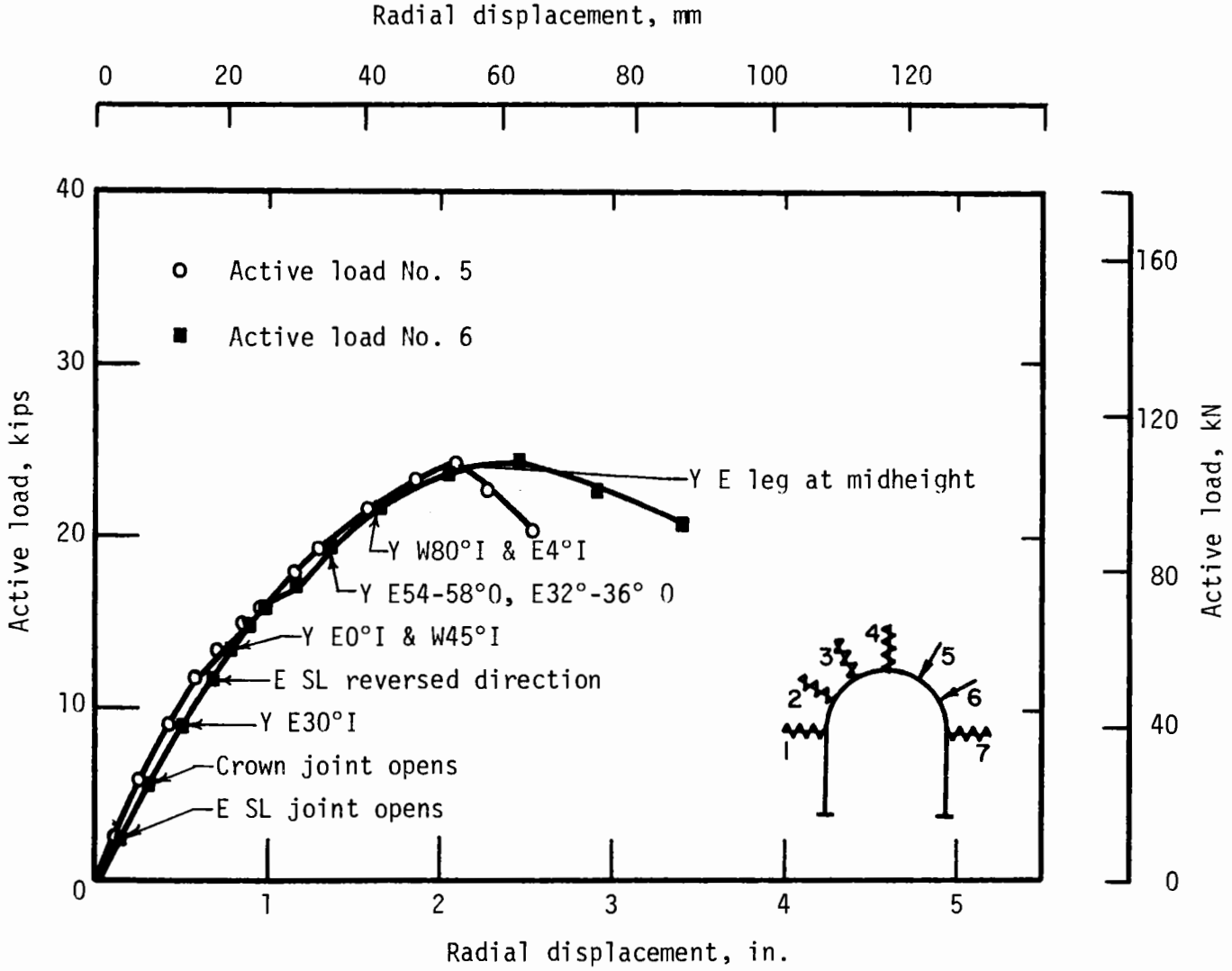

FIG. 2.16 ACTIVE LOAD-DISPLACEMENT IN TEST P18

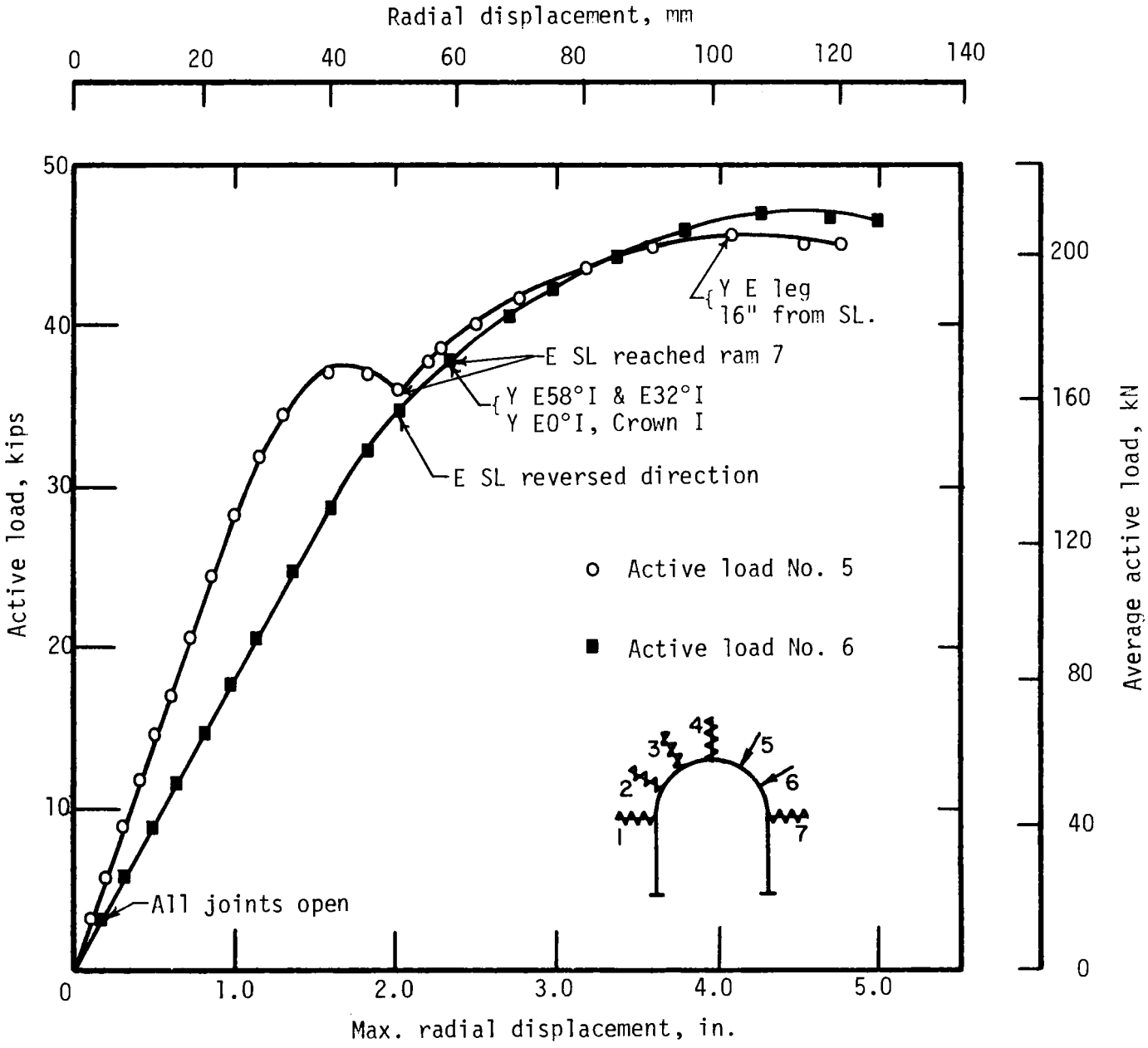

FIG. 2.17 ACTIVE LOAD-DISPLACEMENT IN TEST BC12

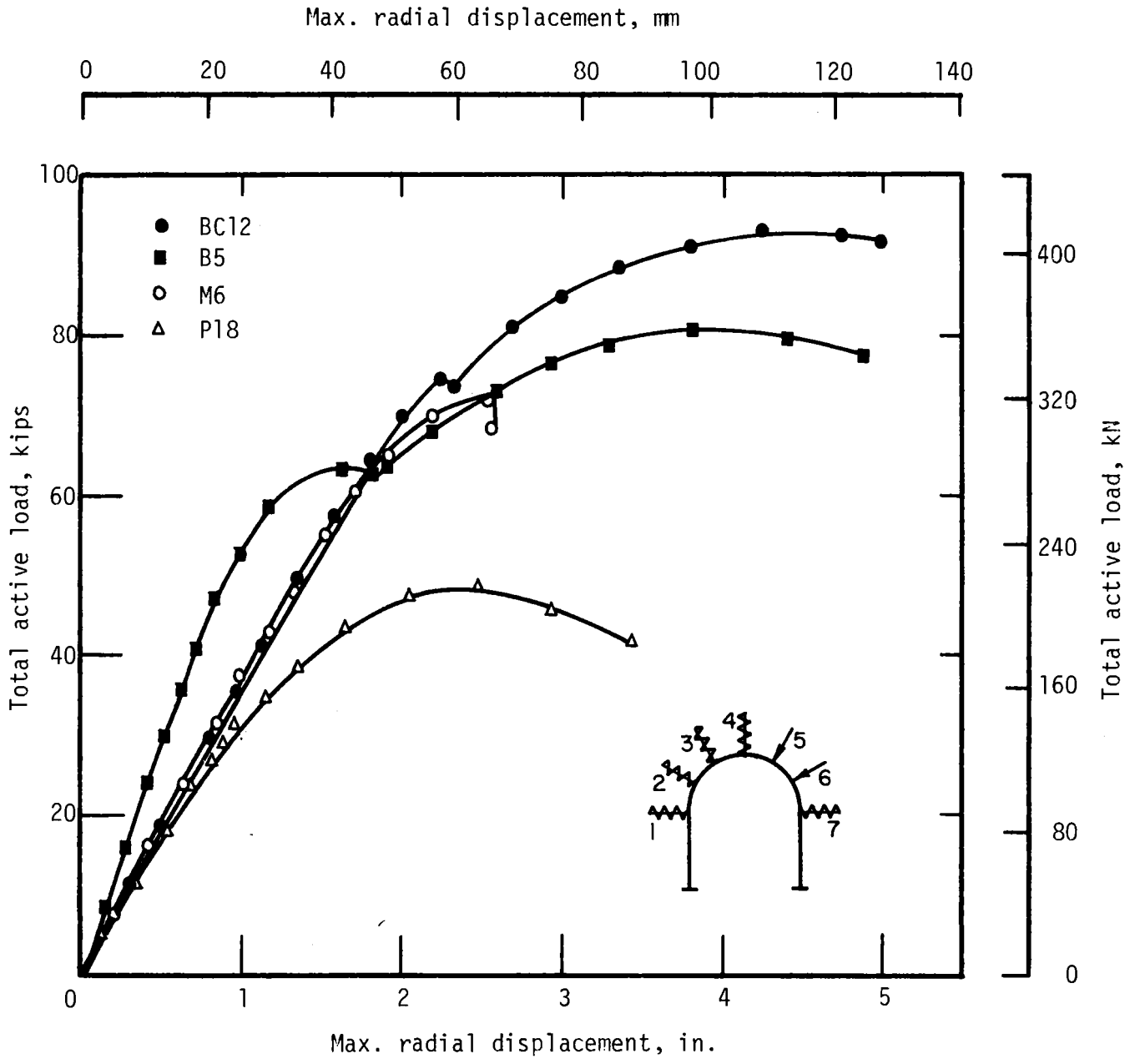

FIG. 2.18 TOTAL ACTIVE LOAD-MAXIMUM DISPLACEMENT IN TESTS M6, B5, P18 AND BC12

observed on the outside of the section between the active loads at 32 to 36 deg and 54 to 58 deg. This yielding grew as load increased, and a load was reached at which deflection continued at no increase in load for ram No. 5 except in test P18 (in that test this yield plateau was not reached for ram No. 5). Finally, the east springline contacted ram No. 7 (passive ram) where it had started when the test began. Thus, ram No. 7 began to take load, which increased the stiffness of the rib so that the total load began to increase more rapidly until a peak load was reached in both active rams. If ram No. 7 had not been present the first plateau would have constituted the maximum load and can be taken as the capacity of the rib if the blocking at ram No. 7 were to fall out because of the initial inward movement of the rib. The second maximum load can be interpreted as the rib capacity if the blocking does not fall out or is replaced if it does. Finally, a mechanism was formed with yielding at the crown, ram Nos. 5 and 6, and at the east springline, after which the load began to decline.

A definite peak load was not reached in test M6 because of twisting of the section at ram No. 6, which finally allowed the load block to slip off the rib. The mechanism had formed and a peak load was imminent, so the remainder of the load-deflection diagram has been estimated as shown dashed in Fig. 2.14. The definite tendency of the wide-flange section to twist even under very small eccentricity of load relative to the web is shown by this test.

In test P18 the initial plateau in the load-deflection curve was not very pronounced. The yield regions were similarly located when the east springline changed its direction of movement; and when it contacted ram

No. 7 yielding developed in the east leg which then began to bow outward. By the end of the test most of the upper two-thirds of the leg was yielded and the leg was deflected outward about 3 in. (76 mm). The springline connection was able to transmit enough moment to bend the leg because the connection is stronger relative to the leg than in the previous tests.

Photographs in Fig. 2.19 show the deformation and yielding of specimen B5. The flattening of the east arch is due primarily to the large deformations between the active loads and the rotations at the crown and east-side joints. Yielding of the straight leg below the east-side joint and around the crown joint are also shown. Significant local buckling of the section was not observed in this group of tests.

2.2.3 GROUP C

Four tests were performed on wide-flange and structural tube specimens with active loads applied 2 in. (51 mm) out of the plane of the rib. Loading was symmetrical for tests M10 and B13 and unsymmetrical for M7 and B9. The behavior of the two section shapes was dramatically different.

Figures 2.20 and 2.21 show the active load-deflection curves and the general behavior for specimens M10 and B13. In each case the crown joint began to open at 6 kips (26.7 kN) average active load, and at the same load the M section started to twist. Twist was not detected in the TS section until a load of 17 kips (75.6 kN) was reached. The structural tube rib behaved much the same as test B2, loaded in-plane, with opening of the side joints at about 23 kips (102 kN) and yielding at 38 deg in both east and west arches. Yielding occurred near the crown connection

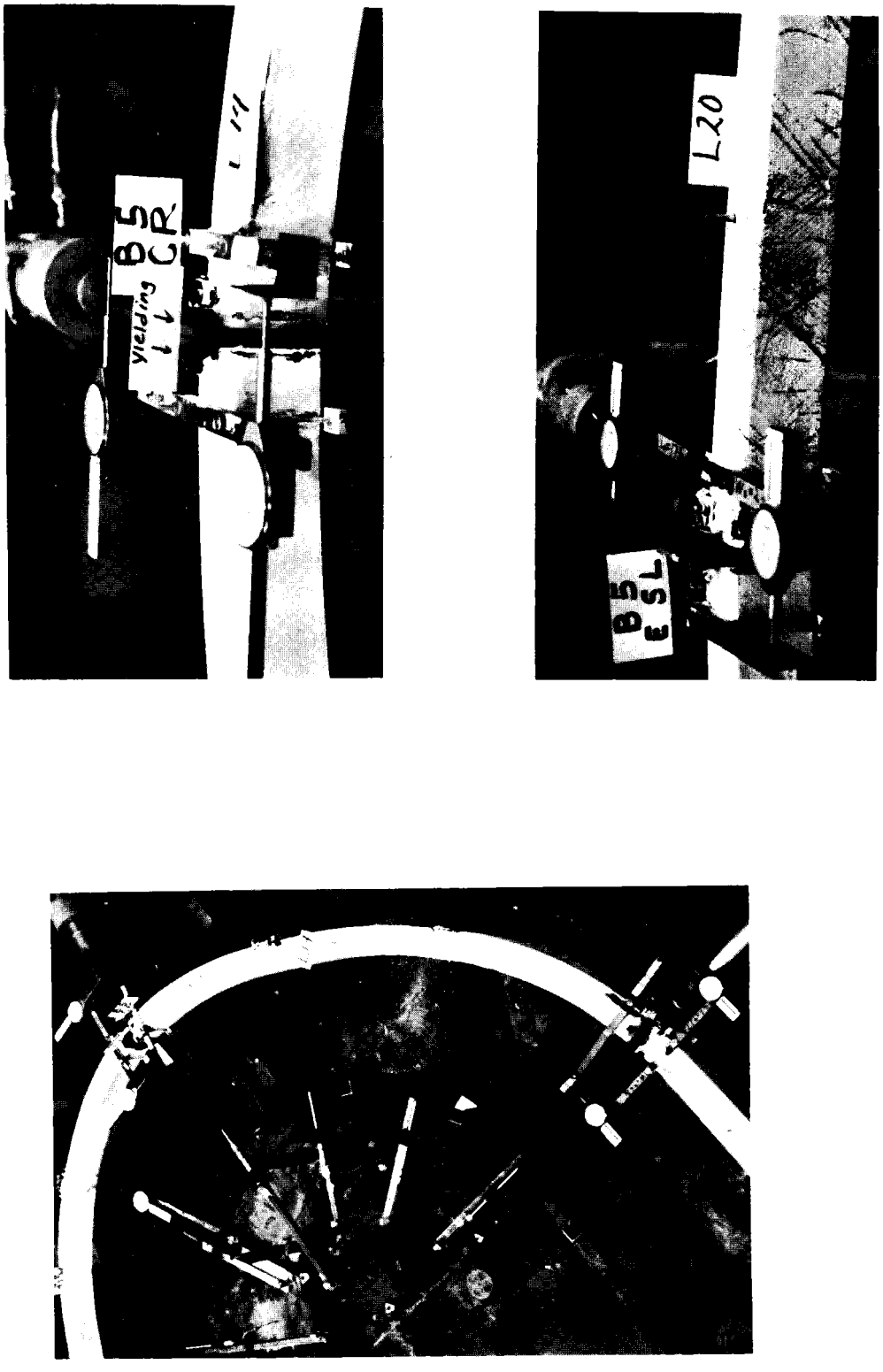

FIGURE 2.19 PHOTOGRAPHS OF SPECIMEN B5

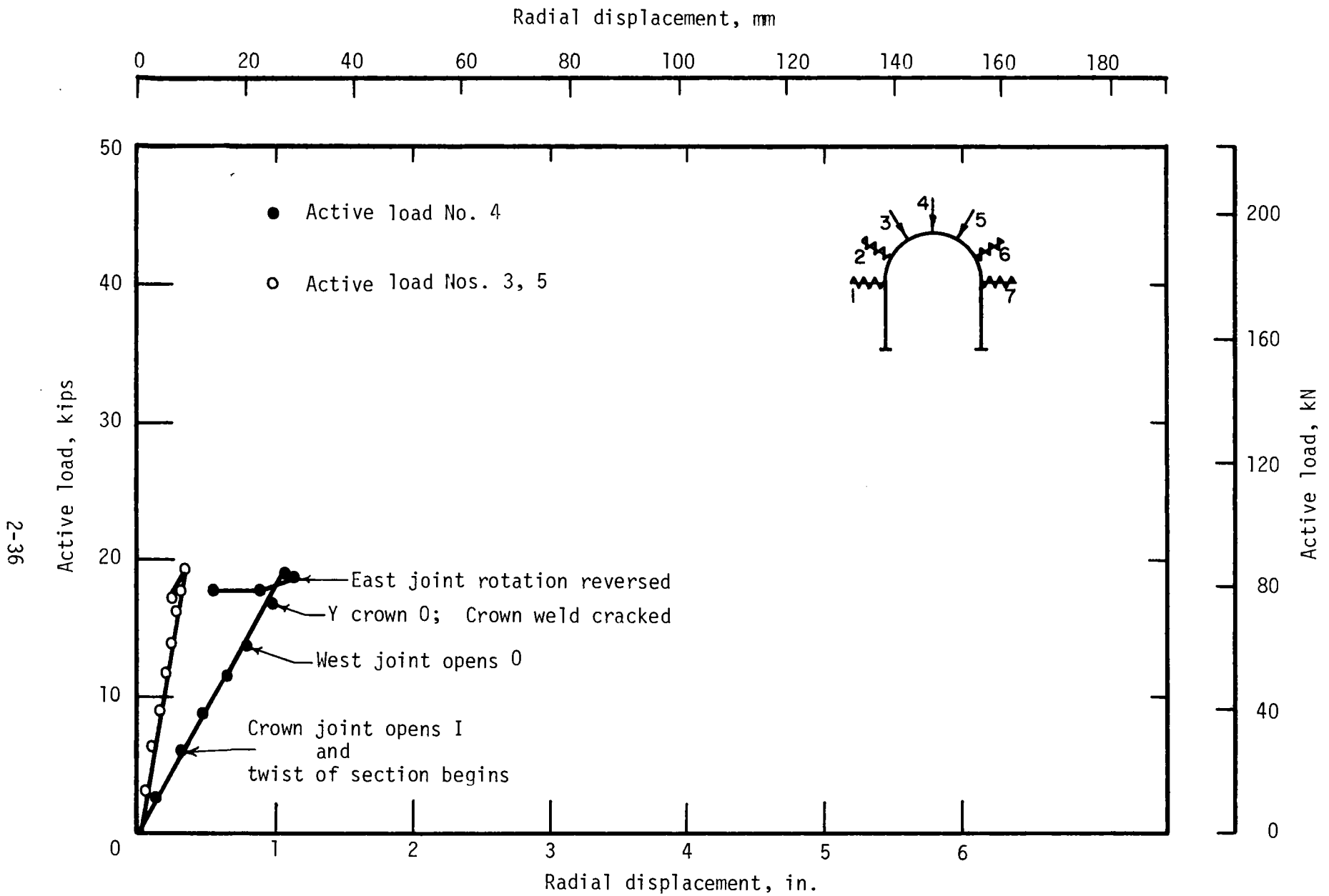

FIG. 2.20 ACTIVE LOAD-DISPLACEMENT IN TEST M10

at 29 kips (129 kN) average active load and the joint rotation reversed at a slightly higher load. Only after the peak load had been reached was local buckling of the walls of the tube detected.

The yielding of the M section rib was confined to the crown at an average active load of about 17 kips (75.6 kN), but the twist was much greater and determined the rib capacity. Twisting of the sections at the active load points are compared for the two tests in Fig. 2.22 where it is seen that the twist at maximum load was 4.5 deg for the box section and 19 deg for the M section. Figure 2.20 shows that the deflection of the mid-section of the M section at the crown reversed after peak active load was reached, although the section continued to twist as shown in Fig. 2.22. This twisting caused the peak load of test M10 to be substantially smaller than that of test M1 in which the load was not eccentric. The difference in section rotation at the active loads is shown in the photographs of Fig. 2.23, taken near peak load in each test.

Figures 2.24 and 2.25 show the load-deflection curves and the important events in the behavior of M7 and B9. Initially the deformation was similar to that of tests M6 and B5 in which the load was in-plane. The east springline moved inward until yielding began and then it reversed direction, but rotation of the M section at the active loads was much larger. When the east joint contacted ram No. 7 the active loads increased in test B9, but twisting dominated the deformation of M7 and the loads fell off. Twisting of the active load section of both ribs is shown in Fig. 2.26, where the large difference can be noted. The photograph of Fig. 2.27 also shows the extent of twisting in M7. It is seen to be rather local and to

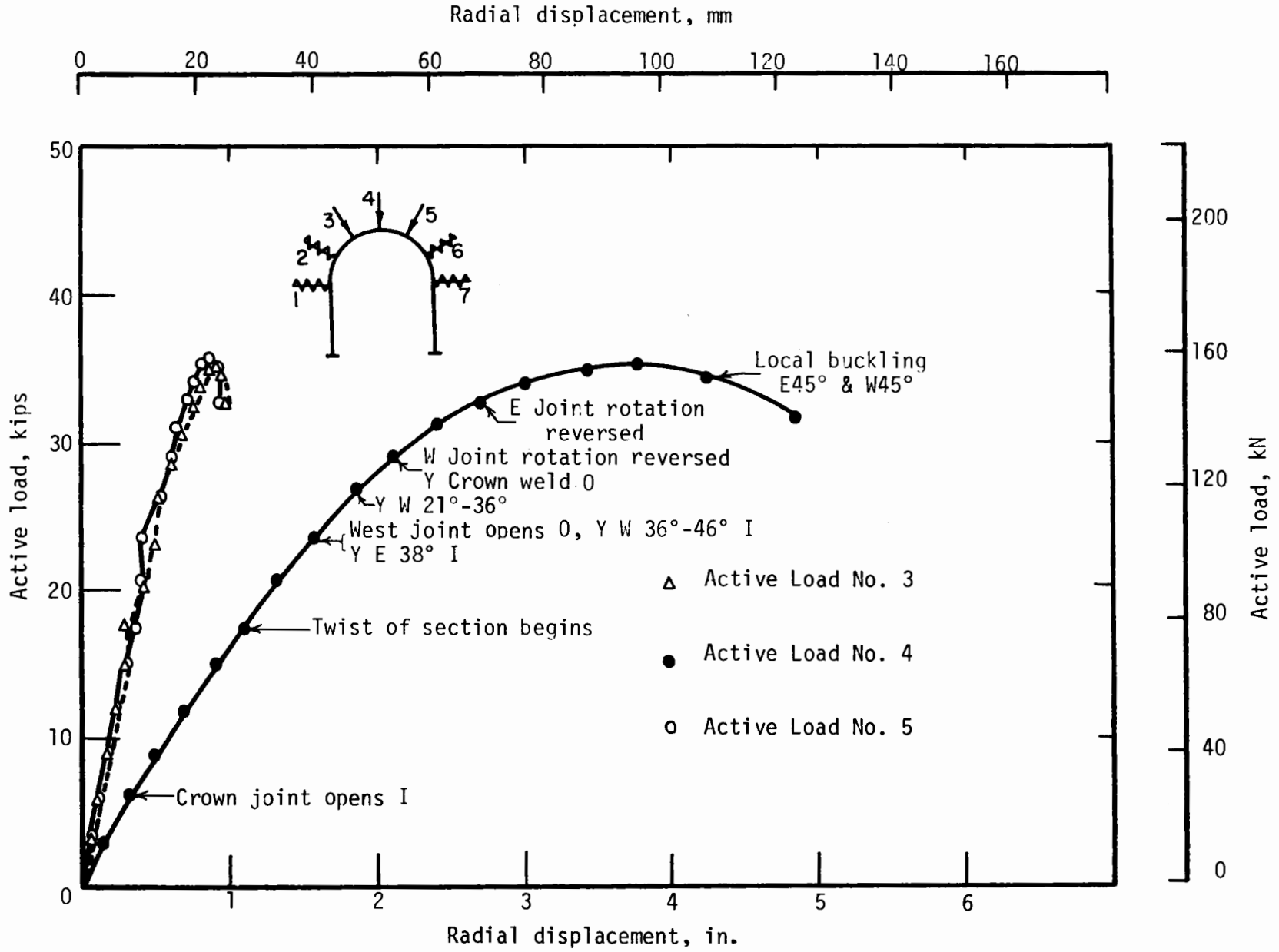

FIG. 2.21 ACTIVE LOAD-DISPLACEMENT IN TEST B13

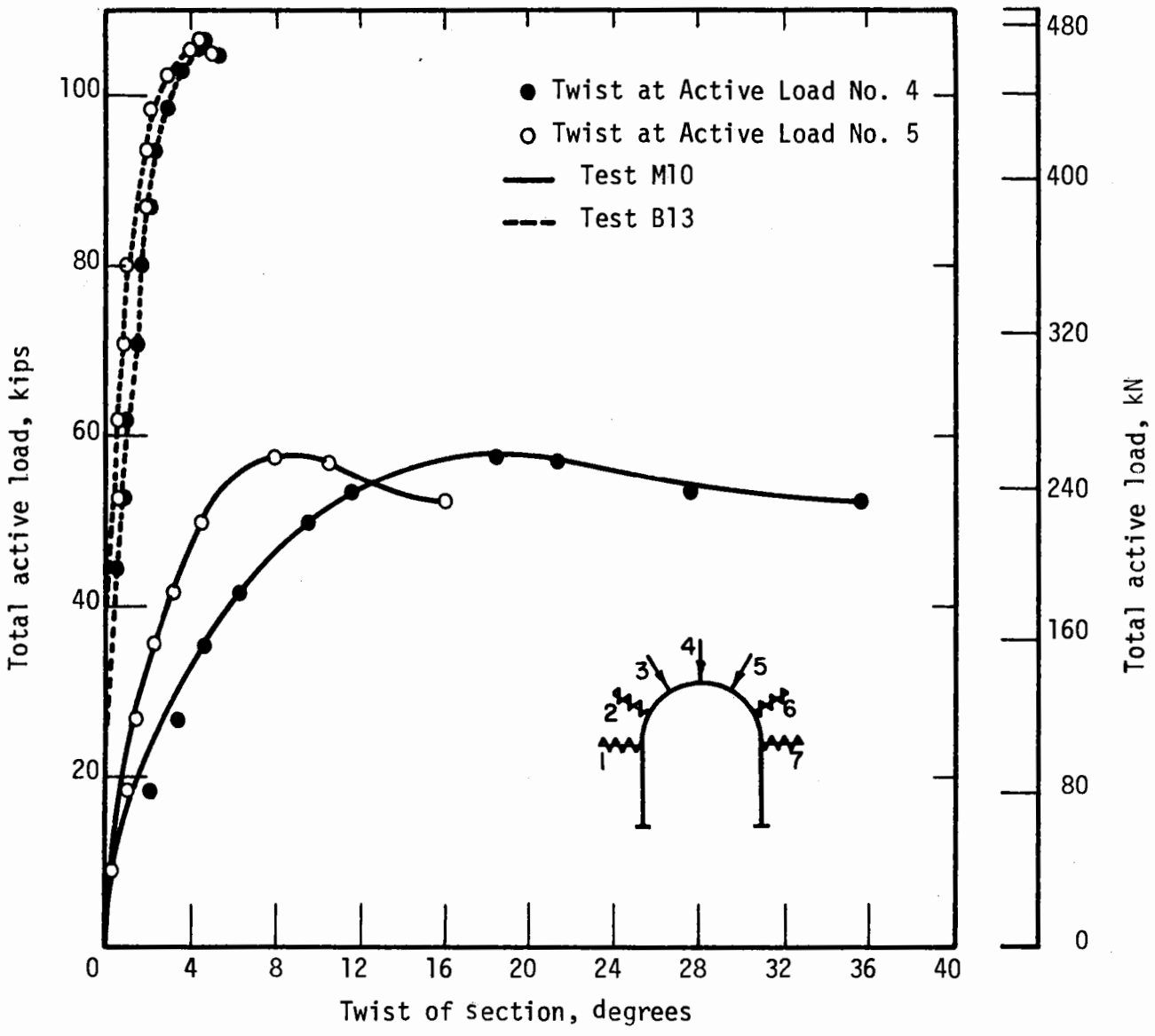

FIG. 2.22 TOTAL ACTIVE LOAD - TWIST IN TESTS M10 AND B13

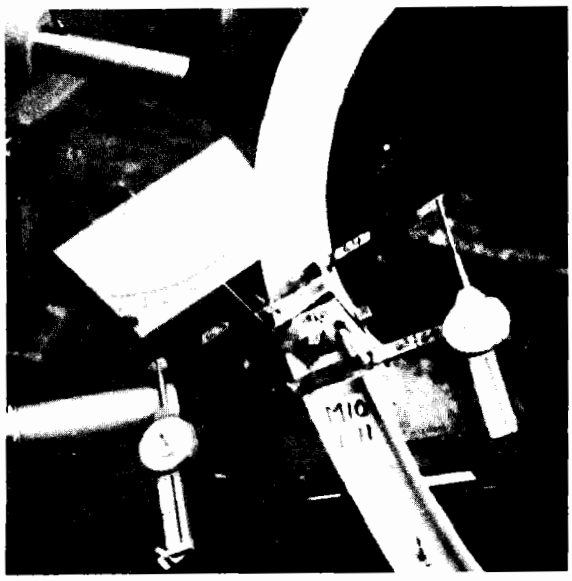

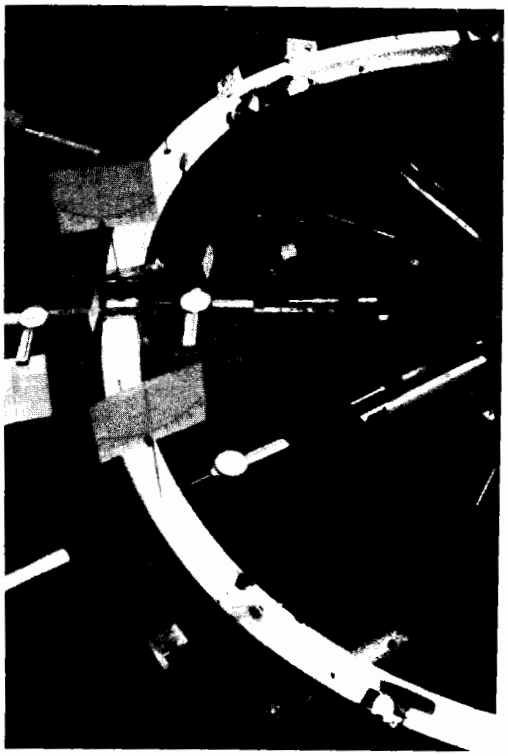

FIGURE 2.23 PHOTOGRAPHS SHOWING SECTION ROTATION IN TESTS M10 AND B13

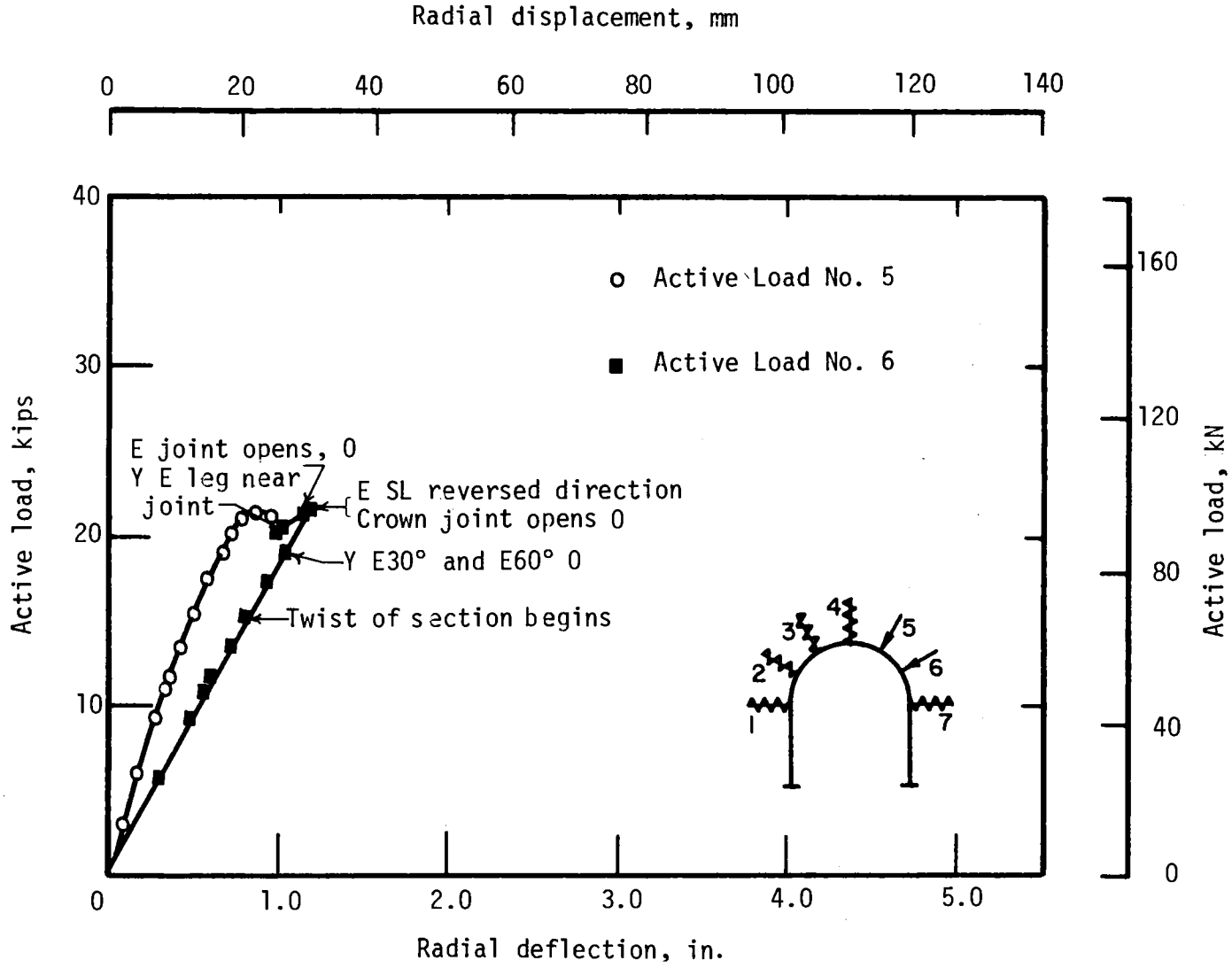

FIG. 2.24 ACTIVE LOAD-DISPLACEMENT IN TEST M7

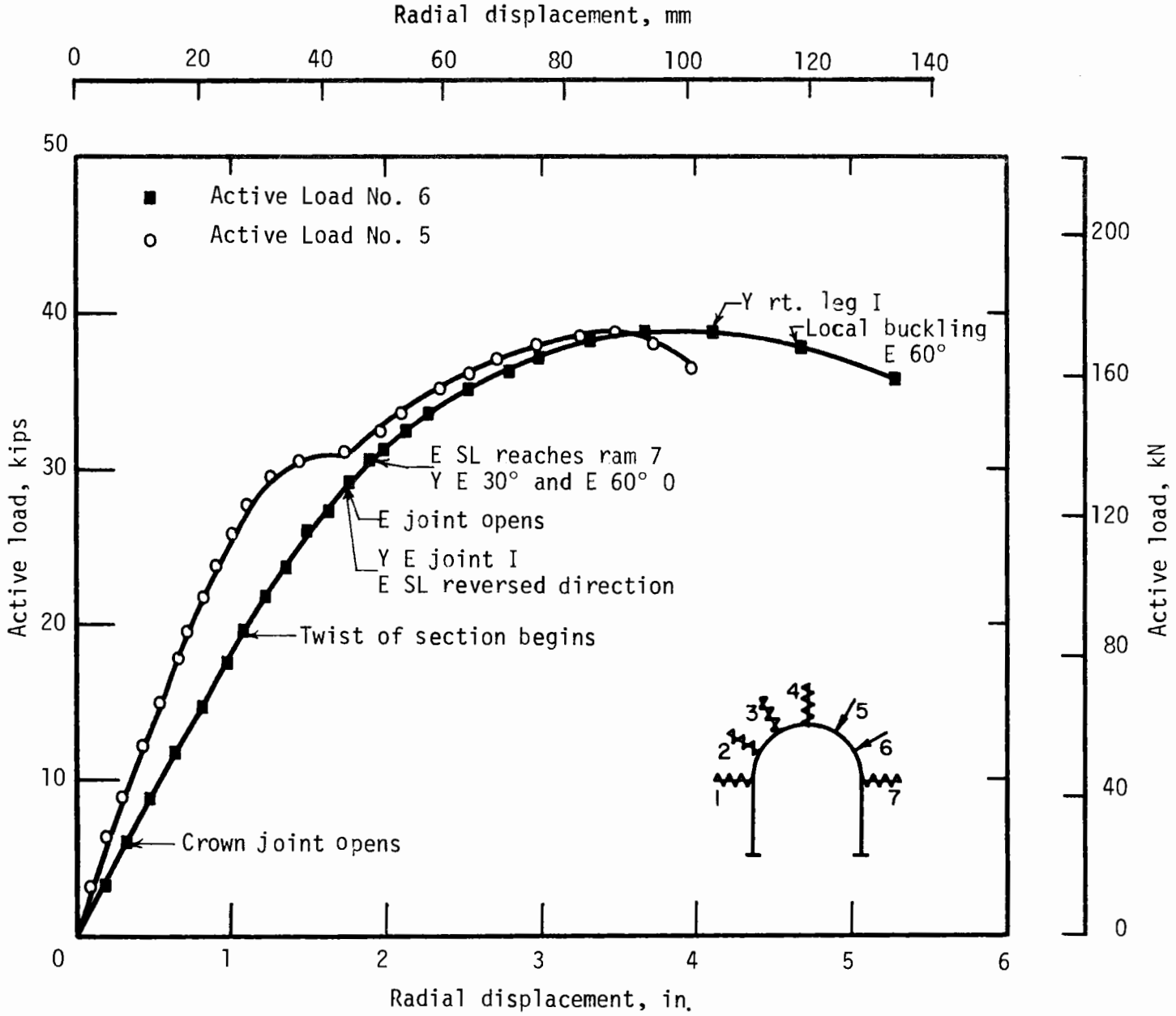

FIG. 2.25 ACTIVE LOAD-DISPLACEMENT IN TEST B9

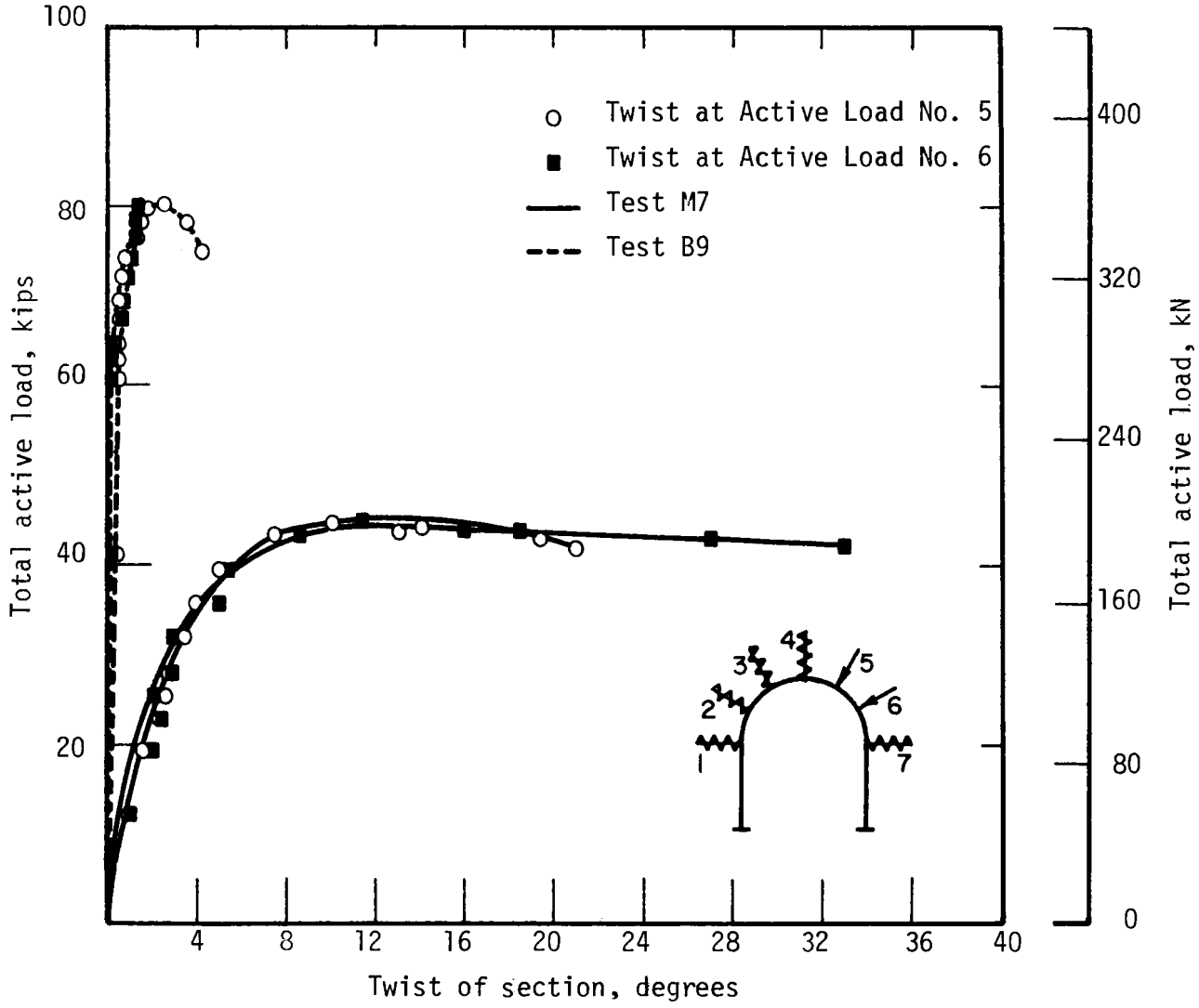

FIG. 2.26 TOTAL ACTIVE LOAD - TWIST
IN TESTS M7 AND B9

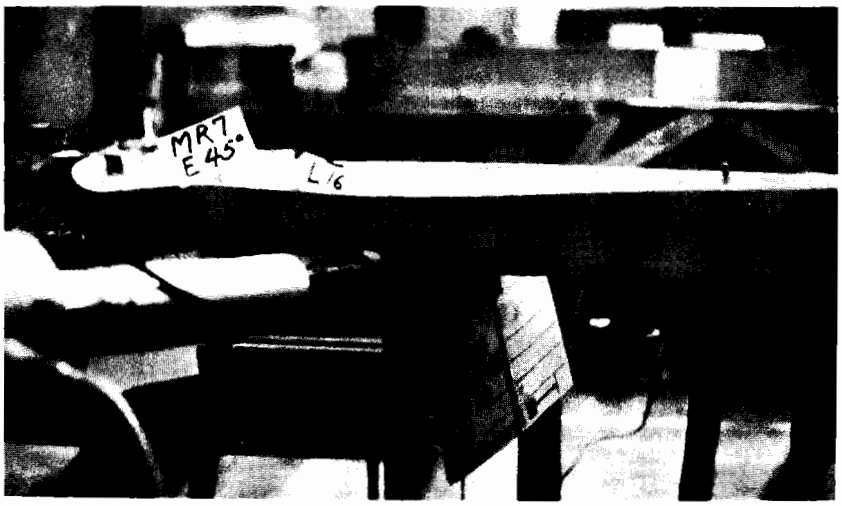

FIGURE 2.27 PHOTOGRAPH OF SECTION TWIST IN TEST M7

reduce rapidly toward the lateral support sections. The structural tube section developed a mechanism with plastic hinges at 30 and 60 deg on the east side (at the active loads), at the crown, and just below the east joint. The east joint did not open as much as in the M section tests, but a yield hinge formed just below the joint in the leg. This general yielding and mechanism formation was prevented in test M7 when the east side joint contacted ram 7 because of the premature twisting failure. The total active load-displacement curves are compared in Fig. 2.28 for the tests in this group.

2.2.4 GROUP D

The passive ram at blocking point No. 2 (Fig. 2.1) was omitted

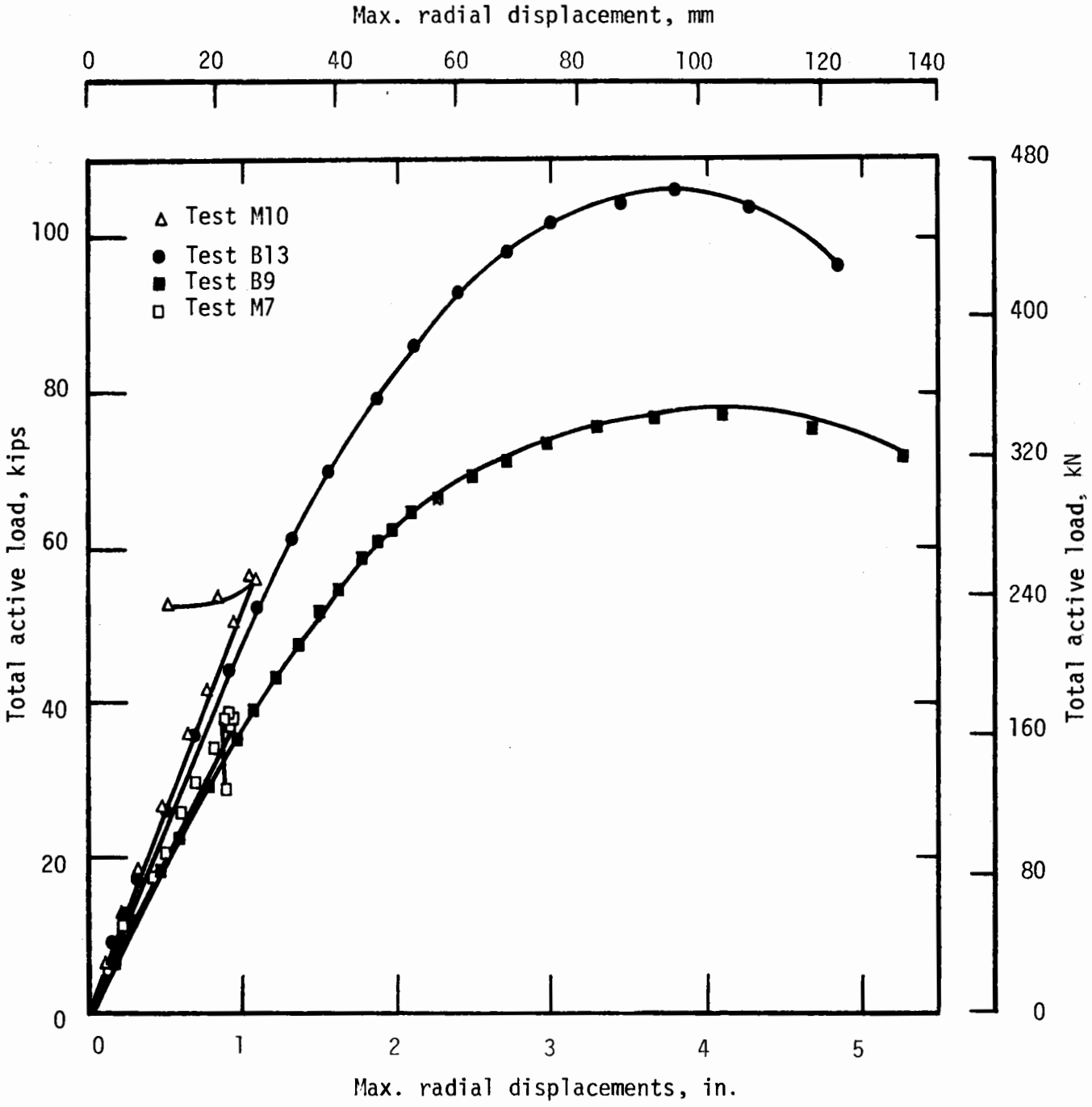

FIG. 2.28 TOTAL ACTIVE LOAD - MAXIMUM DISPLACEMENT IN TESTS M7, M10, B9, AND B13

in tests M3 and B4 with the symmetrical active loading applied in the plane of the rib. Overall response was very similar for the M and TS section ribs as shown in Figs. 2.29 and 2.30 with the crown joint beginning to open on the inside at about 6 kips (26.7 kN) average active load and the east joint on the outside at about 9 kips (40.0 kN). At 21 to 22 kips (93 to 98 kN) yielding began at blocking point 2 (30 deg on west arch) and the west joint started to open on the inside. This load level was very close to the peak load in both tests, as the mechanism, which consisted of plastic hinges at the crown, 30 deg west, and about 22 deg east, formed very quickly. This mechanism and the resulting deformed rib are shown in Fig. 2.31(a).

The M section began to twist at 45 deg in the west arch after the peak load was reached, and local buckling of the inside flange occurred, as shown in Fig. 2.31(b), two load increments after the twist began. There was no twist of the section in the TS rib, but local deformation of the section at the west yield hinge occurred after the peak load with the inside face of the tube buckling inward and the sides outward. This same type of local deformation was observed in the square TS section tests of Group A.

The passive ram at blocking point No. 2 was omitted in test M8 with unsymmetrical active load. Active load-deflection curves are shown in Fig. 2.32. The joints at the crown and west opened first, and at 25 kips (111 kN) average active load yielding began at 30 deg in both the east and west arches. The peak active load occurred at 28.5 kips (126.8 kN), and the section began to twist at 60 deg on the west arch after the peak

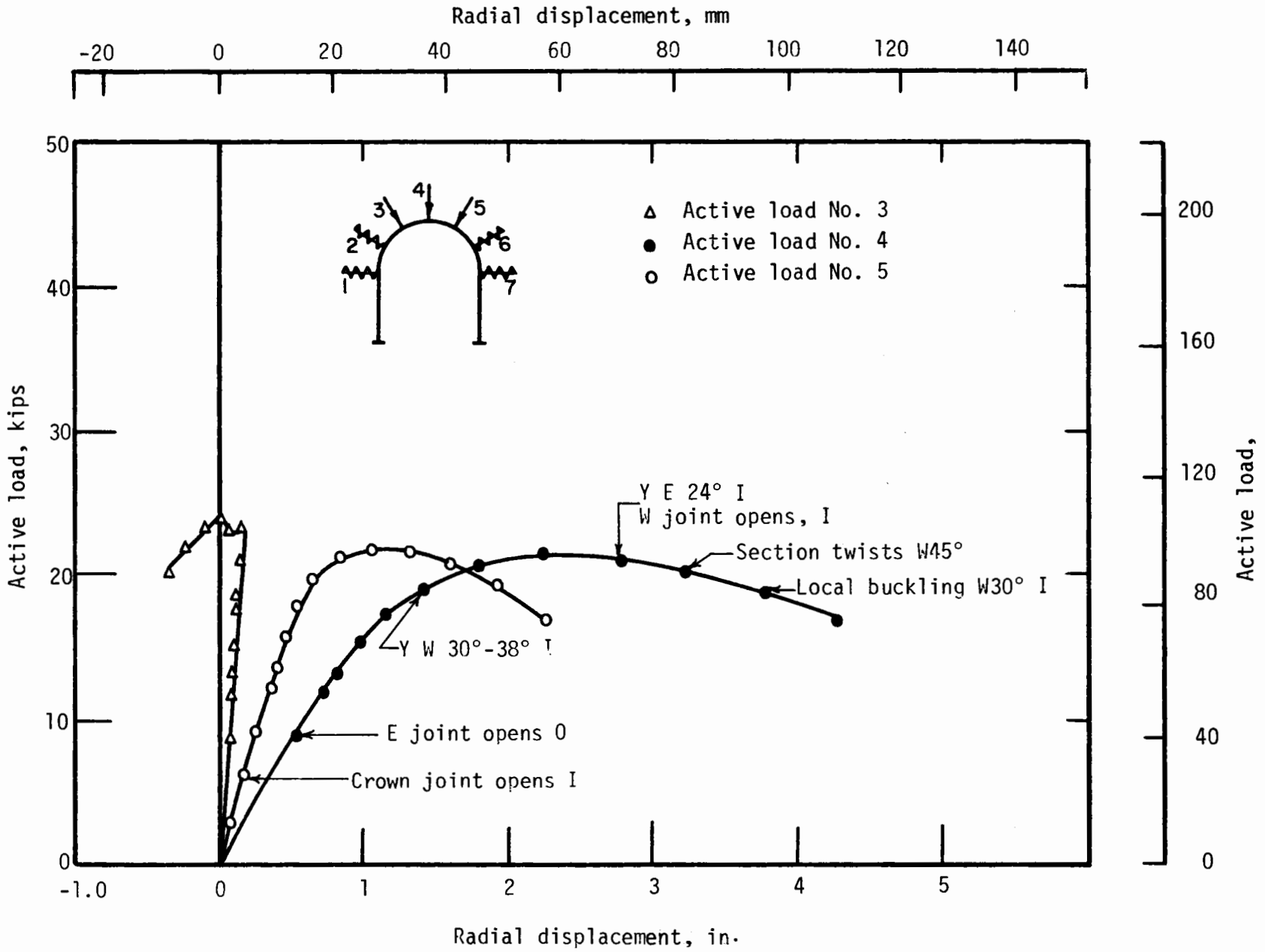

FIG. 2.29 ACTIVE LOAD-DISPLACEMENT IN TEST M3

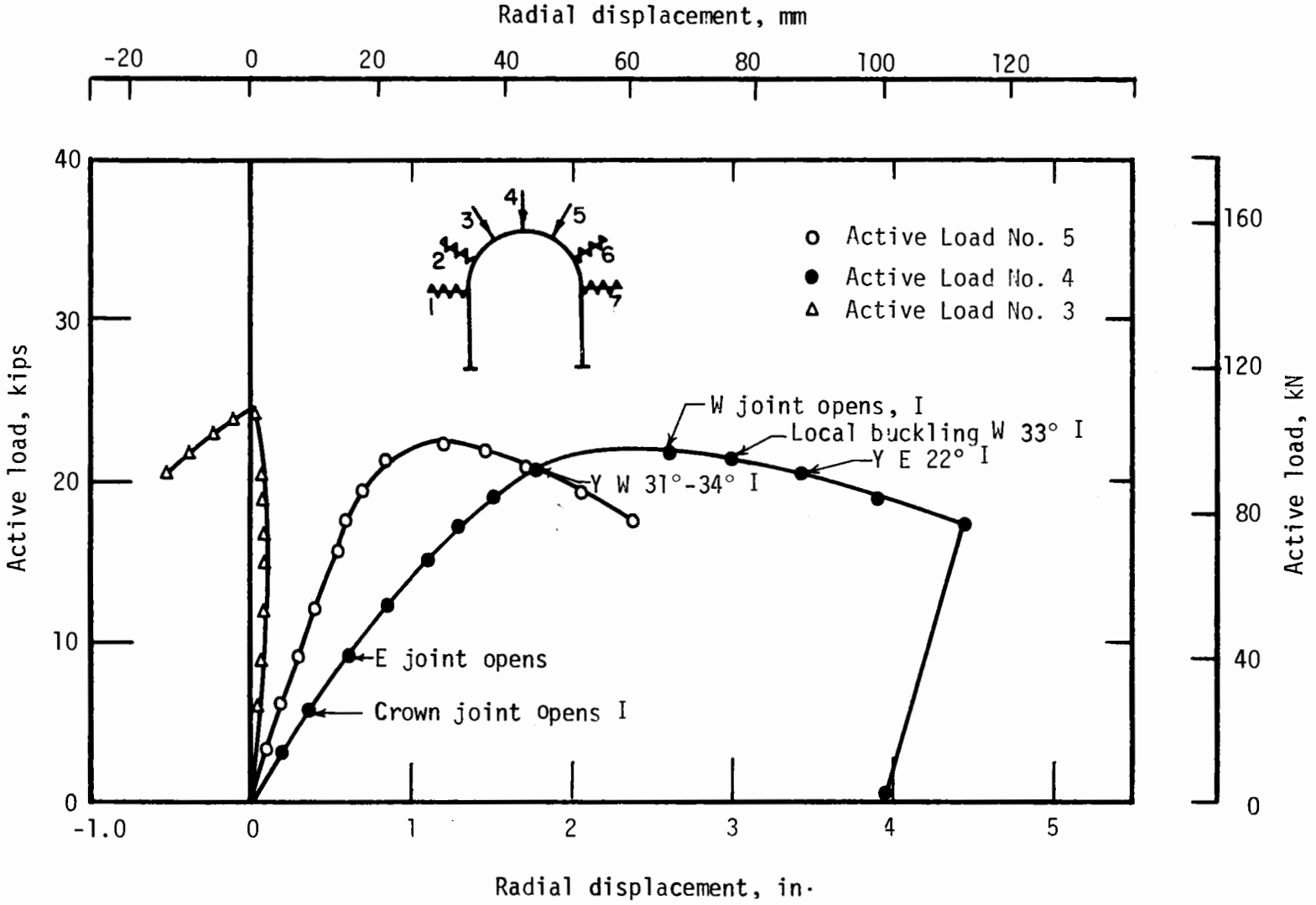

FIG. 2.30 ACTIVE LOAD-DISPLACEMENT IN TEST B4

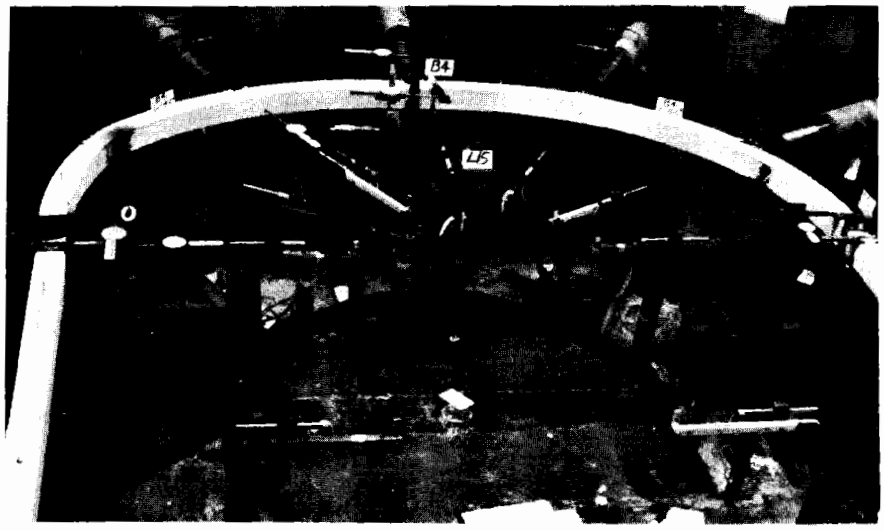

(a) Specimen B4

(b) Specimen M3

FIGURE 2.31 PHOTOGRAPHS OF SPECIMENS M3 AND B4

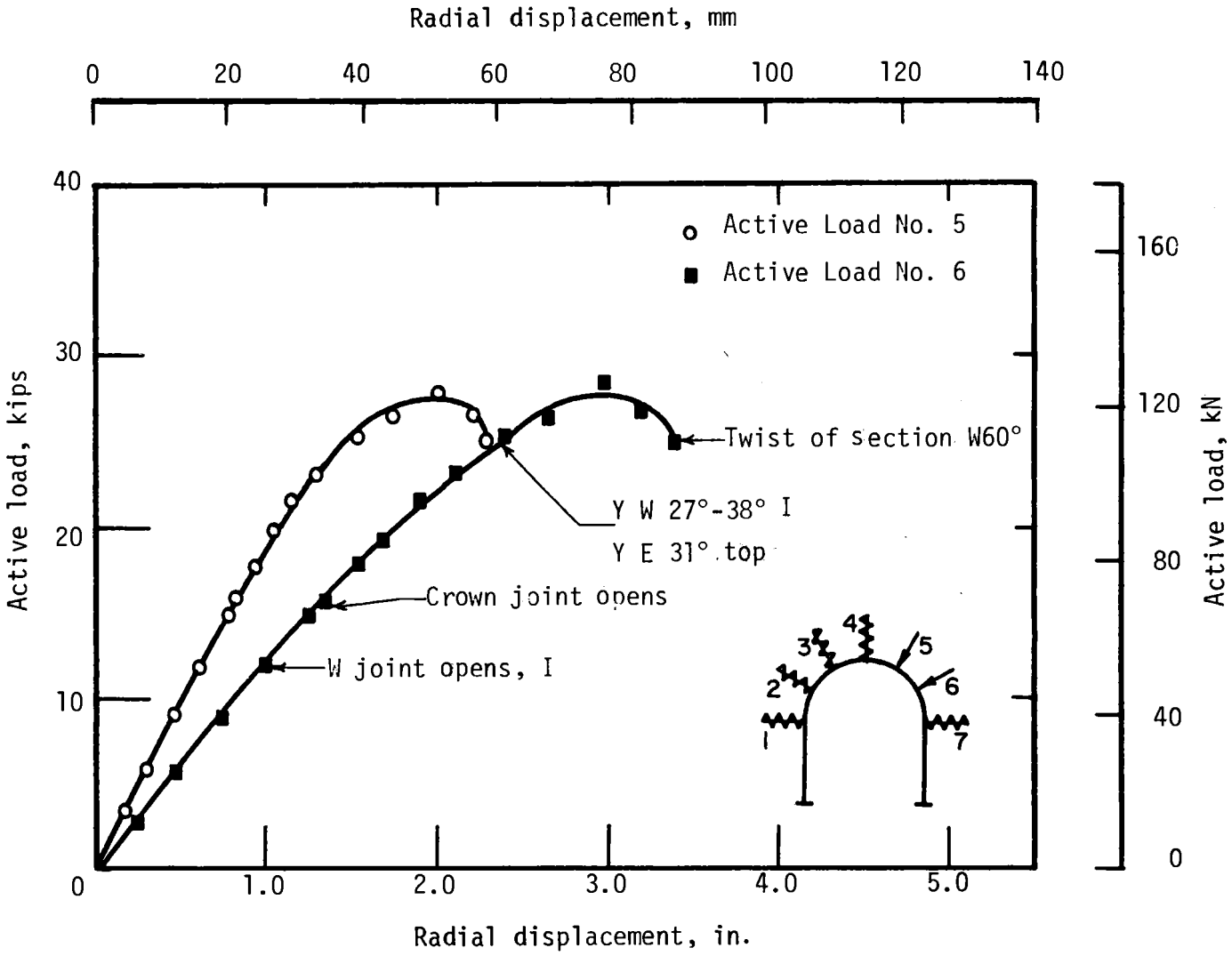

FIG. 2.32 ACTIVE LOAD-DISPLACEMENT IN TEST M8

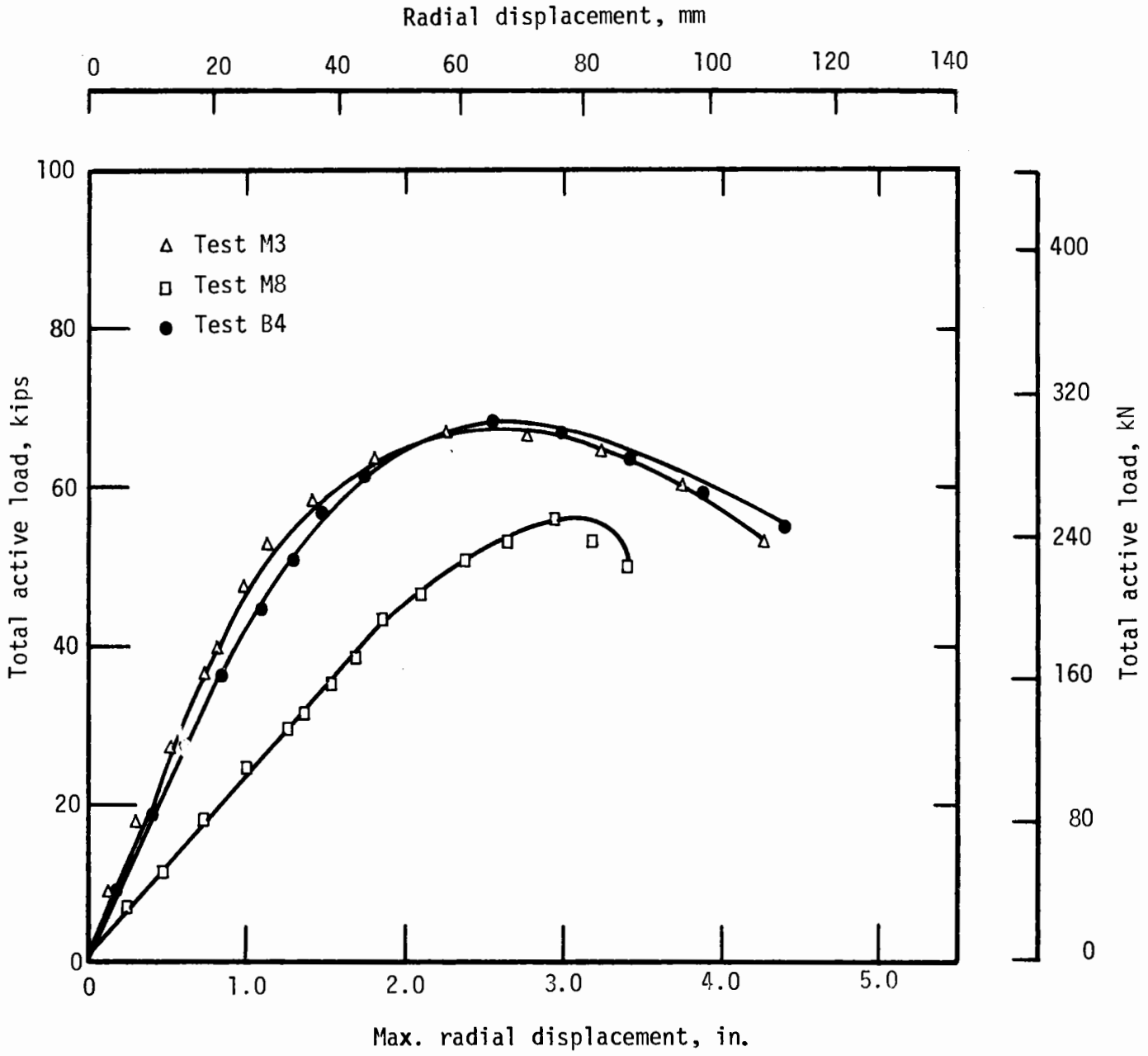

FIG. 2.33 TOTAL ACTIVE LOAD - MAXIMUM DISPLACEMENT IN TESTS M3, M8, AND B4

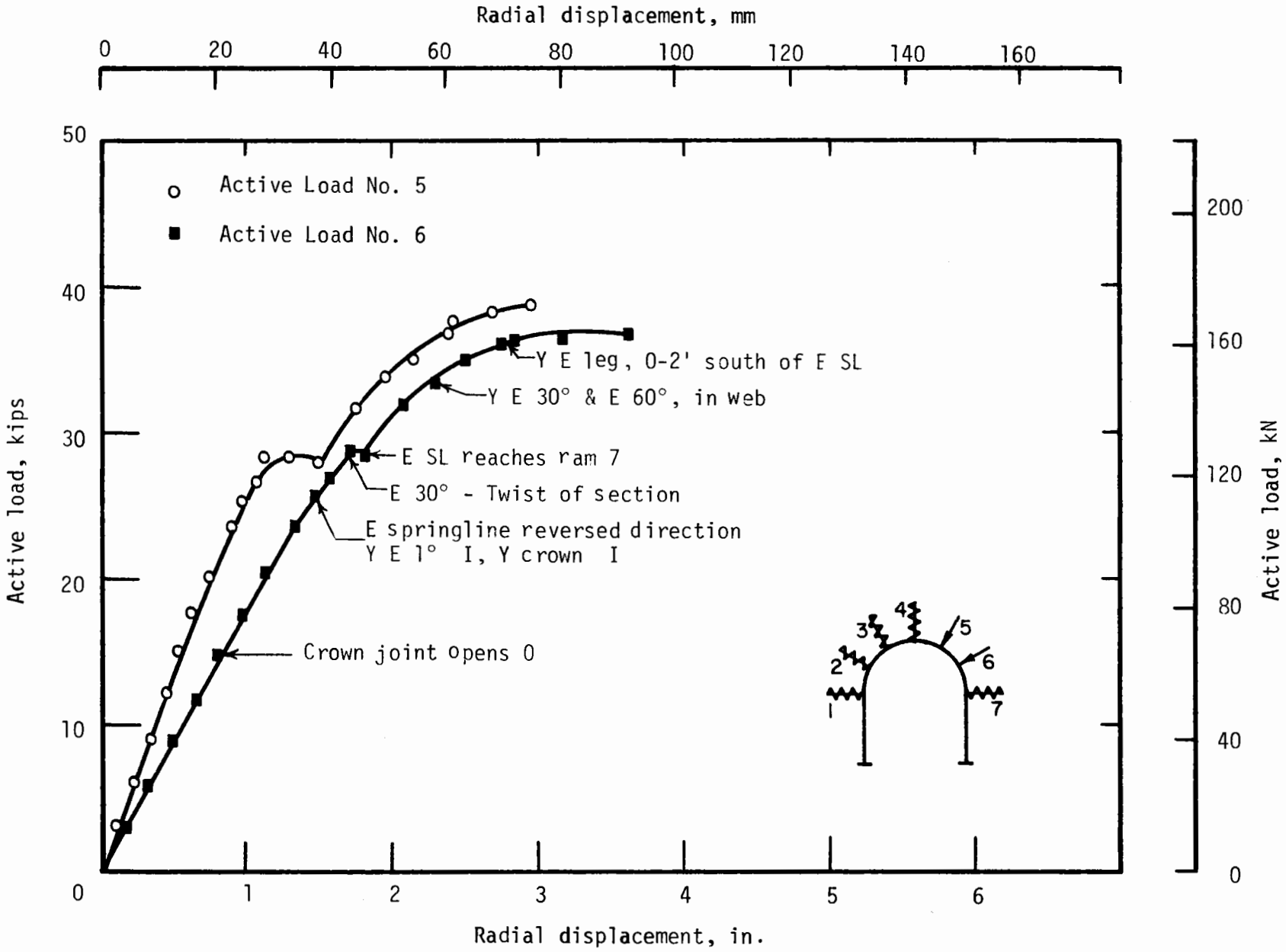

FIG. 2.34 ACTIVE LOAD-DISPLACEMENT IN TEST M11

load. The east joint moved inward from the start of loading and never reversed its direction as it had in the previous unsymmetrical loading tests.

Total active load-deflection curves for the tests in this group are compared in Fig. 2.33.

2.2.5 GROUP E

Test M11 was the same as M6 except that the bolts in the east joint were left loose so that 1/8 in. (3.2 mm) of threads remained exposed adjacent to the butt plate. Active load-deflection curves are shown in Fig. 2.34. The overall behavior was quite similar to that of test M6. The east joint moved inward until yielding began, when it reversed direction. An initial yield plateau then developed but load increased again when the east joint contacted ram No. 7. A maximum load was again obtained when a general yield mechanism formed. The total active load-displacement curve is shown in Fig. 2.35.

Test BS15 was similar to B2 (symmetrical load in the plane of the rib) except that a sleeve connector, shown in Fig. 2.2, was used at all joints. The active load-displacement and general behavior are shown in Fig. 2.36. Yielding developed at a rather low load of about 6 kips (26 kN) in the east arch at 40 deg, but was not noted at other locations until about 15 kips (66.7 kN), when yielding occurred at 45 deg in the west arch and at the next load increment at 62 deg on the east and 25 and 75 deg on the west. Loading continued as yield hinges formed at 25 and 75 deg on the west and 40 deg on the east to form a mechanism, as shown in Fig. 2.37(a).

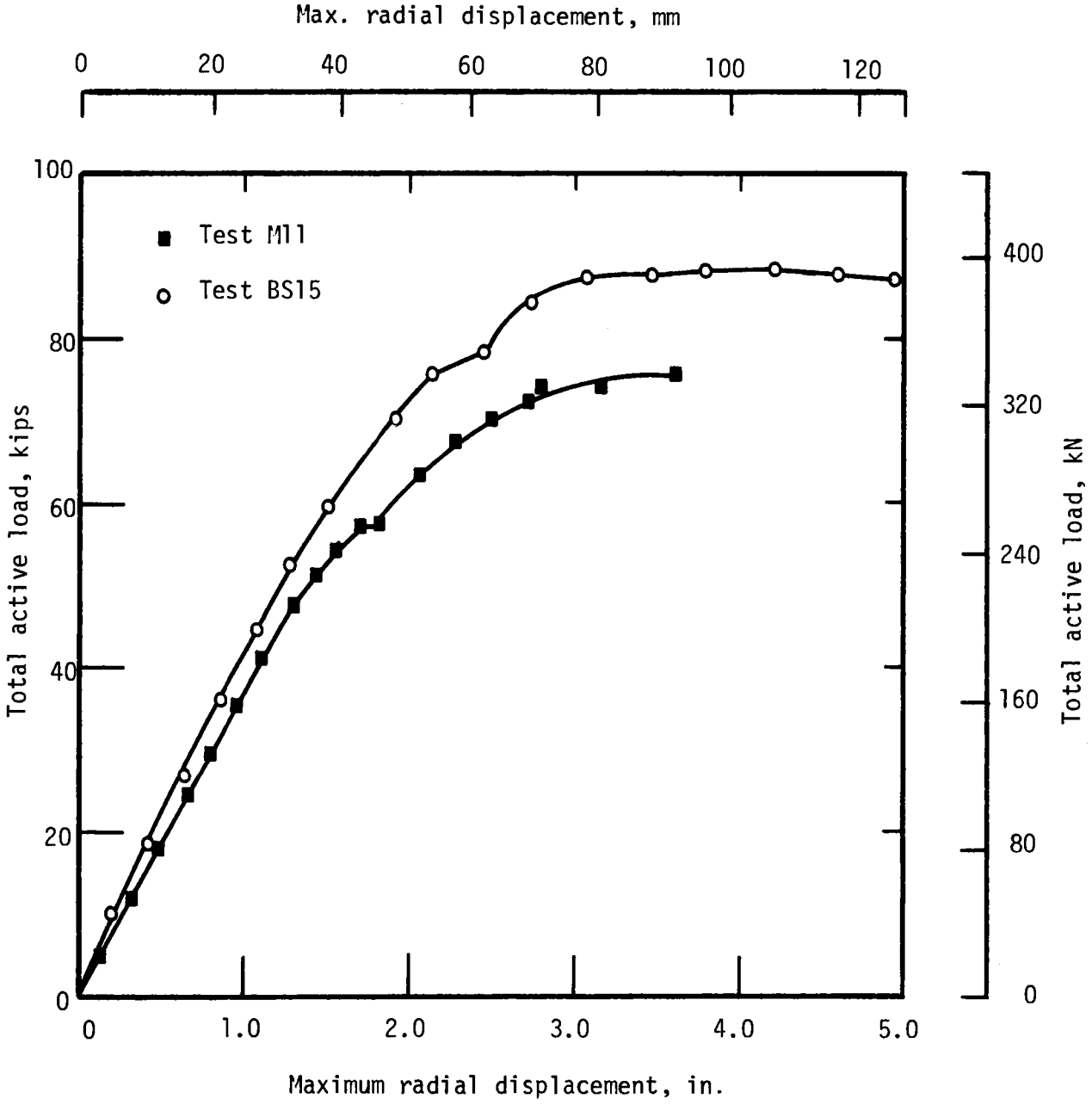

FIG. 2.35 TOTAL ACTIVE LOAD - MAXIMUM DISPLACEMENT IN TESTS M11 AND BS15

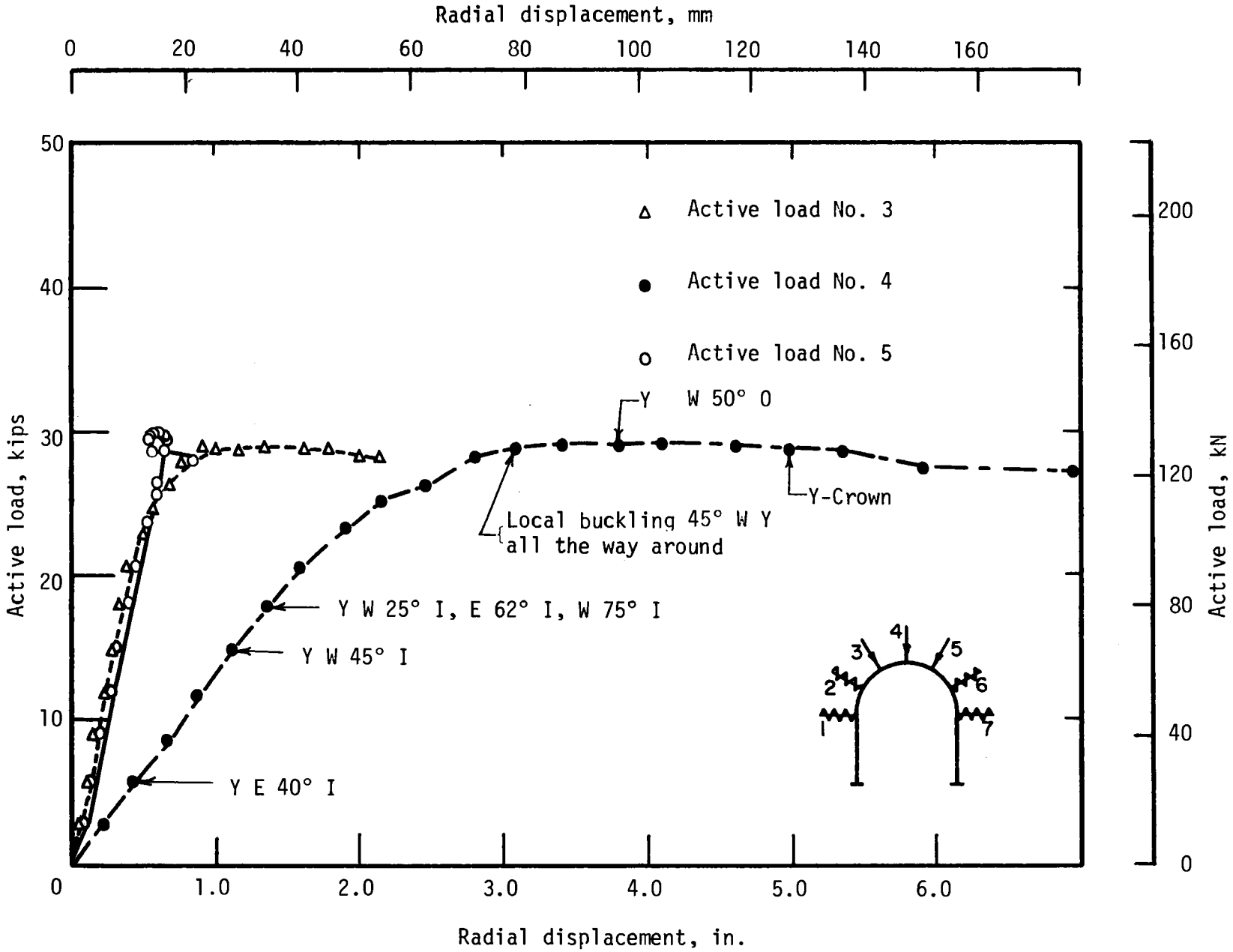

FIG. 2.36 ACTIVE LOAD-DISPLACEMENT IN TEST BS15

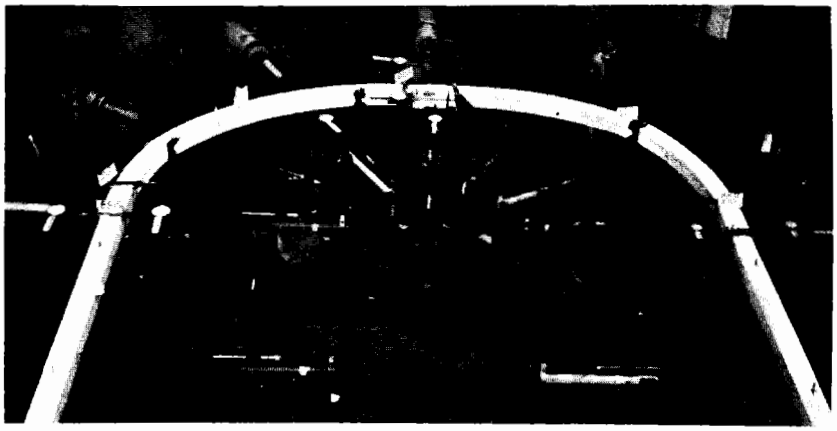

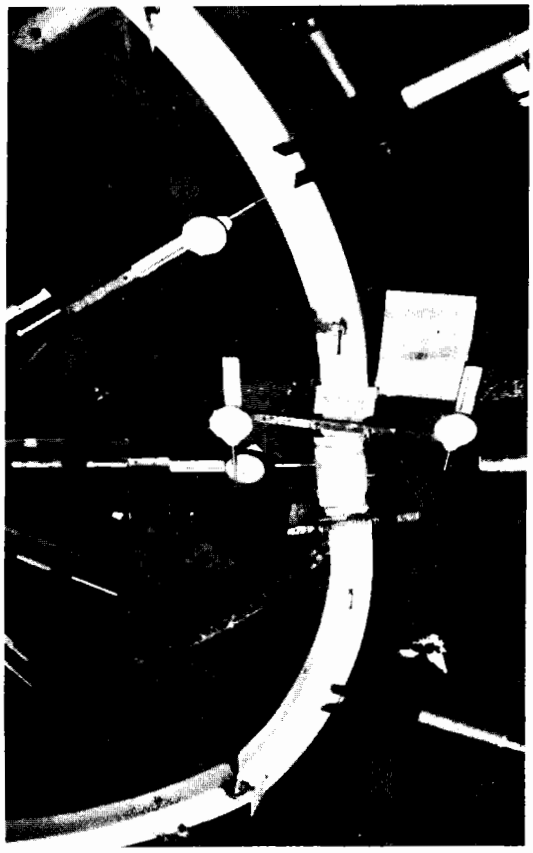

(a) Rib at end of the test

FIGURE 2.37 PHOTOGRAPHS OF SPECIMEN BS15

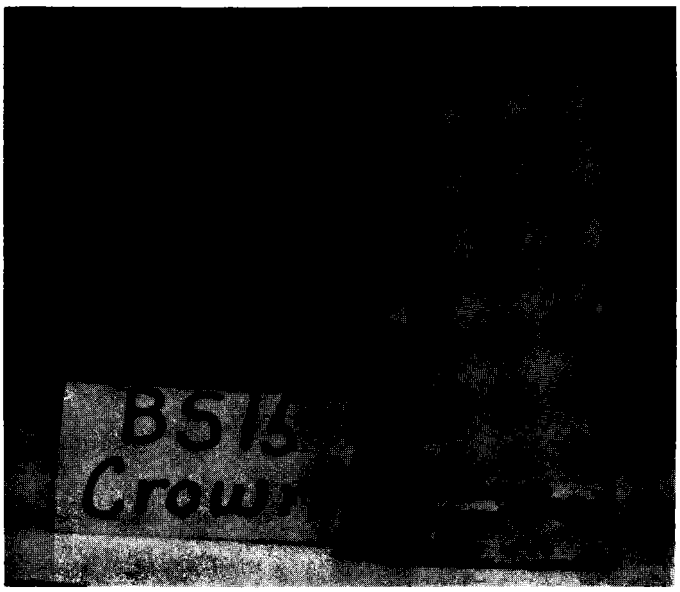

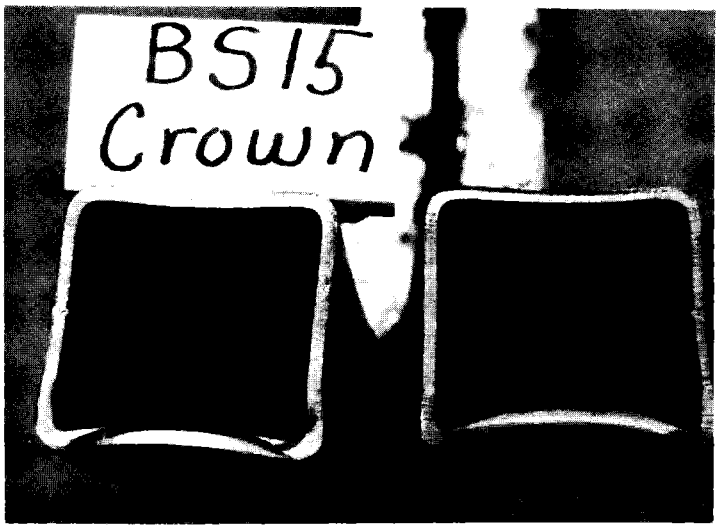

(b) Crown deformation after the test

FIGURE 2.37 PHOTOGRAPHS OF SPECIMEN BS15

The load-deflection curve broke over more sharply at the knee than in previous tests, and is flatter.

The sleeve connector allowed more rotation at the joints than the butt plate connection, as shown in Fig. 2.38 where joint rotations are compared for several representative tests. In the linear range of the curve the rotation of the sleeve connection is about twice that of the butt plate connection. The strength of the rib with sleeve connectors was about 20 percent less than for the comparable test B2 with butt plate connections. The sleeves did not fail, but deformed more and allowed large deformation of the crown joint as shown in Fig. 2.37(a). It appears that the greater deformation reduced the rib capacity. The sleeve deformation is shown in Fig. 2.37(b), where the bumps on the right side are caused by the end of the arch within the sleeve bearing on it. Bearing of the ends of the structural tube section was concentrated at the outside at the crown connection because of the bending in the connection. The resulting plastic deformation of the ends of the tube is also shown in Figure 2.37(b).

2.3 DISCUSSION OF RESULTS

The effects of loading configuration, rib cross section, type of connection, etc., can be compared best in terms of maximum strength and overall behavior as regards ductility and mode of failure. Strength depends on geometrical properties of the cross section if all other variables are the same. Therefore, some scaling of the loads is necessary to compare the M, the square TS, and the circular TS. Since the cost per pound is the same for all three, and since costs of fabrication and erection will be

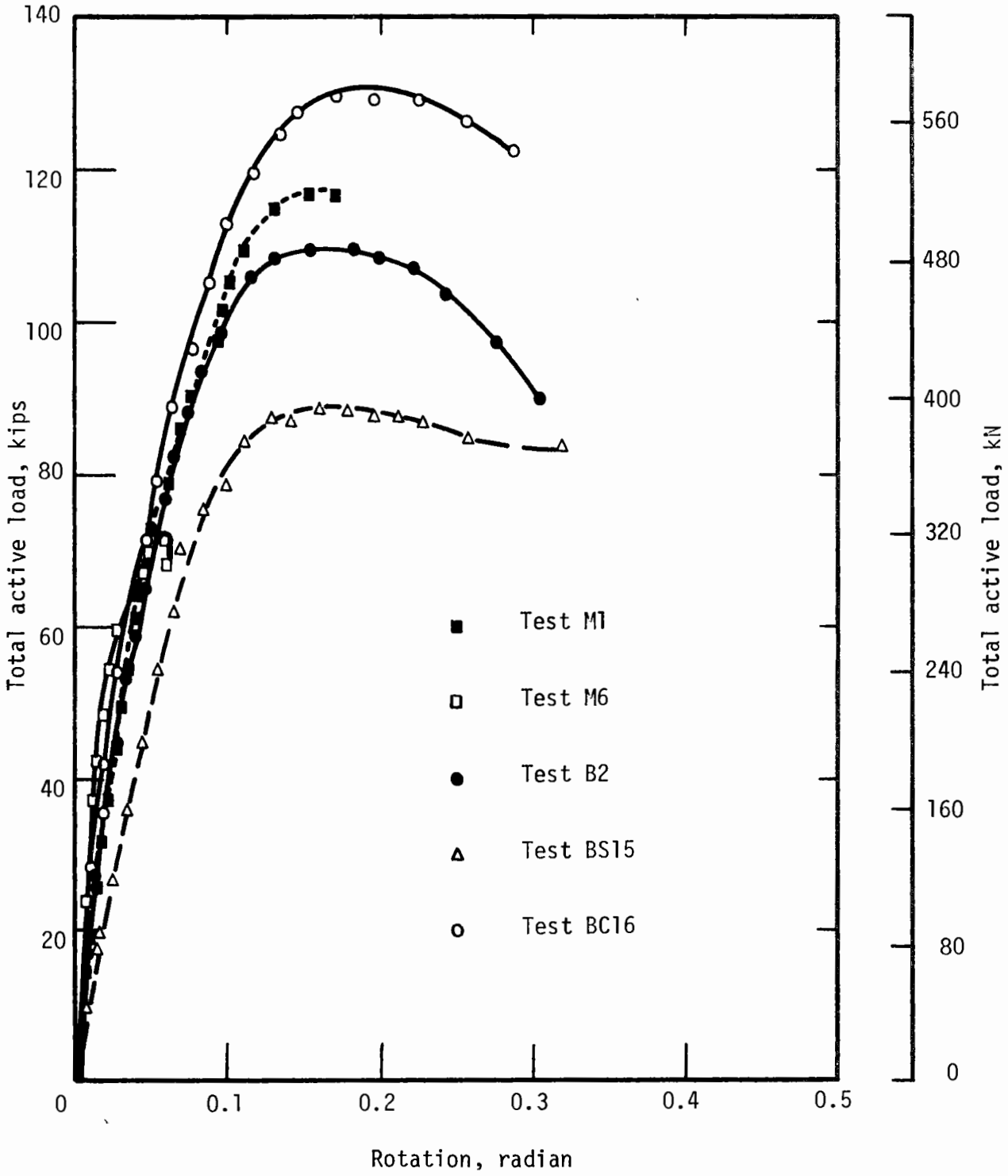

FIG. 2.38 TOTAL ACTIVE LOAD - CROWN ROTATION
IN TESTS M1, M6, B2, BS15, BC16

essentially the same, scaling in terms of cross-sectional area, which is equivalent to scaling in terms of weight, is appropriate. Also the circular TS ribs were scaled upward to account for their lower yield stress relative to the other specimens. From the yield stresses discussed in Section 2.1.1 this ratio is 1.20.

Comparisons of the total vertical load, which is the sum of the vertical components of all the ram loads, both active and passive, are of interest because the usual procedure for the design of ribs (described in Chapter 6) is based on the weight of a block of rock across the full width of the opening. However, as was noted in Chapter 1, rock usually loosens in only part of the opening, so that comparisons of active radial loads on portions of the rib are also of interest.

Table 2.1 gives a comparison of all the tests with respect to total active load, which is the sum of the loads in all active rams, the average load on each active ram, and the total vertical load. Comparisons of the effects of section shape, load geometry, and other variables are given in tables that follow, in terms of total active load and total active load scaled according to cross sectional area and for yield stress as well as for the circular TS ribs.

2.3.1 SECTION SHAPE

Table 2.2 shows a summary that allows comparisons of section shape on the basis of maximum capacity under various loading conditions. Maximum total active loads and their scaled values are listed.

The tests in Group I were on ribs with symmetrical loading.

TABLE 2.2

SECTION SHAPE

Group	Test	Load 2 omitted	Load geometry	Eccentric load	Max. total active load		Scaled total active load	
					kips	kN	kips	kN
I	M1	No	S	No	119.0	529.3	119.0	529.3
	M17	No	S	No	123.3	548.4	123.3	548.4
	B2	No	S	No	109.7	488.0	117.4	522.1
	P14	No	S	No	71.6	318.5	121.7	541.3
II	M10	No	S	Yes	56.4	250.7	56.4	250.7
	B13	No	S	Yes	106.5	473.7	114.0	507.1
III	M6	No	U	No	71.8	320.0	71.8	520.0
	B5	No	U	No	80.1	356.3	85.7	381.3
	P18	No	U	No	48.2	214.4	81.9	283.0
IV	M7	No	U	Yes	42.8	190.4	42.8	190.4
	B9	No	U	Yes	77.0	342.4	82.4	366.4

Tests M1 and B2 had scaled peak loads that were nearly equal, indicating that there is little difference in the M and square TS shapes in resisting in-plane loads. The M section is slightly stronger, which could be normal variation in test specimens, but it should be somewhat stronger because the M section is more efficient in resisting moment. Test M17 had a capacity about 3.6 percent higher than M1, which may be due to the difference in the supports at the bottom of the leg. The circular TS test, P14,

should be compared with test M17 as the supports were the same. The circular tube capacity was only 1.3 percent less than that of the M section after scaling.

The total active load-displacement curves for the Group I specimens are shown in Fig. 2.11. They all show essentially the same behavior. The initial stiffnesses are the same and the overall deformability is quite similar if the differences in capacity are taken into account. Failure modes were of a type that does not lead to sudden failure; general yielding of the section occurred at certain sections until a mechanism was formed and the load began to decline gradually. There was some local deformation of the M and square TS sections, but this was observed only after the peak load was reached.

The tests in Group II were on ribs loaded symmetrically about the crown of the rib with the active loads applied parallel to the plane of the rib but 2 in. (51 mm) from it. A comparison of test B13 with test B2 of Group I shows that eccentric load reduced the strength by only 3 percent. However, a comparison of M10 with M17 shows a reduction of 54 percent for the M section. These tests demonstrate the great advantage of the structural tube in resisting loads that tend to twist the section. The active test load for B13 was 89 percent more than for M10, but when the two are scaled for area the strength of B13 is more than double that of M10.

Tests in Group III were on ribs with unsymmetrical, in-plane loading. They show an advantage of the square TS over the M section of 19 percent (tests M6 and B5), which resulted from the M section's greater

tendency to twist even when the active loads were in the plane of the rib. The scaled strength of the circular TS section rib was 14 percent above that of the M section (tests M6 and P18); again due to the reduced capacity of the M section from twisting.

The Group IV tests with unsymmetrical loads eccentric to the plane of the rib show again the advantage of the structural tube, which has a scale strength 92 percent higher than that of the M section. A comparison of M7 with M6 and B9 with B5 shows a reduction in strength of 40 percent for the M section but only 4 percent for the box because of eccentric loading. The corresponding figures for symmetrical loading were 54 and 3 percent, respectively.

The advantage of the box section also appears in the overall behavior of the rib as shown by the total-load deflection curves. Figure 2.28 shows these curves for symmetrically loaded specimens M10 and B13 and unsymmetrically loaded specimens M7 and B9, all of which were loaded eccentrically. In both loading configurations the difference in behavior is significant. The square TS section rose gradually to a peak load at 3.8 to 4.3 in. (97 to 109 mm) of deflection and then dropped off gradually. On the other hand, the M-section ribs lost load immediately when the peak was reached, and at a deflection of only about 1 in. (25 mm). Under gravity load in a tunnel, the M section would almost certainly collapse because of the sudden loss of strength while the square TS sections might not because of their gradual loss of strength during which time the ground might be able to mobilize the small additional resistance required to maintain stability. For the square TS ribs the mode of failure was the same as for

in-plane loads, while for the M-section ribs it was primarily a twisting failure.

The M section is efficient in resisting bending moment but has very low torsional resistance, while the box section is efficient in both. However, some moment of inertia is sacrificed in the box because of the two webs. Even when the loads were aligned quite accurately with respect to the web of the M section the small accidental eccentricity caused considerable twist of the section as the peak load was approached. With intentional eccentricity of load twisting developed almost from the start of loading and was as high as 30 deg at peak load. Thus, the box section has a definite advantage when eccentric loads are encountered.

2.3.2 ECCENTRIC LOADING

Eccentricity of load reduces the strength of the box section only slightly, but failure is sudden and at relatively low deflection for the eccentrically loaded M-section rib. The eccentricity in these tests represents the worst condition that can occur; the active condition in the ground probably lies between the in-plane and eccentric loadings. However, some twisting of the rib probably occurs in most cases. It may result from application of load near the edge of the section, particularly if wedges are driven from only one side or if blocking extends only partially across the rib. Furthermore, ground movement will generally not be parallel to the plane of the rib, and the resulting component of load normal to the plane is somewhat limited because it can only be transmitted by friction between the ground and the blocking and between the blocking and the rib.

On the other hand, the tests show that the M section twists significantly under relatively small torque.

Twisting of a rib may be restrained under the conditions in which it is used in a tunnel. Restraint can result from the tie rods and collar bracing. There was some restraint from this source in the tests. Bearing of the blocking against the rib may also limit twist to some extent, even when the blocking applies load at an edge of the section. This is because the other edge of the flange may contact the blocking and restrain further rotation. This restraint is limited, however, because it was observed in the tests that the flanges twist differentially because of the low bending capacity of the thin web.

2.3.3 LOAD GEOMETRY

Strengths of ribs under various load geometries are compared in Table 2.3. The tests in Group I were loaded in-plane either symmetrically or unsymmetrically. For the M section ribs the total unsymmetrical active load was 40 percent less than that for symmetrical loading. The corresponding reduction was 27 percent for the square TS rib and 33 percent for the circular TS. Thus, it is clear that capacity is considerably larger under symmetrical load. This results from more arch action and correspondingly less bending.

Symmetrical and unsymmetrical eccentric loadings are compared in Group II of Table 2.3. The total unsymmetrical active load was 24 percent below that for symmetrical loading of the M section and 28 percent

TABLE 2.3

LOAD GEOMETRY

Group	Test	Load 2 omitted	Load geometry	Eccentric load	Max. total active load		Scaled total active load	
					kips	kN	kips	kN
I	M1	No	S	No	119.0	529.3	119.0	529.3
	M6	No	U	No	71.8	320.0	71.8	320.0
	B2	No	S	No	109.7	488.0	117.4	522.1
	B5	No	U	No	80.1	356.3	85.7	381.3
	P14	No	S	No	71.6	318.5	121.7	420.4
	P18	No	U	No	48.2	214.4	81.9	283.0
II	M10	No	S	Yes	56.4	250.7	56.4	250.7
	M7	No	U	Yes	42.8	190.4	42.8	190.4
	B13	No	S	Yes	106.5	473.7	114.0	507.1
	B9	No	U	Yes	77.0	324.4	82.4	366.4
III	M1	No	S	No	119.0	529.3	119.0	529.3
	M3	Yes	S	No	66.5	295.6	66.5	295.6
	B2	No	S	No	109.7	488.0	117.4	522.1
	B4	Yes	S	No	66.9	297.8	71.6	318.6
IV	M6	No	U	No	71.8	320.0	71.8	320.0
	M8	Yes	U	No	55.9	248.6	55.9	248.6
V	M3	Yes	S	No	66.5	295.6	66.5	295.6
	M8	Yes	U	No	55.9	248.6	55.9	248.6

below for the TS rib. The effect of this loading geometry on overall behavior is shown in Figure 2.28, where it is seen that the symmetrical and unsymmetrical active loadings yield the same shape of curve for the two

M-section ribs and the two square TS ribs. The effect of both symmetry and eccentricity of load is shown by comparing M7 and B9 with M1 and B2 of Group I. The strength of M7 is 64 percent less than the strength of M1 while that for B9 is only 30 percent less than for B2.

The test results in Group III indicate the effect on rib capacity of unequally spaced blocking, or possible loss of blocking, by comparing the tests with symmetrical in-plane load with and without the No. 2 passive force. A reduction in total active load of 44 percent results for the M-section and 39 percent for the TS rib. The importance of tight uniform blocking is emphasized by this comparison. Figure 2.39, where the overall behavior for these tests is compared, shows that the stiffness is somewhat reduced in the linear range by the elimination of the No. 2 blocking point, but the general shape of the load-deflection curve remains the same.

The test results of Group IV provide the same comparison as in Group III except that the active loads are applied unsymmetrically. Omitting the No. 2 passive force reduced the capacity of the M-section rib 22 percent, compared to 44 percent for the symmetrical loading noted above. The effect of symmetry of load with No. 2 blocking omitted is further shown by the tests in Group V, where the strength for unsymmetrical loading is 16 percent less than that for symmetrical loading.

2.3.4 CONCRETE FILLED SQUARE TS

Results of the tests of the concrete filled box section are compared with the unfilled box and the M in Table 2.4. Capacity of the

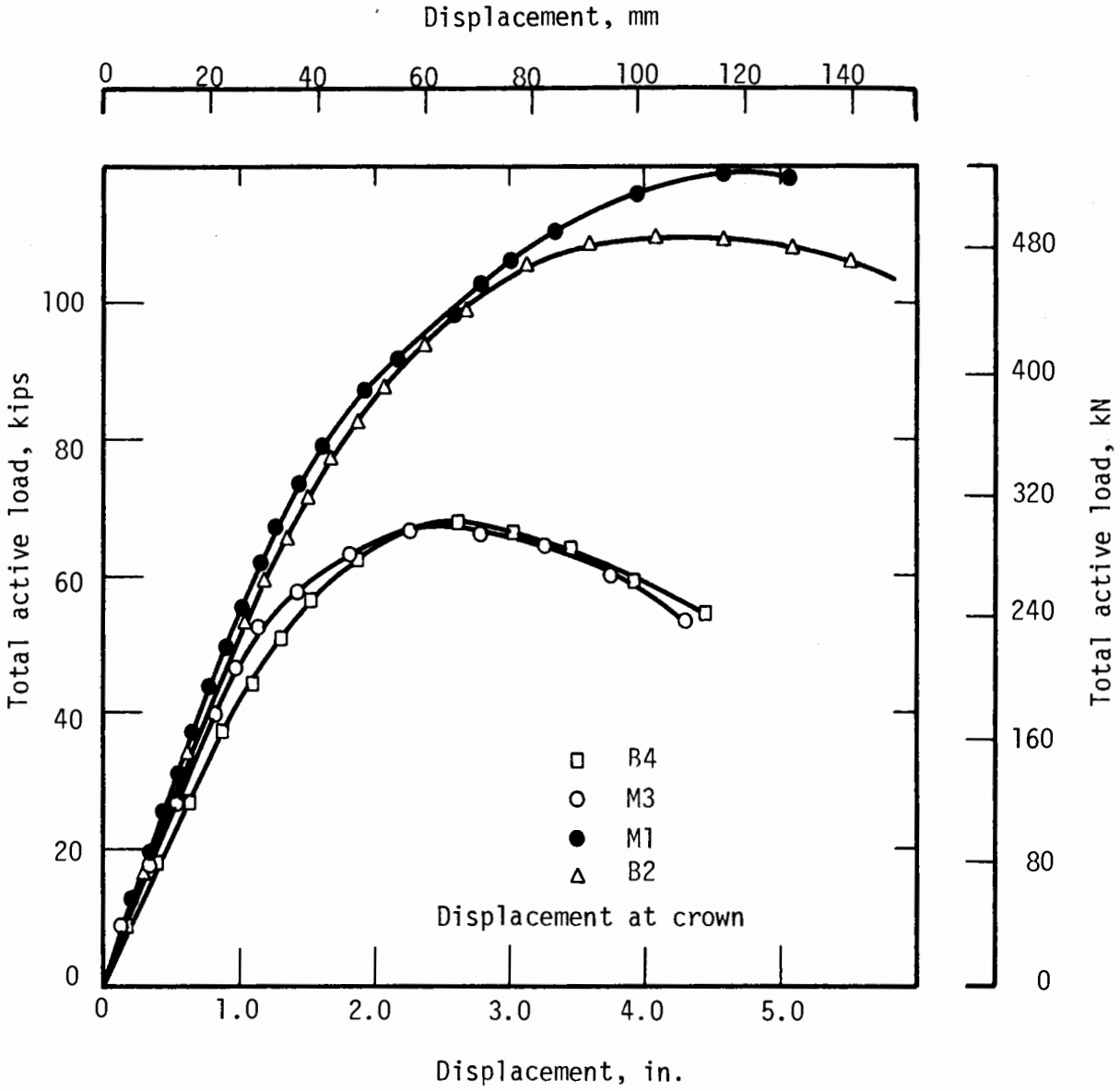

FIG. 2.39 TOTAL LOAD VS. DISPLACEMENT SYMMETRICAL LOADING WITH AND WITHOUT RAM NO. 2

TABLE 2.4

CONCRETE FILLED SQUARE TS

Group	Test	Load 2 removed	Load geometry	Eccentric load	Max. total active load		Scaled total active load	
					kips	kN	kips	kN
I	BC16	No	S	No	129.9	577.7	139.0	618.3
	B2	No	S	No	109.7	488.0	117.4	522.1
	M1	No	S	No	119.3	529.3	119.3	529.3
II	BC12	No	U	No	93.1	413.9	99.6	443.1
	B5	No	U	No	80.1	356.3	85.7	381.3
	M6	No	U	No	71.8	320.0	71.8	320.0

concrete filled rib is scaled according to area as for the unfilled ST rib, so that the difference between the two results from the concrete alone. With the symmetrical loading of Group I the concrete filled rib was 18 percent stronger than the unfilled rib and 17 percent stronger than the M-section rib. The load-displacement diagrams for the three tests shown in Fig. 2.11 indicate the same initial stiffness and shape of curve with essentially the same deflection at peak load.

The unsymmetrically loaded ribs in Group II of Table 2.4 show that the concrete-filled rib is 16 percent stronger than the unfilled rib and 39 percent stronger than the M-section rib. The larger difference for

the M section results from the reduced capacity because of twist. Load-displacement diagrams for the three tests of Group II are shown in Fig. 2.18. Rib B5 has a larger initial stiffness than the others, but ribs M6 and BC12 are essentially the same. Ribs B5 and BC12 have similar load-displacement curves except that BC12 has a larger displacement at peak load and drops off more slowly. The curve for test M6 descends prematurely because of the twisting tendency of the section.

Local deformation of the concrete filled section was much less than that of the other sections. The M section twisted and developed some local waving of the compression flange, while the unfilled TS section buckled inwardly on the inside (compression side) of the tube and outwardly at the sides where yield hinges formed. These buckles did not generally form until the peak load was reached, however. The concrete filled tube buckled slightly on the compression side of the tube at the plastic hinges but there was no noticable deformation of the sides. This deformation occurred well past the peak load.

The concrete in the TS section rib increased the capacity by 16 to 18 percent and reduced the local deformation of the tube. The rate at which load declined beyond the peak was reduced by the decrease in local buckling. However, these results are not conclusive since they are based on only two tests.

2.3.5 LOOSE CONNECTION BOLTS

Test M11 was performed on an M section rib with unsymmetrical loading and with the bolts in the east springline connection left loose

so that 1/8 in. (3.2 mm) of threads were exposed. The maximum loads for this test and the corresponding M section rib test with tight joints are given in Table 2.5. Loose bolts appear to have increased the capacity

TABLE 2.5

LOOSE CONNECTION BOLTS

Test	Load 2 removed	Load geometry	Eccentric load	Max. total active load		Scaled total active load	
				kips	kN	kips	kN
M11*	No	U	No	75.7	336.6	75.7	336.6
M6	No	U	No	71.8	320.0	71.8	320.0

*East side joint bolts loose.

of the rib over the corresponding M-section rib 5 percent. M6 failed prematurely, as discussed earlier, because of twist; this is demonstrated in Fig. 2.40 where the total-load displacement curves are compared. The loads on rib M11 were probably aligned in the plane of the rib more accurately so that twisting was avoided. Thus, it should not be concluded that loose bolts increases rib capacity, although the test does suggest that they may not reduce it significantly. However, no broad conclusion can be drawn from the results of one test.

The deformations in test M11 were similar to other tests that were loaded unsymmetrically, with the initial inward movement of the east

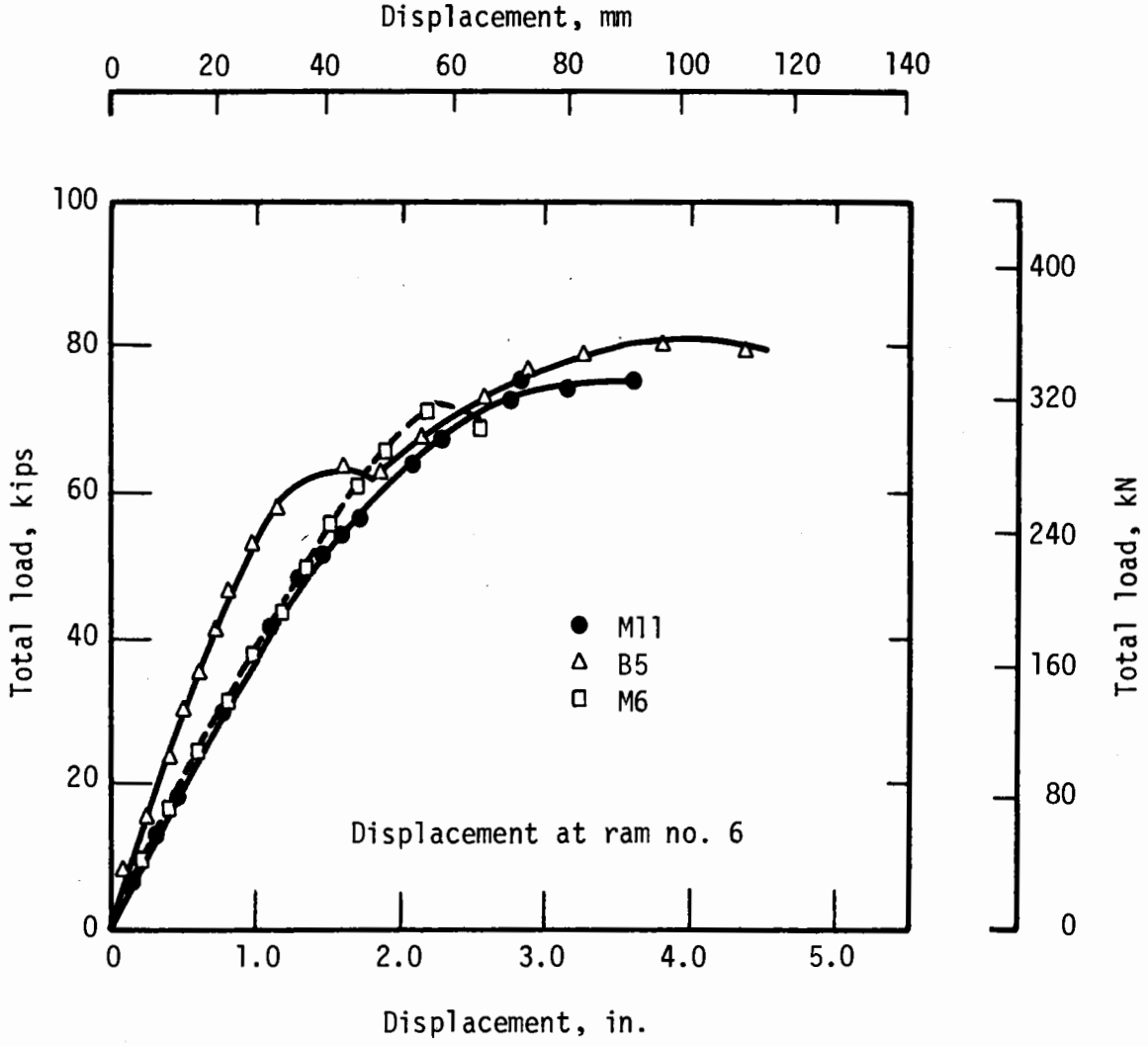

FIG. 2.40 TOTAL ACTIVE LOAD VS DISPLACEMENT FOR UNSYMMETRICAL LOADING WITH AND WITHOUT LOOSE JOINTS

side joint, yielding accompanied by reversal of direction of movement of this joint, and stiffening of the structure with contact of the east joint and ram 7. The initial stiffness of the rib was the same as that of test M6 and the first plateau in the load-displacement diagram, which is associated with first yielding, is not as distinct as in some of the other unsymmetrically loaded tests.

2.3.6 SLEEVE CONNECTION

Test BS15 was performed on a square TS rib with sleeve connectors of the type shown in Fig. 2.2 and discussed in Chapter 4. Rib capacity is compared in Table 2.6 with the other TS rib loaded similarly. The scaled

TABLE 2.6

SLEEVE CONNECTORS

Test	Load 2 removed	Load geometry	Eccentric load	Max. total active load		Scaled total active load	
				kips	kN	kips	kN
BS15	No	S		88.2	392.4	94.4	419.9
B2	No	S	No	109.7	488.0	117.4	522.1

capacity is less than that of the TS section rib with standard connections by 20 percent. The sleeve connector at the crown deformed as shown in Fig. 2.37(c) and allowed about twice the rotation of the crown joint as the

standard connection, as shown in Fig. 2.38, but it did not fail. At the end of the test a small crack at one corner of the sleeve was detected, but it was hair size and about 0.5 in. (13 mm) long. This sleeve was only 1/8 in. (3.18 mm) thick, compared with 1/4 in. (6.35 mm) for the walls of the TS section. A thicker sleeve might have reduced these deformations and increased the strength of the rib.

Load-displacement response of the two ribs of Table 2.6 is compared in Fig. 2.41. The initial stiffness of BS15 is about 25 percent less than for B2 because of the reduced stiffness of the connections. Ductility of the rib is maintained, however, and there appears to be a tendency to hold the load constant to a somewhat larger displacement. This tendency to maintain ductility also appears in the load-rotation curves of Fig. 2.38. Yield hinges formed near the 45 deg regions and at the crown joint in test B2 (Fig. 2.13(b)), but the latter hinge formed just to the west of the crown in test BS15 (Fig. 2.37(a)). This shows the crown sleeve joint was stronger than the standard connection at this stage of loading.

Rib strength depends to a considerable extent on the bending moments, which depend in turn on the deflection of the rib. Therefore, the lower capacity of the rib with sleeves probably results from the larger displacements rather than the moment capacity of the sleeve itself. Whether sleeve connectors with adequate bending strength and stiffness can be developed for ribs of this size and larger can only be determine by further tests. Advantages and disadvantages of sleeve connectors is discussed further in Chapter 4.

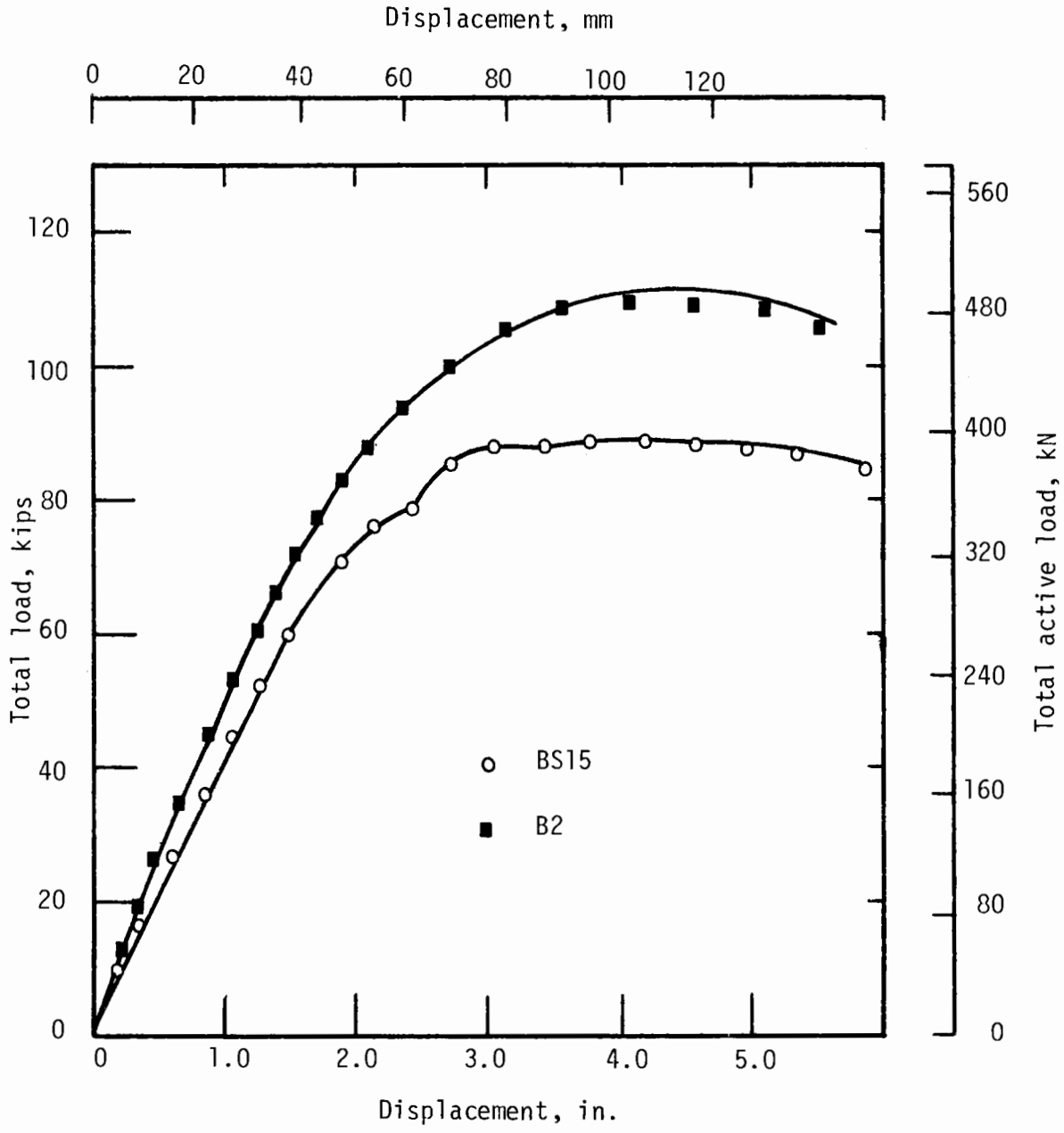

FIG. 2.41 TOTAL LOAD VS. DISPLACEMENT FOR SYMMETRICALLY LOADED SECTIONS

CHAPTER 3

TELESCOPING RIBS

3.1 INTRODUCTION

A telescoping steel pole for electric power transmission lines has been marketed. It consists of nested tapered sections, with erection accomplished by pumping concrete into the inner section after the assembly is erected. This operation pushes the various segments upward, one at a time, beginning with the smallest, until the pole is fully extended (Fig. 3.1).

Tunnel ribs are shipped in sections, brought into the tunnel on cars, and erected in the location they are to occupy. Horseshoe-shaped sets are made of two legs and two or more arch segments. Circular sets for transportation tunnels may be shipped in four or six segments, each of which must be lifted from the car, swung 90 deg, put in position, and bolted to the preceding piece. This is a time-consuming operation. Therefore, anything that can be done to simplify the procedure has a potential for saving in cost of tunnels. This might be accomplished by using round or box shaped telescoping sets that could be expanded by pumped grout or concrete or by pulling the segments around the opening from the invert with an erector arm.

Three things contributed to the success of telescoping transmission poles (1) the pole is straight, (2) the elements are tapered so that the movement of each is self-limiting since it is stopped when it reaches

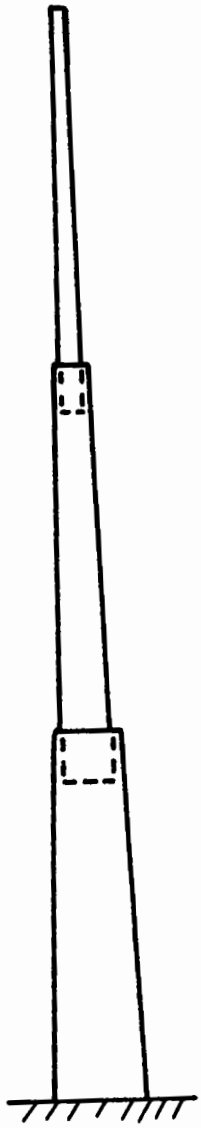

FIGURE 3.1 TELESCOPING STEEL POLE FOR ELECTRICAL TRANSMISSION LINES

a predetermined position, and (3) the required cross section in terms of bending strength decreases with height so that the tapered section tends to produce an optimum structure. Although tapered arch elements can be made they would be more expensive to fabricate. Therefore, in this study nesting elements of uniform cross section are also considered.

3.2 TELESCOPING SETS WITH UNIFORM CROSS SECTION

The simplest application of telescoping ribs would be the horseshoe, with three arch segments (Fig. 3.2). The segments could be square

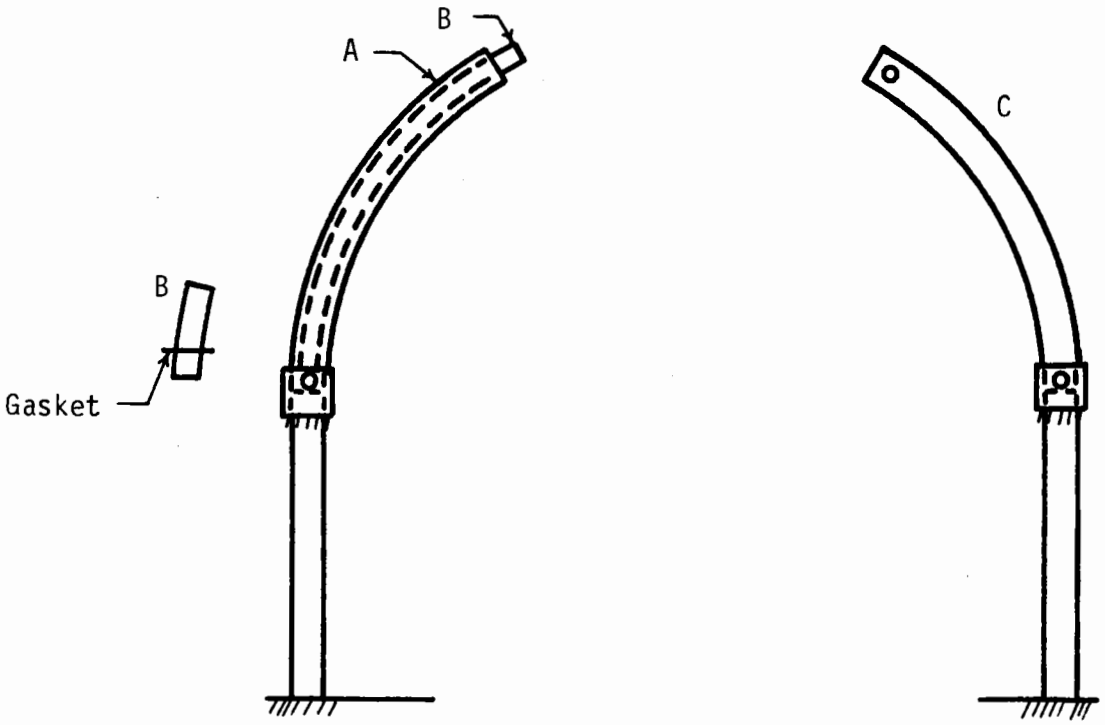

FIGURE 3.2 TELESCOPING HORSESHOE RIB WITH THREE ARCH SEGMENTS

or round. Two arch segments could be nested as shown in the figure. The nested pair would be inserted and pinned (or bolted) in a sleeve, shop-welded to the leg. The third arch segment could be connected in the same way to the other leg. Although the load to be transferred at these connections is primarily axial compression, the pins are needed to hold the segments in place when concrete is pumped into them or when segment B is pulled into position if concrete is not used.

If pumped concrete is used to expand the set the upper end of segment B would be capped so that pressure of the concrete pumped into the leg would force it out of segment A. It would have to be guided into segment C where a pin tack welded in the shop to this element would stop segment B in the correct position. A pin would also be required for load transfer between A and B when B is extended so that blocking could proceed without waiting for the concrete to set. Because of clearances required between the nesting elements a gasket would have to be attached near the lower end of segment B to prevent leaking of mortar into segment A. The gasket would be located so that it would allow concrete to enter the space between the two segments for a short distance to achieve a tight connection at the upper end of segment A.

A horseshoe rib with four arch elements is shown in Fig. 3.3. Here a sleeve could be shop-welded to the upper end of segment B and segment D would be guided into it during the pumping operation. The obvious difficulty here is controlling the sequence of operations so that segment B is not pushed out of segment A. It may be possible to develop a spring-loaded pin to be installed inside element B which would engage holes in

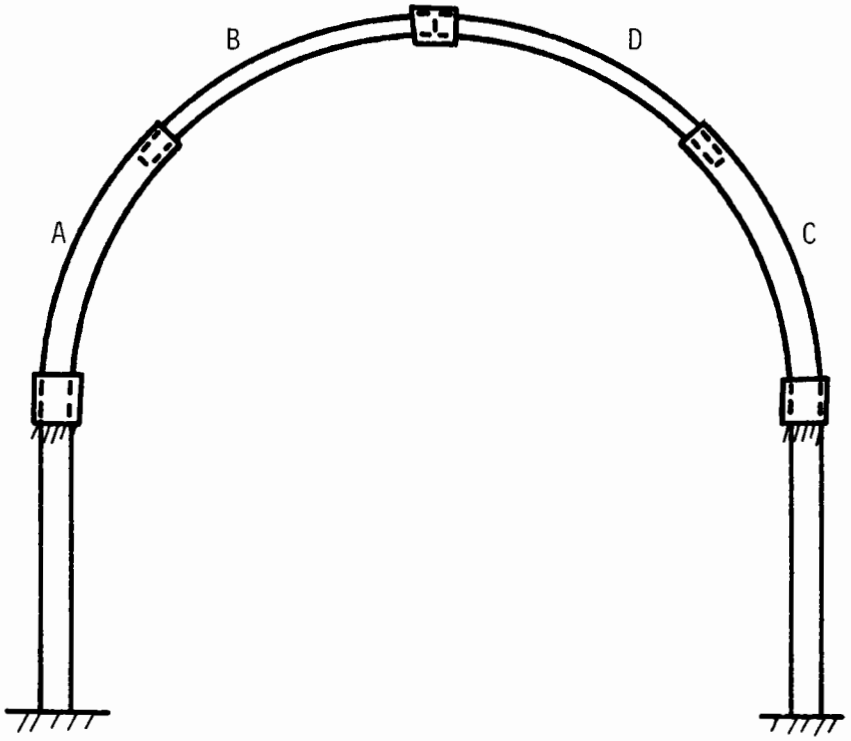

FIGURE 3.3 TELESCOPING HORSESHOE RIB WITH FOUR ARCH SEGMENTS

element A when B reaches its correct position. Axial compression at the crown would be transmitted by direct bearing while any moment that could not be transmitted by contact would be resisted by bearing against the sleeve.

A telescoping arrangement for circular ribs is shown in Fig. 3.4a. Two nested segments A-B and C-D would be brought in the tunnel and connected as shown by means of a sleeve shop-welded to element C, using a pin to connect element A. A and C would be open at both ends but B and D would be capped at the upper ends. A sleeve would be shop-welded to element B.

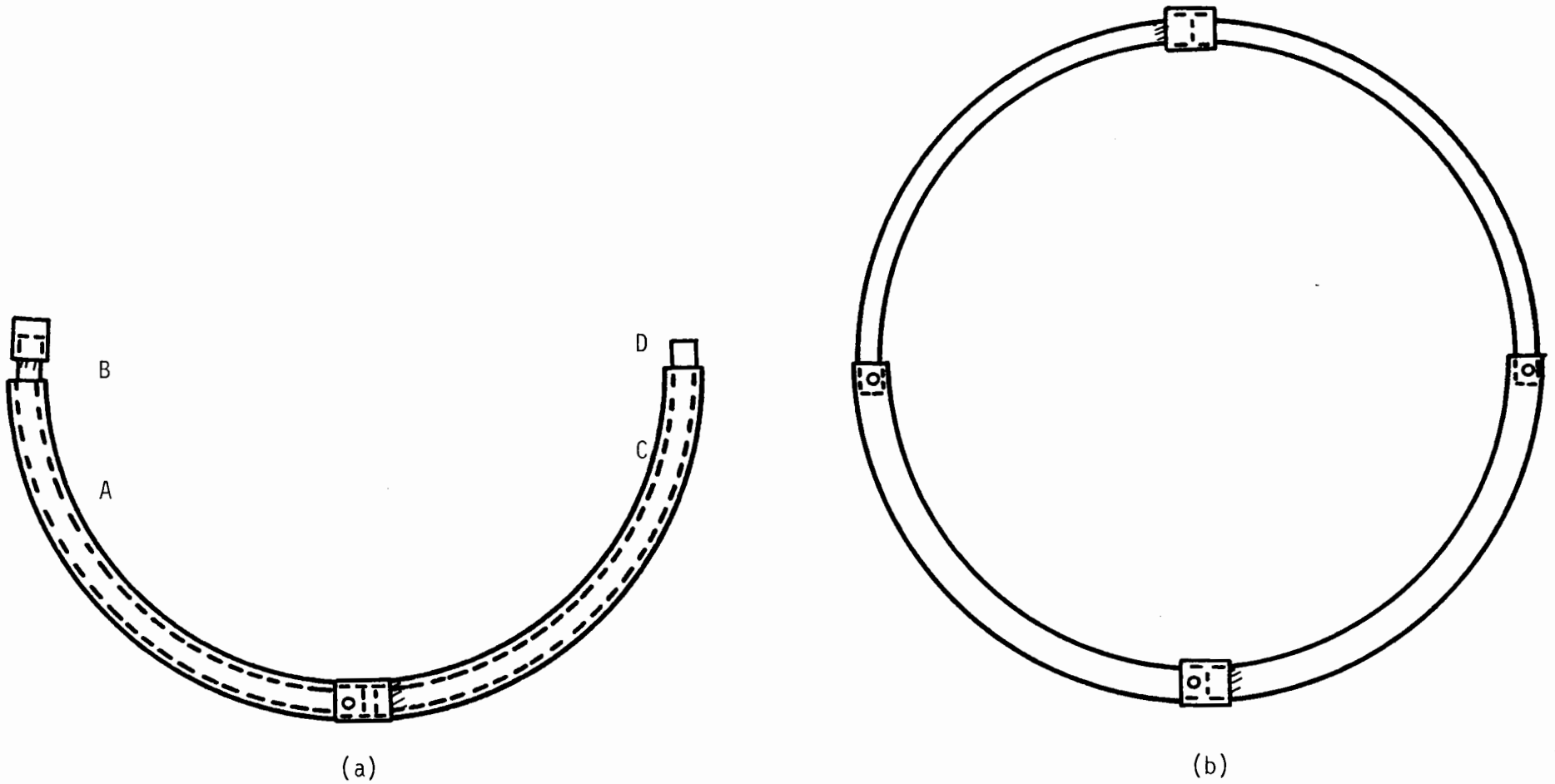

FIGURE 3.4 TELESCOPING CIRCULAR RIB WITH FOUR SEGMENTS

Pumping concrete into the assembly through an opening in the bottom sleeve would force B and D out into position. The completed ring would be as shown in Fig. 3.4b. Gaskets would be required near the lower ends of elements B and D as for element B in Fig. 3.2. The sequence of operations would have to be controlled to prevent B or D from being forced completely out. It would probably be necessary to pump concrete into one side first, say A-B, and then pin B to A after B is extended to the correct position. This would be a difficult operation unless the internal spring-loaded pin mentioned above could be installed. If this were done both A-B and C-D could be pumped simultaneously. Of course, the alternative to using a concrete fill would be to pull B and D into position as mentioned earlier. In either case, the pins connecting B to A and D to C are needed.

A possible scheme for tunnels large enough to require ribs to be shipped in six segments is shown in Fig. 3.5. The sequence of operations here would be even more difficult to control, unless spring-loaded pins or some other scheme could be devised to stop the movements of the various elements when they reach their intended positions.

3.3 CROSS SECTIONAL SHAPE

Although a variety of standard pipe and box sections is available, clearances for nesting limit the choices to a considerable extent. Examples of possible combinations of box sections (square structural tubes) are as follows: A standard 5 x 5 section will nest in a 6 x 6 x 3/16ths with 5/16ths in. (7.94 mm) clearance all around, in a 6 x 6 x 1/4 in. (6.35 mm) clearance all around, etc. A 6 x 6 will nest in a 7 x 7 and a 7 x 7 in an

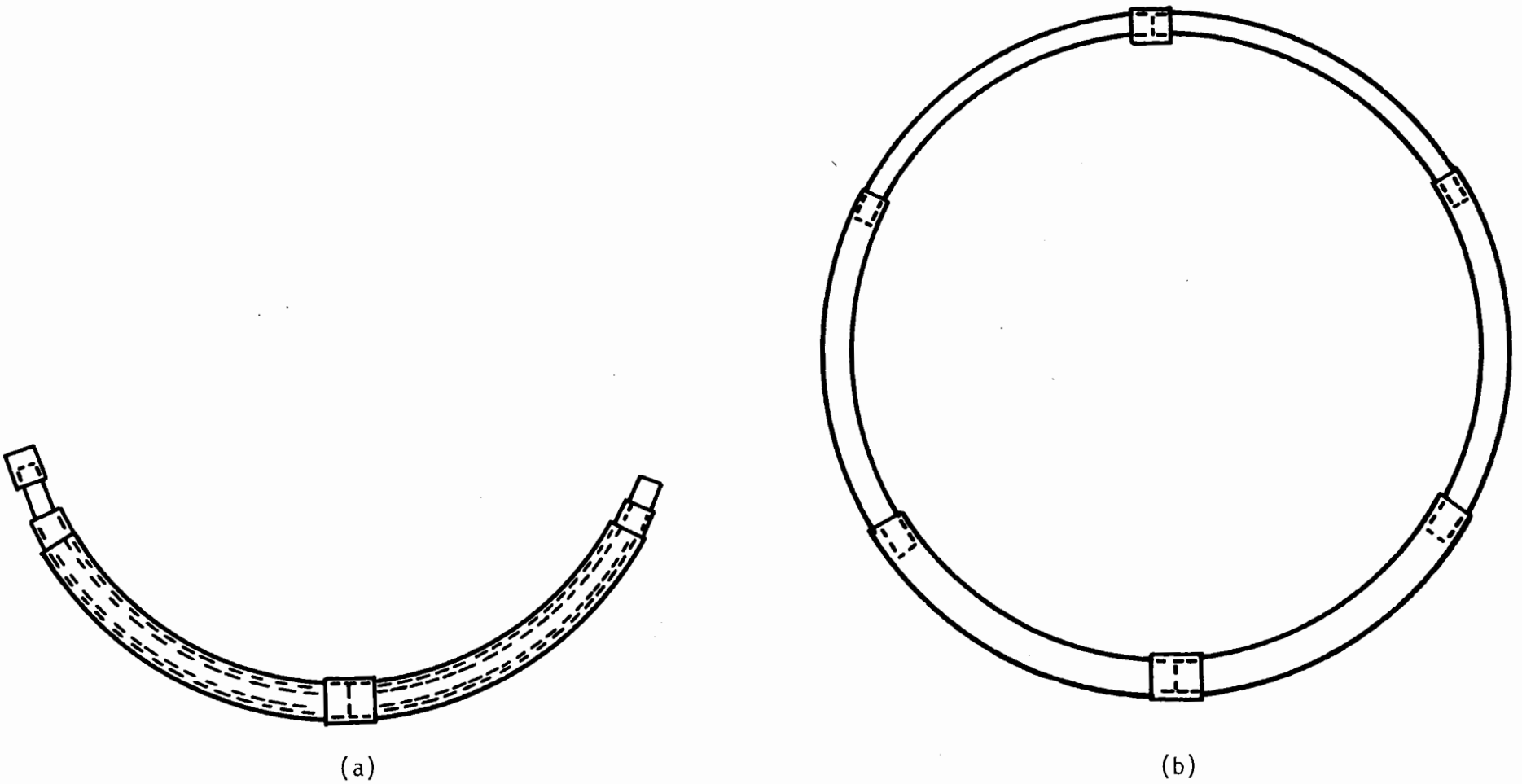

(a) (b)

FIGURE 3.5 TELESCOPING CIRCULAR RIB WITH SIX SEGMENTS

8 x 8 with the same clearances. Special sizes cold formed in press brakes are also commercially available.

3.4 TOLERANCES

Round tubing two inches and over and square or rectangular tubing with the largest outside dimension over 5-1/2 in. (140 mm) are produced to a tolerance of ±1 percent from the standard outside dimension. An additional departure from the specified dimensions is permitted in square and rectangular tubing in that adjacent sides may deviate from 90 deg by ±2 degrees. There is also a straightness tolerance of 1/8 in. (3.18 mm) per 5 ft (1.5 m) of length. The most unfavorable combination of these tolerances would require a fairly liberal clearance to allow nesting.

Distortions of the cross section from the forming operation to produce curved segments must be accomodated. These deformations can be considerable, and depend on the procedure used in bending. The 4 x 4 x 1/4 box sections used in some of the earlier tests were filled with sand before bending. This resulted in a bulging of the side walls (the walls parallel to the plane of curvature). Measurements at 1 ft (0.3 m) intervals along the circumference of four 90-deg arches showed widths as much as 0.34 in. (8.64 mm) more than the 4-in. (102-mm) nominal width (Table 3.1). Box sections used in later tests were bent by a different fabricator, this time without a sand fill. This operation resulted in a bowing-in of the sides. Measurements at 1-ft (0.3 m) intervals on two 180-deg arch sections assembled for testing are given in Table 3.2. These are more representative of what would be expected in large-scale production of bent box sections (i.e.,

TABLE 3.1

MAXIMUM WIDTHS OF SECTION OF 90-DEGREE ARCHES*

Distance from end, ft (m)	Section width, in. (mm)			
	Arch 1 in. (mm)	Arch 2 in. (mm)	Arch 3 in. (mm)	Arch 4 in. (mm)
1 (0.3)	4.34 (110.2)	4.31 (109.5)	4.31 (109.5)	4.31 (109.5)
2 (0.6)	4.33 (110.0)	4.28 (108.7)	4.34 (110.2)	4.33 (110.0)
3 (0.9)	4.34 (110.2)	4.28 (108.7)	4.25 (108.0)	4.31 (109.5)
4 (1.2)	4.31 (109.5)	4.31 (109.5)	4.28 (108.7)	4.30 (109.2)
5 (1.5)	4.31 (109.5)	4.28 (108.7)	4.27 (108.4)	4.33 (110.0)
6 (1.8)	4.25 (108.0)	4.28 (108.7)	4.25 (108.0)	4.31 (109.5)
7 (2.1)	4.22 (107.2)	4.31 (109.5)	4.26 (108.2)	4.30 (109.2)
8 (2.4)	4.22 (107.2)	4.22 (107.2)	4.19 (106.4)	4.31 (109.5)
9 (2.7)	4.13 (104.9)	4.17 (105.9)	4.16 (105.7)	4.13 (104.9)

*Sand-filled for bending

TABLE 3.2

DISTORTION OF SHAPE OF 180-DEGREE ARCHES*

Distance from end ft (m)	Arch No. 1			Arch No. 2		
	Top width in. (mm)	Bottom width in. (mm)	Out-of-square in. (mm)	Top width in. (mm)	Bottom width in. (mm)	Out-of-square in. (mm)
1 (0.3)	3.95 (100.3)	3.90 (99.1)	0	3.96 (100.6)	4.00 (101.6)	0
2 (0.6)	3.94 (100.1)	3.94 (100.1)	0.08 (2.0)	3.94 (100.1)	3.98 (101.1)	0.08 (2.0)
3 (0.9)	3.98 (101.1)	3.95 (100.3)	0.05 (1.3)	3.94 (100.1)	3.96 (100.6)	0
4 (1.2)	3.97 (100.8)	3.94 (100.1)	0	3.95 (100.3)	3.98 (101.1)	0.10 (2.5)
5 (1.5)	3.97 (100.8)	3.94 (100.1)	0	4.01 (101.8)	4.02 (102.1)	0.03 (0.8)
6 (1.8)	3.98 (101.1)	3.95 (100.3)	0	4.10 (104.1)	4.02 (102.1)	0.07 (1.8)
7 (2.1)	3.98 (101.1)	3.94 (100.1)	0.05 (1.3)	3.99 (101.3)	3.98 (101.1)	0.08 (2.0)
8 (2.4)	3.97 (100.8)	3.95 (100.3)	0	3.95 (100.3)	3.98 (101.1)	0.10 (2.5)
9 (2.7)	3.98 (101.1)	3.95 (100.3)	0	3.94 (100.1)	3.98 (101.1)	0.07 (1.8)
10 (3.0)	3.97 (100.8)	3.94 (100.1)	0	3.93 (99.8)	3.95 (100.3)	0.07 (1.8)
11 (3.3)	3.98 (101.1)	3.96 (100.6)	0.04 (1.0)	3.96 (100.6)	3.97 (100.8)	0.09 (2.3)
12 (3.6)	3.98 (101.1)	3.90 (99.1)	0	3.94 (100.1)	3.98 (101.1)	0.06 (1.5)
13 (4.0)	3.98 (101.1)	3.96 (100.6)	0	3.96 (100.6)	3.98 (101.1)	0.10 (2.5)
14 (4.3)	3.97 (100.8)	3.95 (100.3)	0	3.94 (100.1)	3.97 (100.8)	0.10 (2.5)
15 (4.6)	3.98 (101.1)	3.96 (100.6)	0	3.94 (100.1)	3.97 (100.8)	0.07 (1.8)
16 (4.9)	3.98 (101.1)	3.97 (100.8)	0.05 (1.3)	3.95 (100.3)	3.98 (101.1)	0.10 (2.5)
17 (5.2)	3.99 (101.3)	3.96 (100.6)	0	3.95 (100.3)	3.96 (100.6)	0.02 (0.5)
18 (5.5)	3.98 (101.1)	3.96 (100.6)	0.03 (0.8)	3.94 (100.1)	3.96 (100.6)	0.10 (2.5)
19 (5.8)	3.97 (100.8)	3.93 (99.8)	0.04 (1.0)	3.96 (100.6)	3.98 (101.1)	0.10 (2.5)
20 (6.1)	3.98 (101.1)	3.95 (100.3)	0	3.93 (99.8)	3.94 (100.1)	0.06 (1.5)

*Cold-bent without sand fill

bending without a sand fill). Although departures from nominal width are smaller than for the sand-filled sections, they range from 3.90 to 4.10 in. (99.1 to 104.1 mm). Furthermore, the cross section was out-of-square at various points by the amounts shown in Table 3.2. These measurements are distances by which one face (perpendicular to the plane of curvature) was displaced sideways relative to the opposite face.

3.5 RADIUS

Measurements on four of the 90-deg 4 x 4 x 1/4 arch sections of Table 3.1 showed a difference of 1/4 in. (6.35 mm) in the perpendicular distance from the chord to the outside walls at mid-length (Fig. 3.6). This difference would require a clearance of 1/4 in. (6.35 mm) all around in a 5 x 5 box for a 4 x 4 to slide through freely. The same clearance

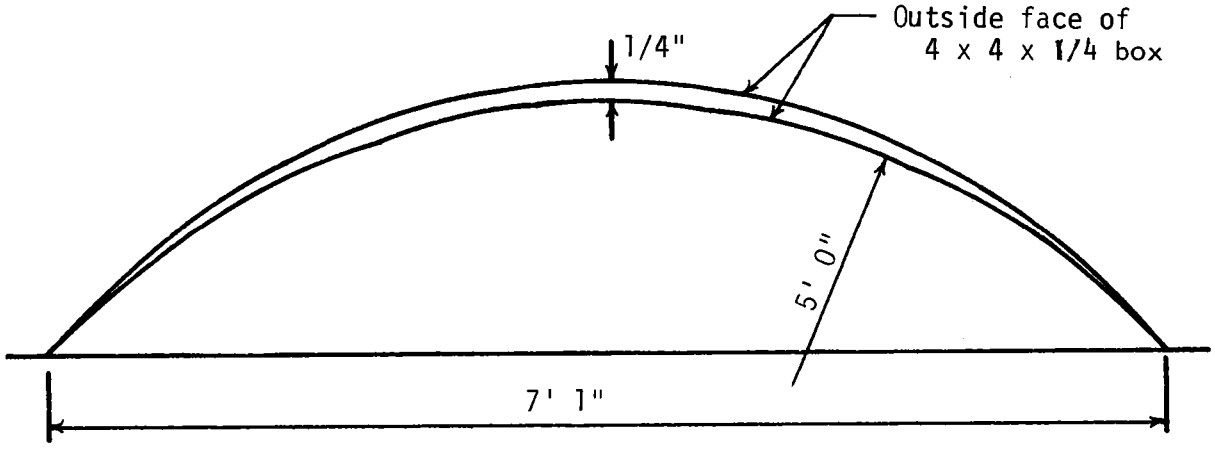

FIGURE 3.6 BENDING TOLERANCE FOR 90 DEG ARCH SEGMENTS

would be required for other sizes differing by 1 in. (25.4 mm) in nominal outside dimension. The effect of these differences in radius should be smaller for segments with subtended angles less than 90-deg.

3.6 JOINTS

The clearance required to accommodate the tolerances in shape and radius discussed above may cause problems of load transfer at the joints since there will be no metal-to-metal bearing between the telescoping segments. Their performance can be evaluated only by tests.

3.7 TAPERED SECTIONS

Some of the problems involved in nesting sections of uniform cross section inside one another might be eliminated by using tapered sections. A tapered horseshoe rib is shown in Fig. 3.7. The legs are not tapered, but the arch segments are tapered so as to maintain a uniform depth in the plane of the rib. The taper would be designed to stop the movement of segments B and D when they reach the correct extended position. However, this direction of taper is also the direction in which the greatest distortion of shape from rolling to radius occurs, so that it is very unlikely that it would be possible to fabricate the segments to the tolerances required to have segments B and D stopped when they reached their intended positions. Furthermore, a pin would be needed for load transfer at the junctures of A-B and C-D if the segments are expanded by an erector arm and for temporary load transfer if they are expanded by pumped concrete. Therefore, it appears that tapered sections would not be practical.

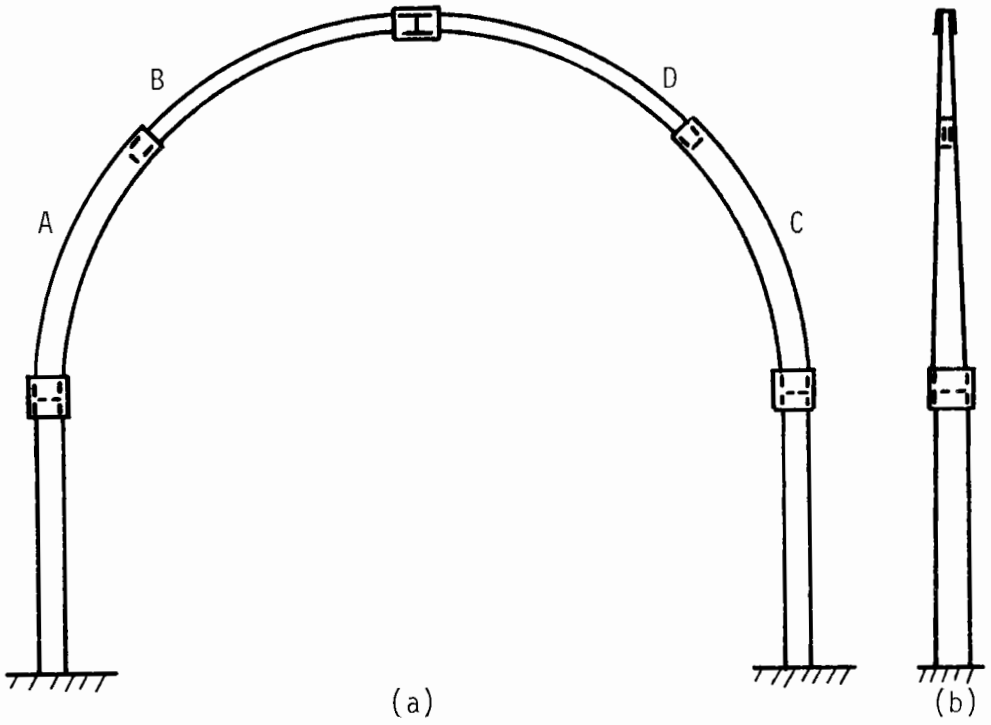

FIGURE 3.7 TAPERED TELESCOPING RIB

3.8 CONCLUSIONS

Several possibilities for developing telescoping steel ribs have been discussed in this chapter. It would appear that the only advantage such an arrangement might have over conventional ribs would be a decrease in time required for erection. Among the problems that would be associated with telescoping ribs are:

1. Effect of mill and fabricating tolerances on the fit of nesting segments.

2. Quality control in manufacturing tubes to guard against jamming while forcing the segments into position.
3. Possibility of local damage during handling that would tend to lock nested segments together.
4. Load transfer at joints.
5. Controlling the operation of expanding the nested segments.
6. Equipment, material and labor costs of pumping concrete if concrete fill is used.
7. Delays because of possible occasional jamming or other problems while the ribs are being expanded.
8. Unless the decrease in area and section modulus of the segments with the smaller outside dimensions is partly offset by increased thickness the resulting structure may not be optimally proportioned for the loadings encountered in tunnels.

CHAPTER 4

INNOVATIVE CONNECTIONS

4.1 INTRODUCTION

The results of six connection tests are discussed in this chapter. Four of the connections are standard, two-bolt, butt-plate connections, and two are sleeve connections. Moment-rotation curves are given for each of the tests and the overall behavior described. The butt plate connections are tested on M4x13 sections and the sleeve connections on TS 4 x 4 x 1/4 sections.

4.2 TESTS OF STANDARD CONNECTIONS

The two-bolt standard connection is shown in Fig. 4.1. The butt plates are 3/8-in. (9.53 mm) thick and the bolts are A307 "fit-up" type. The butt plates are not positioned symmetrically on the M4x13 section. This may or may not be the case in an actual tunnel, depending on the designer. However, this does have the advantage of providing a slightly greater clearance on the outside of the rib because the edge of the plate is flush with the outside edge of the section.

Figures 4.2 and 4.3 show the instrumentation used in the first two tests. Dial gages measured in-plane and out-of-plane displacements. Rotation over a 9-in. (229-mm) section was measured with a pair of LVDT's. A pair of deflection-measuring gages (Fig. 4.4) were fabricated to measure the opening of the butt plates on the tension side and the closing on the

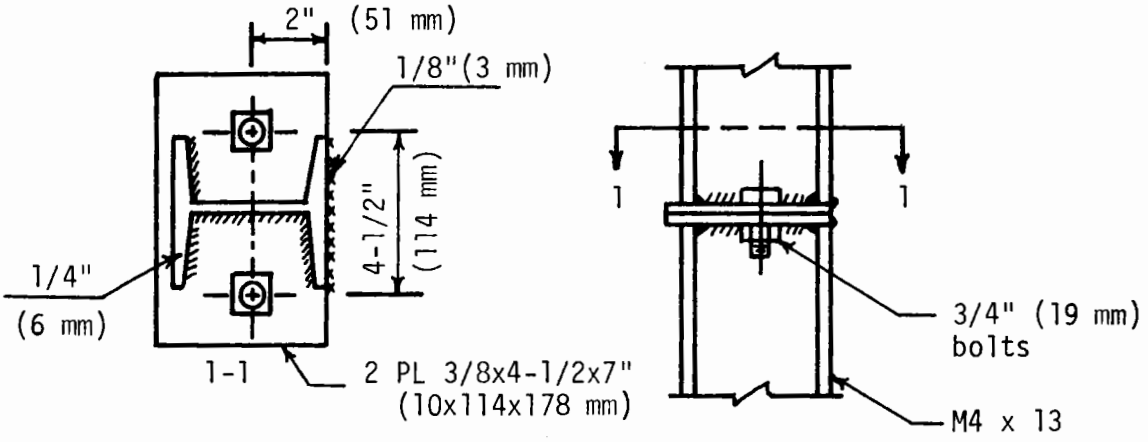

FIGURE 4.1 TWO-BOLT BUTT PLATE CONNECTION

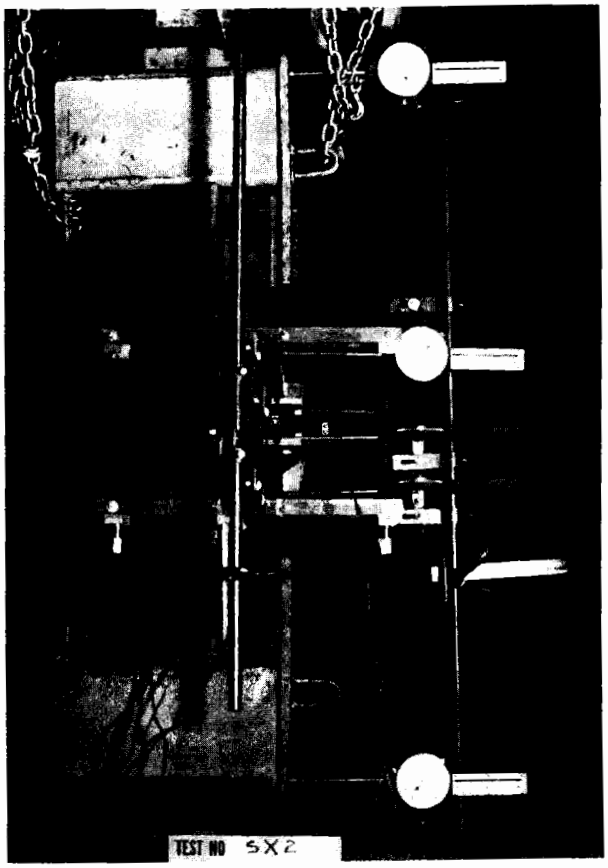

FIGURE 4.2 IN-PLANE DEFLECTION MEASURING ARRANGEMENT

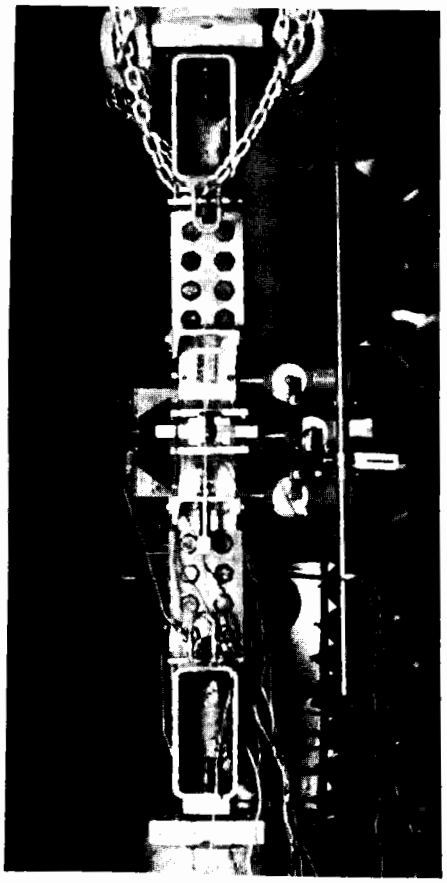

FIGURE 4.3 OUT-OF-PLANE DEFLECTION MEASURING ARRANGEMENT

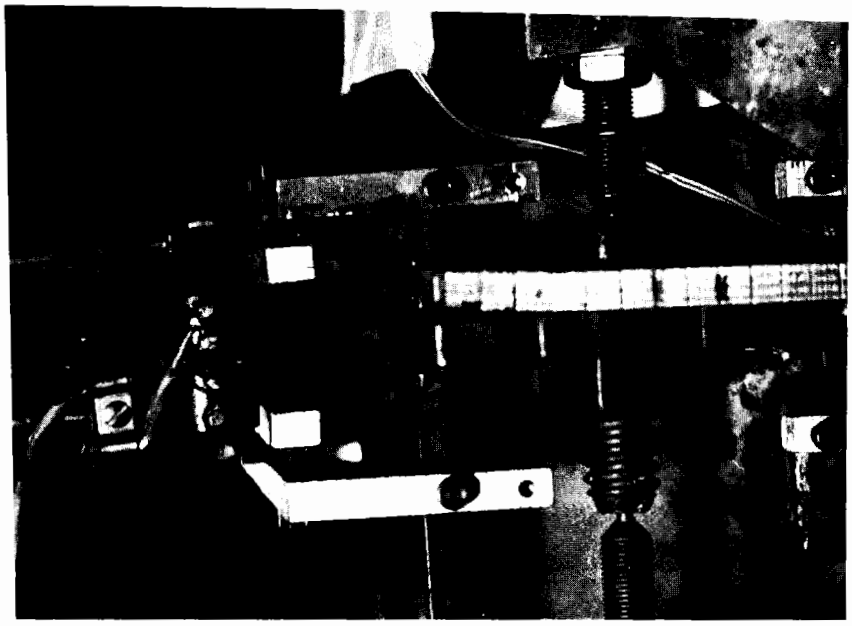

FIGURE 4.4 DEVICES FOR MEASURING JOINT OPENING AND BOLT STRAIN

compression side over a length of 2-1/2 in. (63.5 mm) at the connection. From these readings the rotation at the connection could be calculated. An extensometer was used to measure the change in strain of one of the connection bolts (Fig. 4.4). In subsequent tests the instrumentation was reduced to dial gages measuring displacements in the plane of bending and deflection gages measuring the opening and closing of the butt plates. The reduced instrumentation provided all the necessary data for studying the connection behavior.

Beam-column tests with initial eccentricities of 2, 4, and 6 in. (51, 102 and 152 mm) were performed for the case in which the butt plates protruded on the compression side. From strain gage measurements taken during the large-scale rib tests (Paul, et al., 1974) it was found that 6 in. (152 mm) was usually an upper limit for eccentricities in the rib, except at points of load application. Here, eccentricities were higher because of a steep moment gradient due to concentrated loads, but measurements could not be made.

Moment-rotation curves for these connections are shown in Fig. 4.5. The moment capacity decreases as the eccentricity of the applied load increases. This behavior is analogous to that of a reinforced concrete member that fails in tension. The highest moment capacity of the three connections was about 100 kip-in. (11.3 kN•m) for the connection with 2-in. (51-mm) initial eccentricity. The highest moment capacity of the M4X13 section is about 218 kip-in. (24.6 kN•m) for a yield stress of 36 ksi (248 MPa), assuming elasto-plastic stress-strain behavior. Thus, at most this connection has a moment capacity about half that of the M4X13.

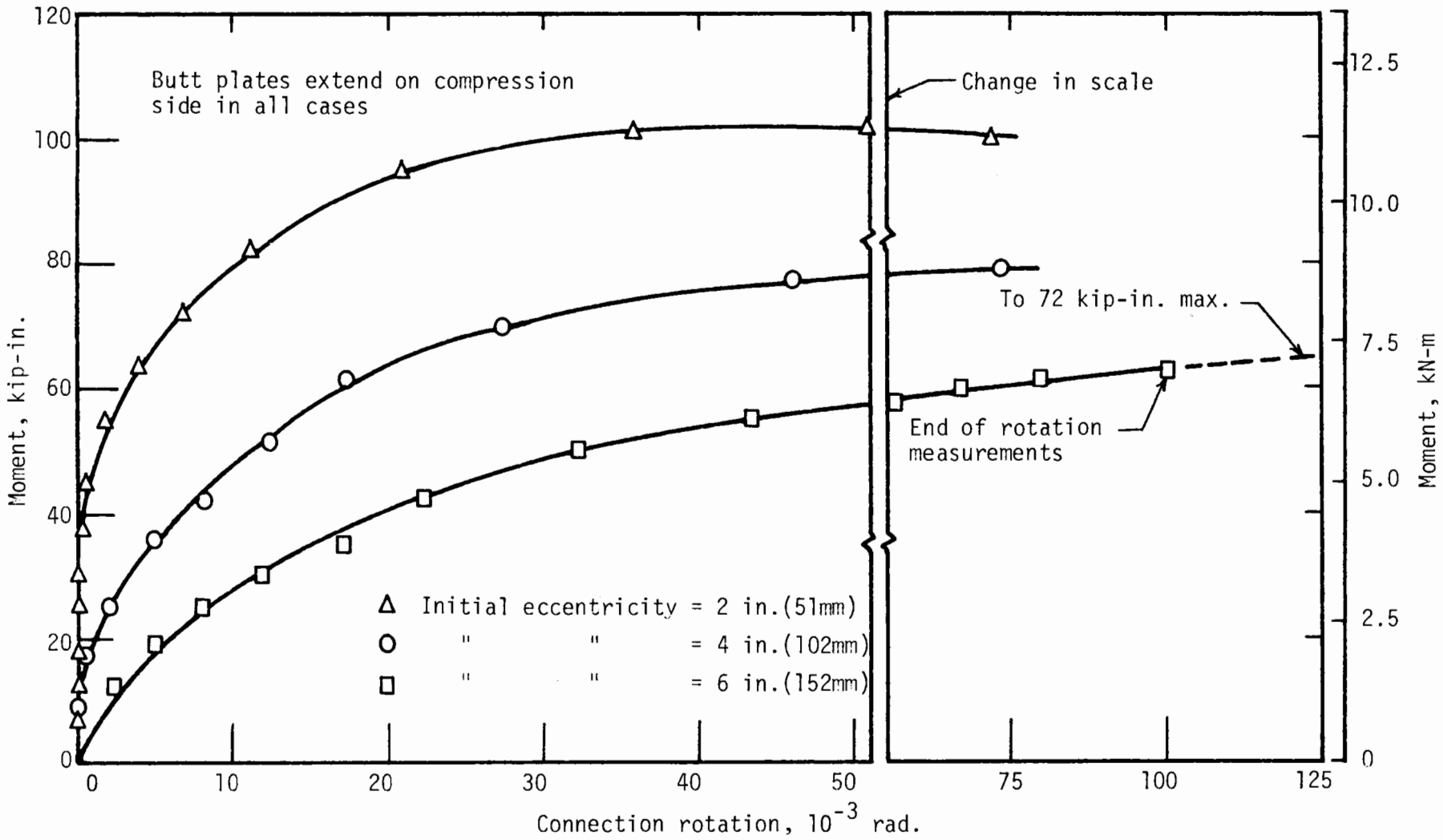

FIG. 4.5 MOMENT-ROTATION FOR BUTT-PLATE CONNECTIONS AND ECCENTRICITIES OF 2, 4 AND 6 IN. (51, 102 AND 152 MM)

But for higher eccentricities, more likely to occur at the connection, its capacity may be as little as one-third that of the M4X13.

The behavior of this connection is primarily affected by the opening of the butt plates on the tension side of the connection. If the butt plates were fastened together here, the connection would behave more as a continuous section, which could carry tension and compression in equal magnitude. The moment capacity of the connection is a result of a compressive force in the portion of the butt plates near the compression flange coupled with the tensile forces in the bolts. Since the butt plates are welded to the M4X13 at its web as well as its flanges, the M4X13 pulls the butt plates apart in the entire region between the bolts as rotation increases (Fig. 4.6). The greatest bending of the plates occur about the strong axis of the section (Fig. 4.7), but there is significant bending about the weak axis as well (Fig. 4.8). The plate bending would occur only about the strong axis if the plates were not welded to the web of the M4X13.

As the connection continued to rotate after the peak axial load had been reached the butt plate welds at the outside edge of the tension flange cracked (Fig. 4.9). The butt plates then began to peel away from the section as the crack progressed towards the web of the section. At this point the ultimate moment capacity of the section generally had been reached. Because of the moment resulting from the increase of eccentricity as the connection rotated (the so-called P-Δ effect), the maximum moment was always reached after the applied load had begun to decrease.

Depending on the loads applied a connection may rotate either to

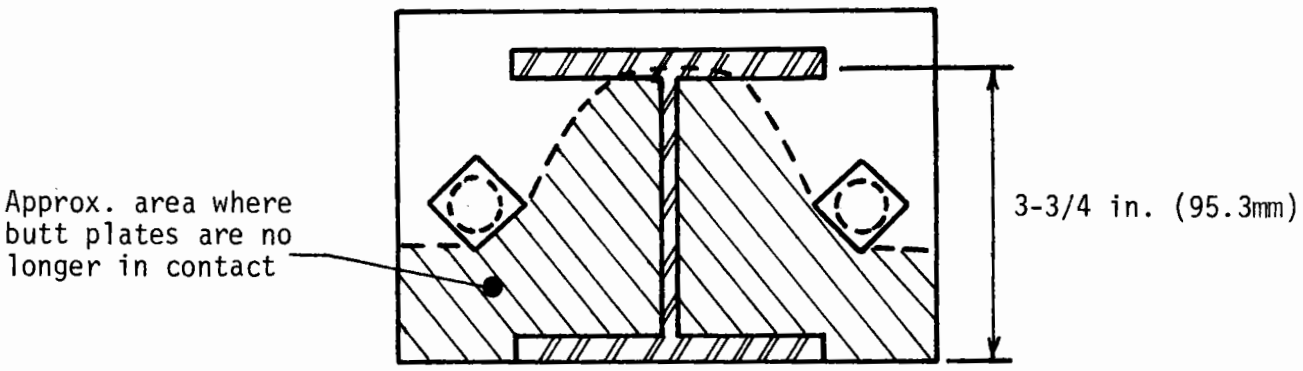

FIGURE 4.6 AREA OF COMPRESSION BETWEEN THE BUTT PLATES

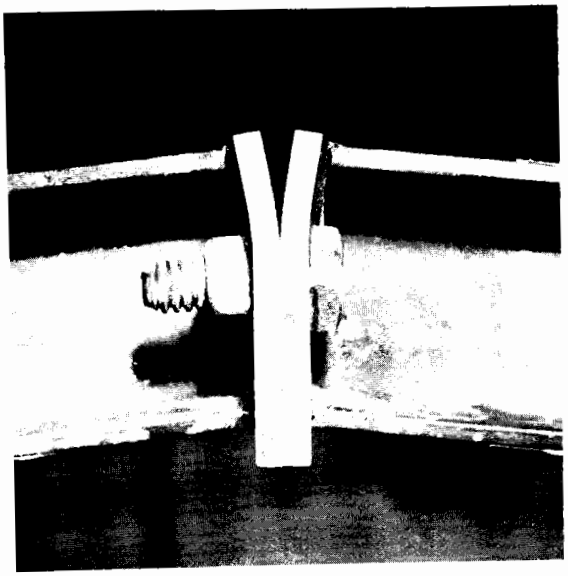

FIGURE 4.7 OPENING OF THE BUTT PLATES ABOUT THE STRONG AXIS OF BENDING

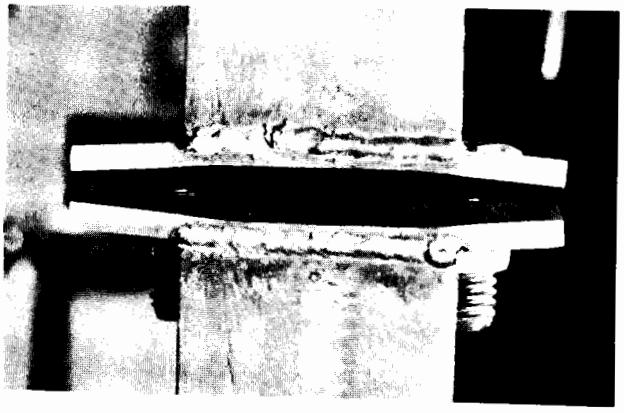

FIGURE 4.8 OPENING OF THE BUTT PLATES ABOUT THE WEAK AXIS OF BENDING

FIGURE 4.9 WELD FAILURE BETWEEN BUTT PLATE AND OUTSIDE EDGE OF TENSION FLANGE

the inside or the outside of a set. For an unsymmetrical connection the behavior may differ with the direction of moment. To determine how much the connection behavior was changed by a moment applied in the opposite direction, an additional test was performed on a connection in which the butt plates extended on the tension side of the section. Figure 4.10 shows the moment-rotation curves for the two connections, both with initial eccentricities of 4 in. (102 mm). There is some reduction in the moment capacity, but the difference is not significant.

4.3 TESTS OF SLEEVE CONNECTIONS

Two types of sleeve connections are considered as a possible means of cutting erection time. Both were designed for the 4 x 4 x 1/4 in. structural steel tube but they could also be used for round or wide-flange cross sections.

The first type of sleeve connection will be referred to as a "solid sleeve" (Fig. 4.11). The inside dimension of the solid sleeve tested was 1/8 in. (3.18 mm) larger than the outside dimension of the 4 x 4 x 1/4 in. tube. This tolerance is required to facilitate positioning the sleeve over the section. The sleeve length was 12 in. (305 mm) and wall thickness 1/8 in. (3.18 mm). Since the sleeve is loose fitting some method of holding it in place is necessary. There are many ways of doing this; one simple method is to put a pin through a pre-drilled hole in the section to prevent the sleeve from sliding.

If the cross sections of the members being connected are not true to shape, which is usually the case, the solid sleeve may not be suitable

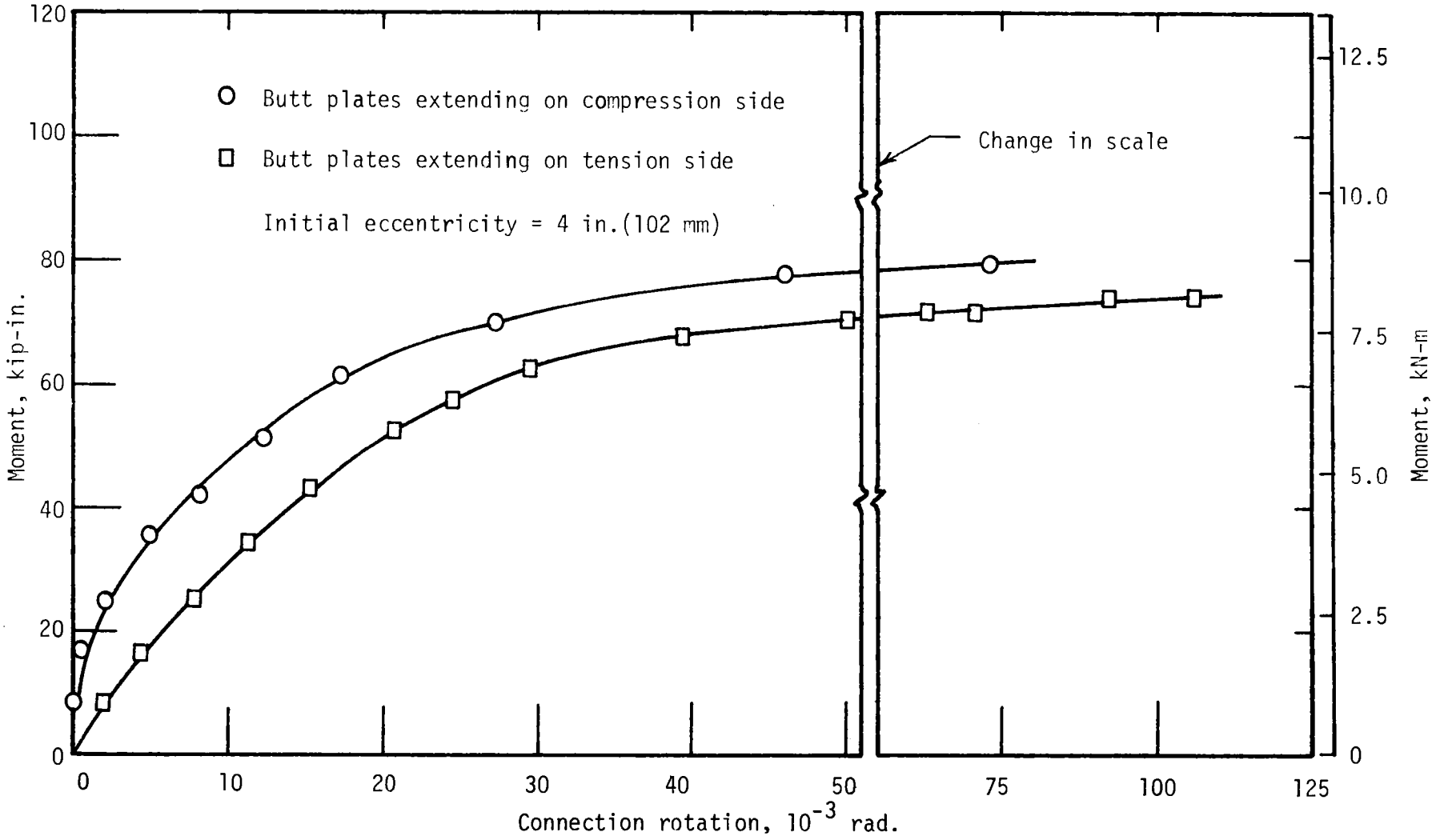

FIG. 4.10 COMPARISON OF MOMENT-ROTATION FOR MOMENT IN EACH DIRECTION ABOUT THE STRONG AXIS

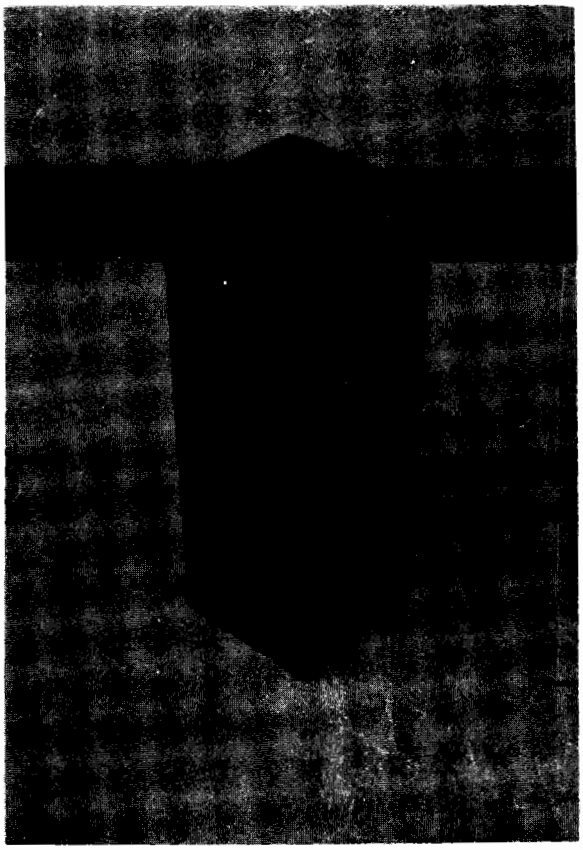

FIGURE 4.11 SOLID SLEEVE CONNECTOR

because the additional inside dimension required to accept extreme variations would result in a very loose fitting connection that would allow considerable rotation before developing any moment resistance. A split-sleeve connection might solve this problem (Fig. 4.12). The split-sleeve tested has inside dimensions approximately the same as the outside dimension of the 4 x 4 x 1/4 in. steel tube, with a wall thickness of 1/8 in. (3.18 mm)

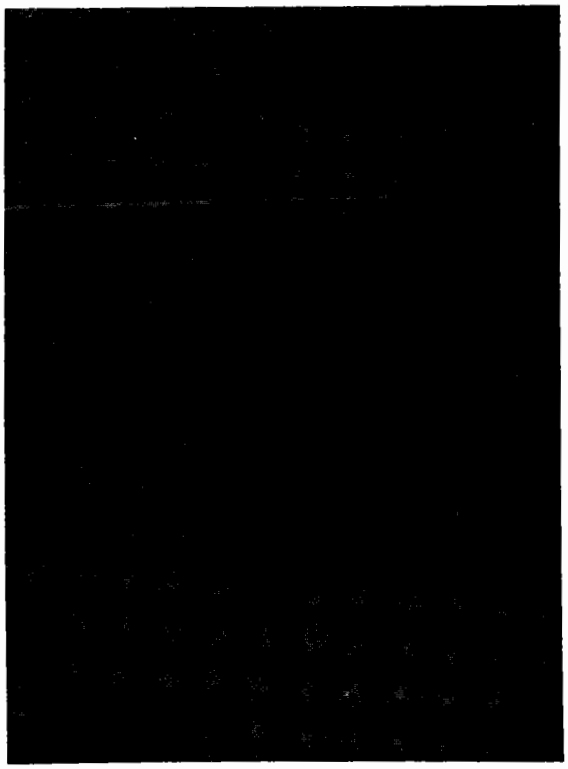

FIGURE 4.12 SPLIT SLEEVE CONNECTOR

and length of 12 in. (305 mm). In one side was a slot of increasing width from one end of the sleeve to the other. The edges of the slot were turned back (Fig. 4.13) to provide a track for a tightening wedge to be driven. This had the advantage of being a loose sleeve, for ease in positioning, that fit tight after the wedge was driven into place.

Both types of sleeves could probably be fabricated most efficiently

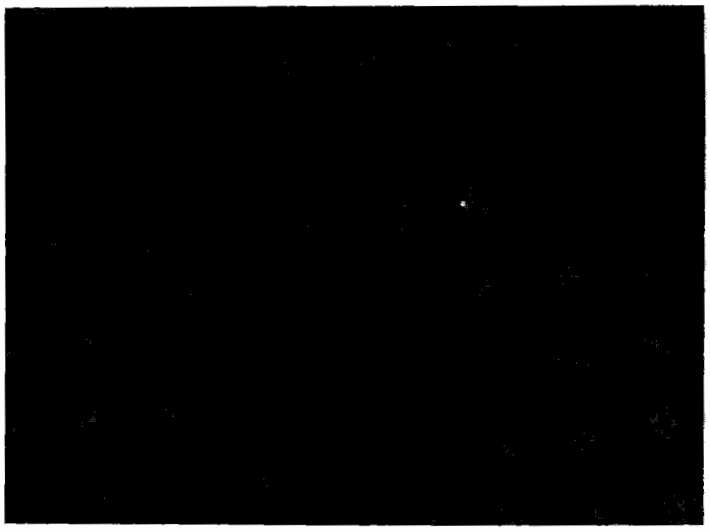

FIGURE 4.13 TIGHTENING SLOT IN THE SPLIT SLEEVE CONNECTOR

by cold forming. Because of shop limitations they were fabricated by welding straight pieces of 1/8-in. (3.18 mm) thick mild steel plate. Consequently, they had low ductility at weld locations. Instrumentation for the joint tests is shown in Fig. 4.14. It consisted of a pair of LVDT's to measure rotation of the section and a dial gage to measure the lateral displacement at mid-length of the connection.

Both sleeves failed as a result of weld fractures. As the connected members rotated the flanges on the tension side pushed out at the top and bottom. Figure 4.15 shows the split sleeve (with the slot on the opposite face) with a weld fracture at mid-length on the tension side. The

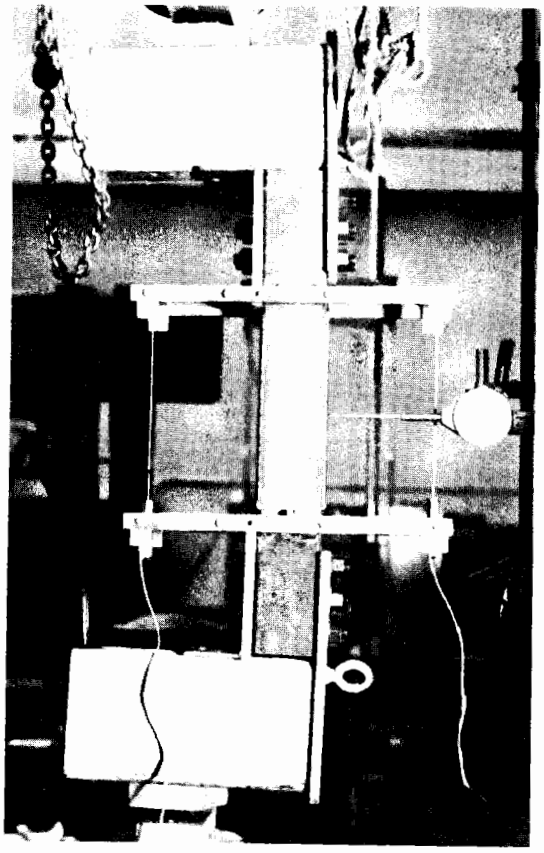

FIGURE 4.14 INSTRUMENTATION FOR THE SLEEVE CONNECTION TESTS

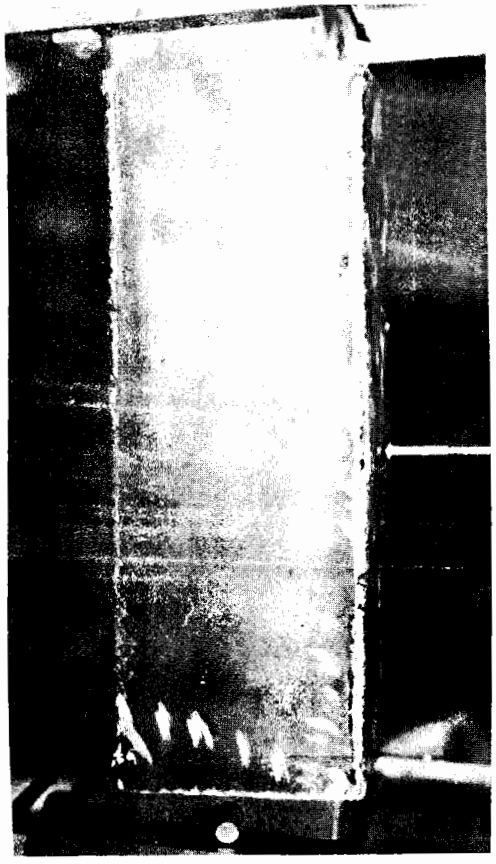

FIGURE 4.15 WELD FAILURE IN SPLIT SLEEVE CONNECTION TEST

solid sleeve, with a fractured weld at the top corner on the compression side, is shown in Fig. 4.16. In each case the fracture occurred at a point of high stress concentration. Once the initial fracture occurred the failure progressed primarily at that location. However, with only two tests there is no basis for relating the initial fracture location to the type of sleeve.

Figure 4.17 shows the moment-rotation curves for the two sleeve connections as well as one for a standard, two-bolt connection, all tested

FIGURE 4.16 WELD FAILURE IN THE SOLID SLEEVE CONNECTOR

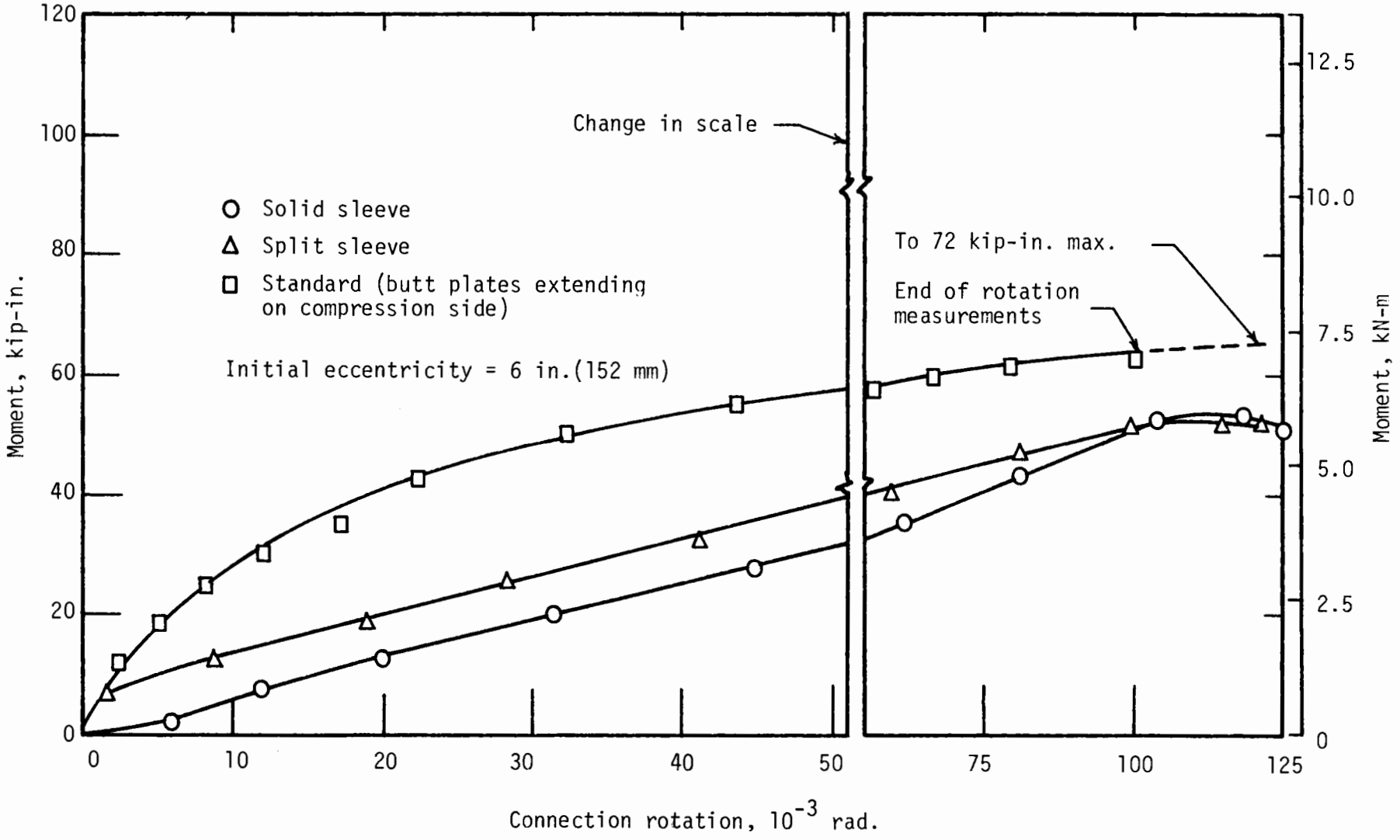

FIG. 4.17 COMPARISON OF MOMENT-ROTATION FOR SLEEVE AND BUTT-PLATE CONNECTIONS

with initial eccentricities of 6 in. (152 mm). The solid sleeve has a lower moment capacity at a given rotation throughout much of the loading, primarily because of its loose fit. Because the split sleeve fits snugly its initial stiffness is somewhat higher. However, both sleeve connections eventually reach the same moment capacity, about 50 kip-in. (5.65 kN•m). This is about 75 percent of the moment capacity of the standard connection (with butt plates extending on the compression side), but it occurs at a lower rotation.

4.4 SUGGESTED SPLIT-SLEEVE CONNECTION

Of the two types of sleeve connections tested, the split sleeve has the advantage of tighter fit and better moment-rotation characteristics. Since cold forming appears to be the only practicable method of producing a split sleeve, several possible configurations were considered. The simplest connection, detailed 3/16 in. (4.76 mm) thick for a 4 x 4 x 1/4 box, is shown in Fig. 4.18. The piece on the right would be tack-welded in the shop to one section of rib, with half its length extending beyond the end of the section and oriented so that the open end of the U would face the tunnel. The mating rib would be slipped into position in the tunnel and the connection made by driving the closing piece into place. This would help make the connection tight in the direction of bending. The slope of the connecting elements accommodates a ±1/8 in. (3.18 mm) variation from the nominal 4-in. (102-mm) dimension if the closing piece tightens with its upper end ±1.3 in. from the top of the mating piece. A large manufacturer of cold-form products was consulted, and it appears that this connection could be produced in

volume at costs commensurate with the cost of welding plates to the ends of rib members for butt-plate connections. However, the minimum radius for cold bending is 3 thicknesses of metal, which tends to make the connection bulky for the thicknesses that would be needed for large cross sections.

4.5 CONCLUSIONS

One test of a rib with sleeve connections was made in the large-scale rib test series described in Chapter 2. This was test BS15 and the results are shown in Table 2.6. It is of interest to note that although the sleeves were only 1/8 in. (3.18 mm) thick the strength of the rib was only 20 percent below that of a rib of the same cross section but with standard butt-plate connections. Considering the possibilities of connections of this type in speeding up erection in the tunnel, it would seem that they merit further study.

Time did not permit tests of split sleeves of the type shown in Fig. 4.18. Therefore, it cannot be finally evaluated. It may prove to be cumbersome in thicknesses that would be needed in larger cross sections, as noted above. However, the solid-sleeve test suggests that the required thickness may be less than that of the section to be connected. Furthermore, the split sleeve connection would probably be cheaper to manufacture than the solid sleeve, since the latter requires welding.

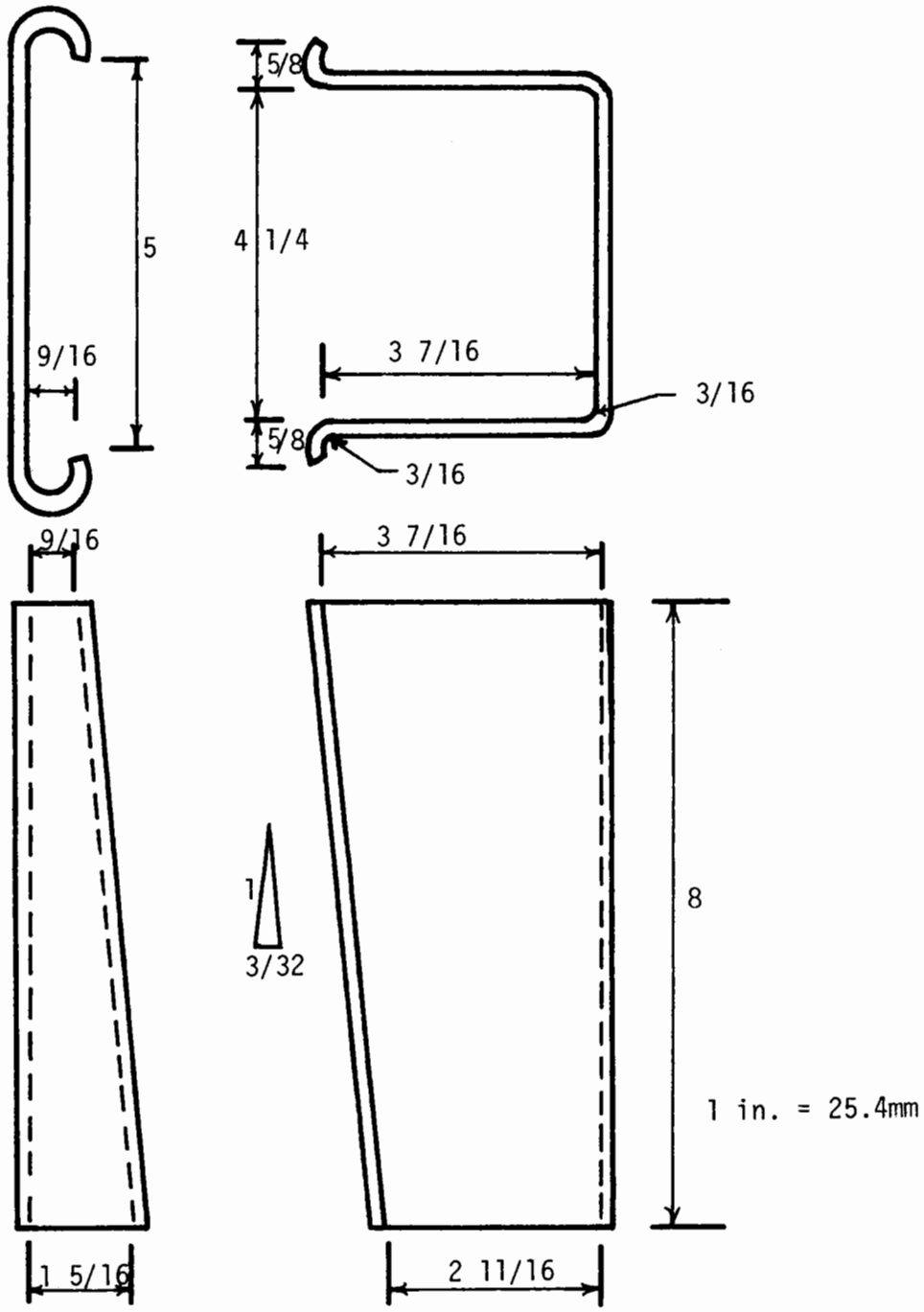

FIG. 4.18 SUGGESTED SPLIT-SLEEVE CONNECTOR FOR 4x4x1/4 BOX SECTION

CHAPTER 5

COMPUTER STUDY OF STEEL SUPPORTS

An analytical investigation of ultimate strength of the horseshoe-shaped steel rib was made with the general purpose structural analysis computer program NASTRAN. Developed by NASA for the space program, NASTRAN contains elements that can be assigned a piecewide linear stress-strain relationship, so it can be used to model nonlinear behavior of the ribs. Such a program enables parameters which affect ultimate strength to be studied more easily and more economically than by performing large-scale laboratory tests.

In tunnels through rock, loads are transferred to the steel rib through wood blocking so the blocking is an essential part of the structure. Stiffness of wood blocking is difficult to control since it depends on the type of wood used, its condition, and the manner in which it is placed. The location of blocking is generally controllable as long as there is some clearance between the rock and the rib. Ideally, it should be placed uniformly around the structure to distribute the load, but this is time-consuming and therefore expensive. The alternative is to place the blocking at intervals along the rib, often at rather random locations. For a given load configuration some blocking locations will be more critical with regard to ultimate strength than others. In this chapter, a study of the effects of both blocking stiffness and absence of blocking on the ultimate strength of a steel rib are described.

Segments of a steel rib are usually joined with bolted butt-plate connections. These connections may have various strengths, depending on the number of bolts used, their strength, location, and other factors. Three connection models, with different moment capacities, are described and their influence on the behavior of the rib reported.

An investigation of the parameters mentioned is intended to give a better understanding of the total structural behavior of the rib. The knowledge gained will be useful in design as well as in the development of alternative primary support structures. These parameters were not considered in the test program described in Chapter 2, so this study was undertaken to determine how important they might be. As discussed in Chapter 1, the active loading considered here is not the same as either of those used in Chapter 2 but corresponds to that used in a previous study (Paul, et al., 1974).

5.1 DESCRIPTION OF ANALYTICAL MODEL

5.1.1 SET MODEL

The horseshoe-shaped rib considered in this chapter is the M4x13 (wide-flange shape), with bolted butt-plate connections at the top of each leg (spring line) and at the crown, that is described in Chapter 2. Figure 5.1 shows the geometry and the unsymmetrical configurations of applied (active) loads and resisting (passive) loads considered. This loading results in relatively high bending moments, and thus a lower ultimate load, than the symmetrical load configuration, so it can be considered the more critical case.

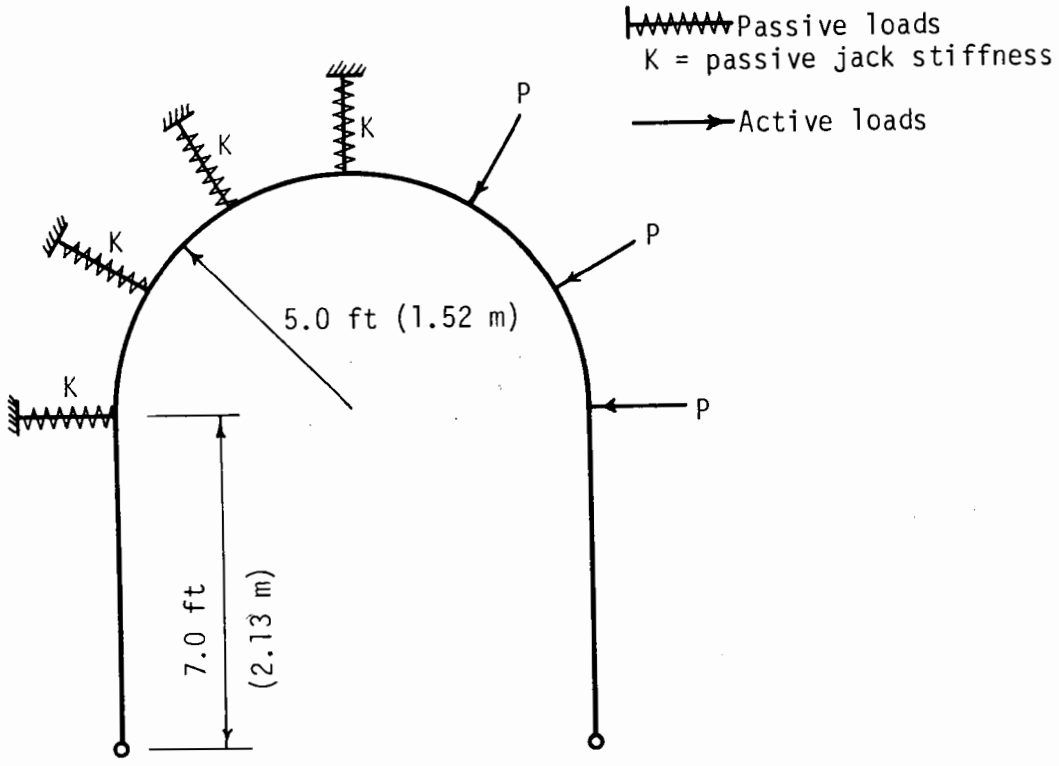

FIGURE 5.1 GEOMETRY AND LOAD CONFIGURATION OF THE STEEL RIB

Figure 5.2 shows how the rib is divided into a series of straight segments in the analytic model. Representation of the M4x13 section is accomplished by using rod elements which can be given nonlinear stress-strain properties for the flanges, and a shear panel, restricted to linear behavior, for the web. Dimensions of these elements are chosen to give the appropriate geometric properties of the section. A more detailed description of this model has been reported by Paul, et al. (1974).

Stress-strain behavior of the steel in the arch portions of the

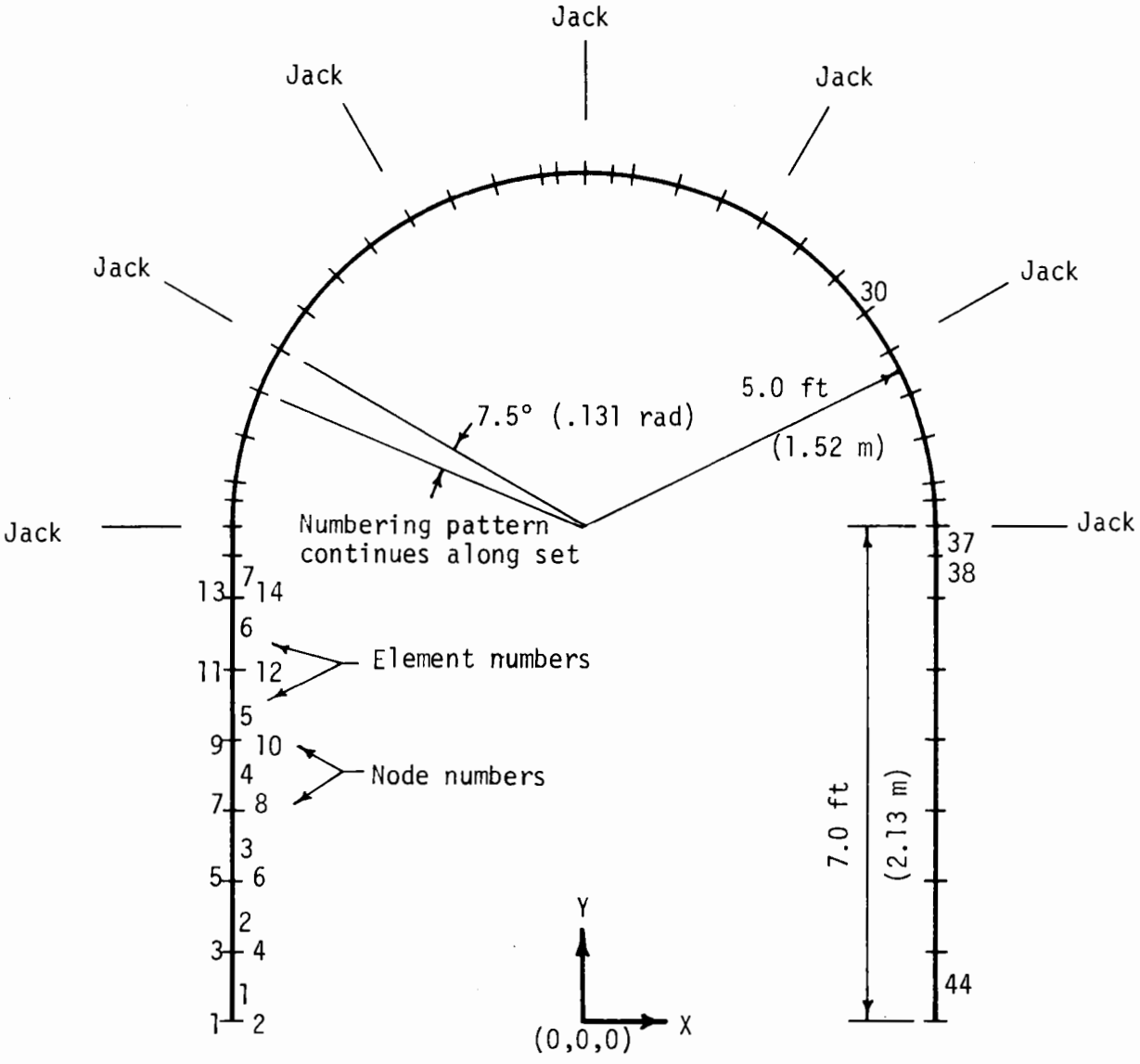

FIG. 5.2 IDEALIZED STRUCTURE IN THE NASTRAN PROGRAM

rib differs from that in the legs. This is due to cold working of the steel in the arches during bending. Stress-strain curves were obtained from a series of coupon tests for the arch and the legs and the difference in strength for these parts was taken into account in the model.

5.1.2 CONNECTION MODEL

Six tests of both moment-resistant and standard connections were reported by Paul, et al. (1974). Data from these tests and from two additional tests on standard connections was used to develop a connection model for use in the NASTRAN analysis.

Two of the standard, two-bolt connections reported by Paul, et al. (1974), were on M4x13 sections using A-325 bolts and 3/8-in. (10 mm) butt plates. Two additional tests, using fit-up bolts, were performed later, and the rotation measured over a 9 in. (229 mm) length of section centered at the connection. Moment-rotation curves from these tests are shown in Fig. 5.3. The rotation in the first tests was measured over a 2.5-in. (64 mm) length in order to eliminate most of the influence of the M4x13 section. To better compare these tests the rotations in the later tests were adjusted by subtracting the portion resulting from 6.5 in. (165 mm) of the M4x13, giving a computed rotation over 2.5 in. (64 mm) of the connection.

From the results of the standard connection tests, it can be seen that there is a reduction in the connection moment capacity with higher eccentricities of applied load. Since the behavior of these connections is fairly complex, depending on such things as butt plate thickness and

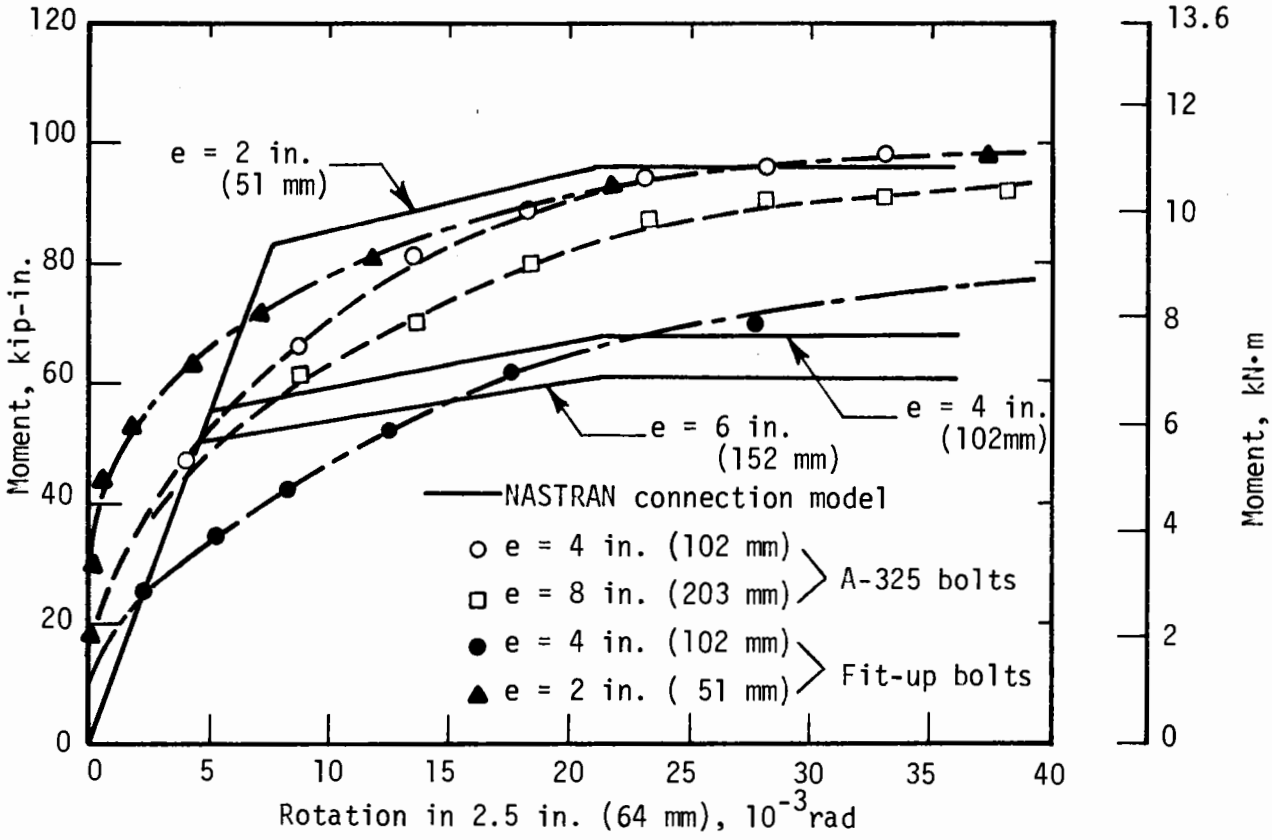

FIGURE 5.3 COMPARISON OF STANDARD CONNECTION TESTS AND NASTRAN STANDARD CONNECTION MODEL

bolt pre-tension, no attempt was made to model them precisely. Instead, the model was developed to give the correct type of behavior.

As used in this study, the connection model consists of rod elements, which can be given nonlinear stress-strain properties, and linear shear panels. The geometry is shown in Fig. 5.4. The moment-rotation behavior of the connection is controlled by the level of stress allowed in the rods and by the slope of the stress-strain curve.

Since for the standard connections there is a reduction in

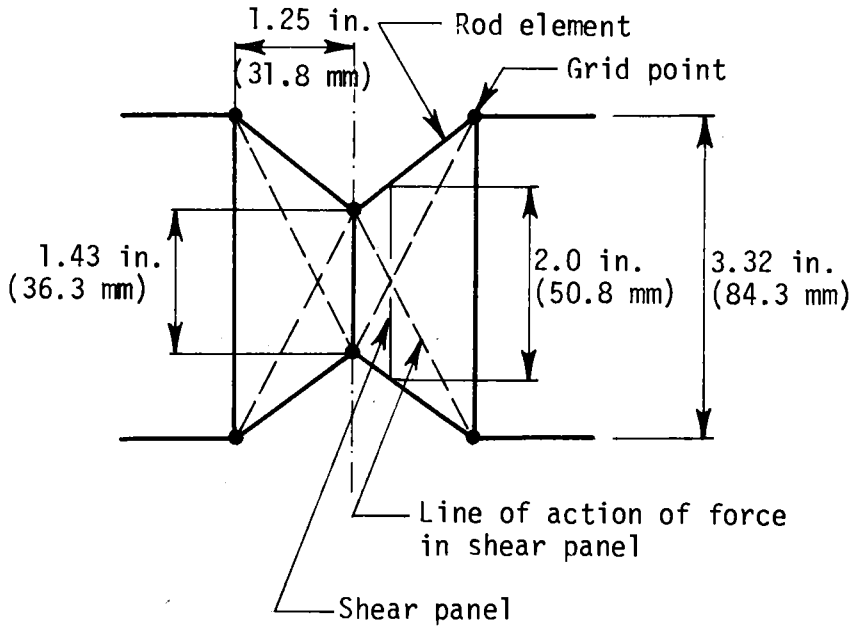

FIGURE 5.4 SIMULATION OF CONNECTION IN NASTRAN PROGRAM

moment capacity with larger eccentricities, the behavior is analagous to that of a reinforced concrete member that fails in tension. Therefore, the stress-strain behavior of the rod elements was chosen to be weaker in tension than in compression. After initial calculations were made, the determination of an appropriate stress-strain curve became a trial-and-error process. The connection was studied in a beam-column model in which the load could be applied at various eccentricities. The moment-rotation behavior of the final connection model used in the analysis is shown in Fig. 5.3.

Two of the four-bolt moment-resistant connections tested were fabricated with 1/2-in. (13 mm) butt-plates identical to those used in

the large-scale tests. The peak moments recorded in these tests were 77 percent and 90 percent of the plastic moment of the M4x13 section for initial eccentricities of 4 in. (102 mm) and 8 in. (203 mm), respectively.

Since eccentricities in the rib were generally less than 6 in. (152 mm), determined from measurements made in the large-scale tests, a moment capacity of 170 kip-in. (19.2 kN•m) at an eccentricity of 4 in. (102 mm) was chosen for the moment-resistant connection model. This is about 78 percent of the plastic moment of the M4x13. At an eccentricity of 8 in. (203 mm), the moment capacity of the model is 195 kip-in. (22.0 kN•m), or 90 percent of the plastic moment of the section. These values correspond quite well with those of the moment-resistant connection tests, as can be seen in Fig. 5.5. Because the initial stress-strain properties of the rods in this connection model were kept the same as in the standard connection model, the initial slopes of the moment-rotation curves are not comparable for the model and the tests.

A third connection model was also used in part of this study. The moment capacities of this connection were less than half that of the standard connection for corresponding eccentricities. Figure 5.6 shows the moment capacities of the three connections plotted against the eccentricity of applied load.

5.1.3 BLOCKING

To simulate blocking stiffness rod elements were connected to the rib model in a radial orientation at locations corresponding to those in the large-scale laboratory tests. Since the stress-strain behavior may be

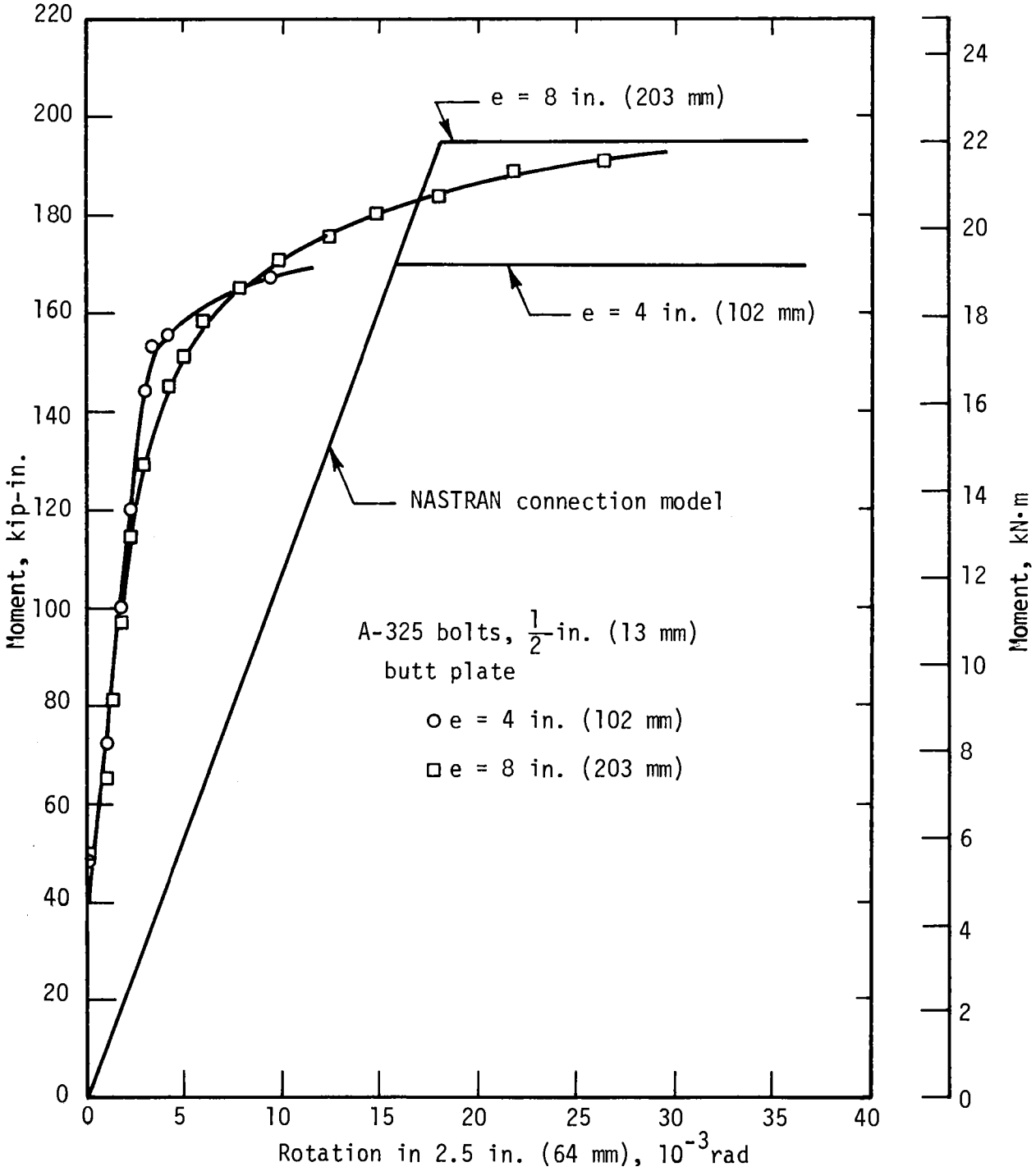

FIG. 5.5 COMPARISON OF MOMENT-RESISTANT CONNECTION TESTS AND NASTRAN MOMENT-RESISTANT CONNECTION MODEL

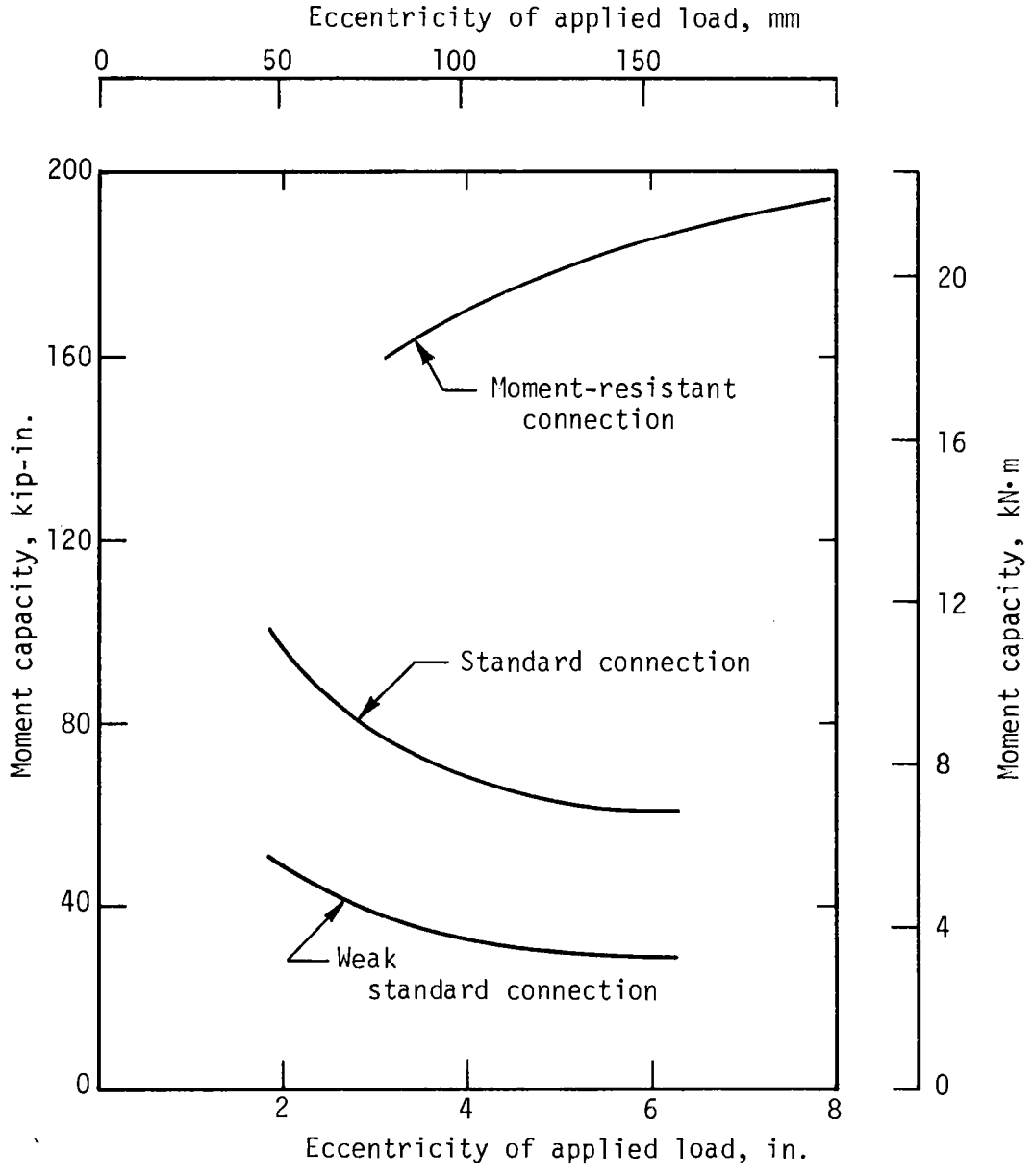

FIG. 5.6 MOMENT CAPACITIES OF NASTRAN CONNECTION MODELS

used for rod elements, the blocking stiffness can be modeled as linear or nonlinear, and can be varied from one blocking point to another. In this manner the effect of blocking stiffness or missing blocking on the behavior of the structure can easily be studied.

5.2 DISCUSSION OF RESULTS

5.2.1 COMPARISON OF ANALYSIS WITH TEST

In order to check the behavior of the nonlinear computer model, it was compared with a large-scale rib test. Of the eleven tests reported by Paul, et al. (1974), four were loaded to failure. However, in only one test (M1b in that reference) was the active loading applied in the plane of the rib (a requirement of the nonlinear model currently being used), so this test was chosen for the comparison. Test M1b had standard connections, hard blocking, and was loaded unsymmetrically (Fig. 5.1).

The accuracy of the nonlinear model was checked by simulating the test with the load-deflection behavior of the passive rams from the large-scale test. Recorded load-deflection of the passive rams were converted to stress-strain relationships for the rod elements that represent passive loads. A comparison of the test and calculated results is shown in Fig. 5.7 in terms of average active load versus radial displacement at the east connection (springline). For the loading considered, the displacement at this location is the largest in the rib. There is good correlation of results, particularly below about 18 kips (80 kN) average active load, which represents 80 percent of the actual ultimate load. At loads

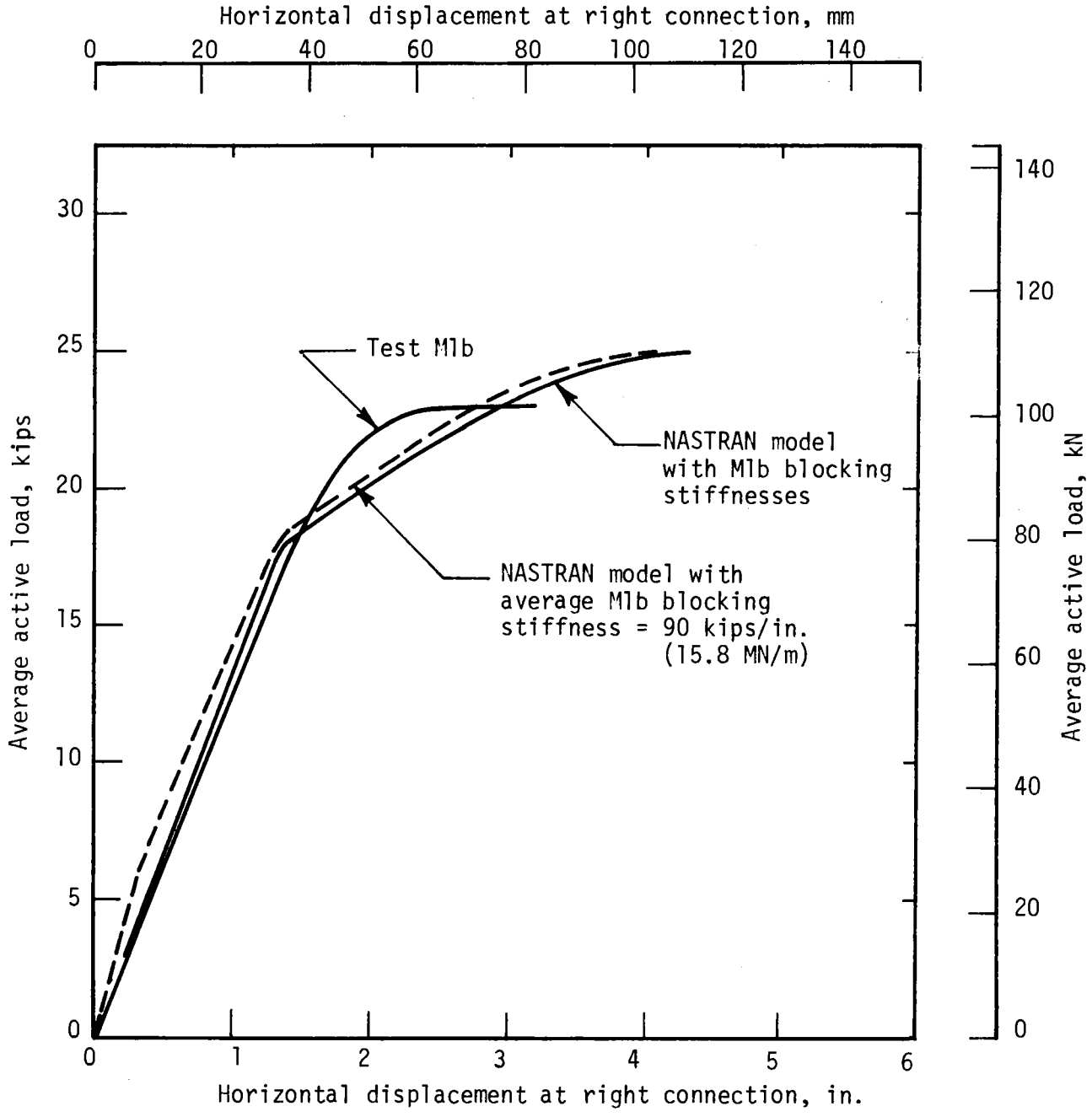

FIG. 5.7 COMPARISON OF TEST M1B AND NASTRAN MODEL

higher than this, the model is more flexible than the rib and has an ultimate load of 25 kips (111 kN), about 10 percent higher than the 22.7 kips (101 kN) ultimate load in the test.

Since the nonlinear model is more important for parameter studies than for simply attempting to reproduce large-scale test behavior, it is convenient to use an average blocking stiffness. From the four individual stress-strain curves used for the passive rams in modeling test M1b, an approximate linear average of 90 kips/in. (15.8 MN/m) was obtained graphically. The corresponding average stress-strain relation was then used for all four passive forces. The resulting load-displacement curve is also shown in Fig. 5.7, and shows that by using this average stiffness the load-displacement behavior at the east connection is somewhat stiffer in the elastic range. However, the slopes of the curves are essentially the same and the ultimate loads converge to the same value, 25 kips (111 kN). Thus, an average linear stiffness for the passive forces is quite reasonable and simplifies the model as well.

5.2.2 EFFECT OF BLOCKING

STIFFNESS OF BLOCKING

Results of the large-scale rib tests reported by Paul, et al. (1974), showed that blocking stiffnesses had a substantial effect on deflections if the rib was loaded from the side. The comparisons were made on ribs with four-bolt, moment-resistant connections. At an average active

load of 9 kips (40 kN) (about 40 percent of the ultimate) the radial displacement was 127 percent greater for soft blocking than for hard blocking. In this case the hard blocking stiffness was on the order of 90 to 100 kips/in. (15.8-17.5 MN/m) and the soft blocking about 40 kips/in. (7.0 MN/m). However, it was not certain that blocking stiffness would substantially affect the ultimate load capacity of the rib since there were no two ribs loaded to failure with blocking stiffness the only variable. For this reason the NASTRAN analysis was used to study the blocking stiffness parameter.

Stiffness of the blocking used in the analysis were the following: 90 kips/in. (15.8 MN/m), an approximate average of the blocking in test M1b; 40 kips/in. (7.0 MN/m), a linear approximation of the soft blocking used in those large-scale tests; 26 kips/in. (4.6 MN/m); and 13 kips/in. (2.3 MN/m) (an extreme low). These stiffnesses are plotted in Fig. 5.8 along with load-deformation curves from wood blocking tests (Paul, et al., 1974) and the soft blocking curve used in the large-scale set tests.

Figure 5.9 shows the load vs. displacement at the east connection for the four blocking stiffnesses. For blocking stiffnesses of 90 and 40 kips/in. (15.8 and 7.0 MN/m) the ultimate load is 25 kips (111 kN), the only difference being in the flexibility of the structure. The rib with a blocking stiffness of 40 kips/in. (7.0 MN/m) is from 50 to 60 percent more flexible than the one with 90 kips/in. (15.8 MN/m) blocking stiffness. Significant decreases in the ultimate loads occur with the lower blocking stiffnesses. For 26 kips/in. (4.6 MN/m) and 13 kips/in. (2.3 MN/m) blocking stiffness, ultimate loads are 14 kips (62 kN) and 9 kips (40 kN) respectively. Figure 5.10 shows a plot of ultimate load vs. blocking stiffness

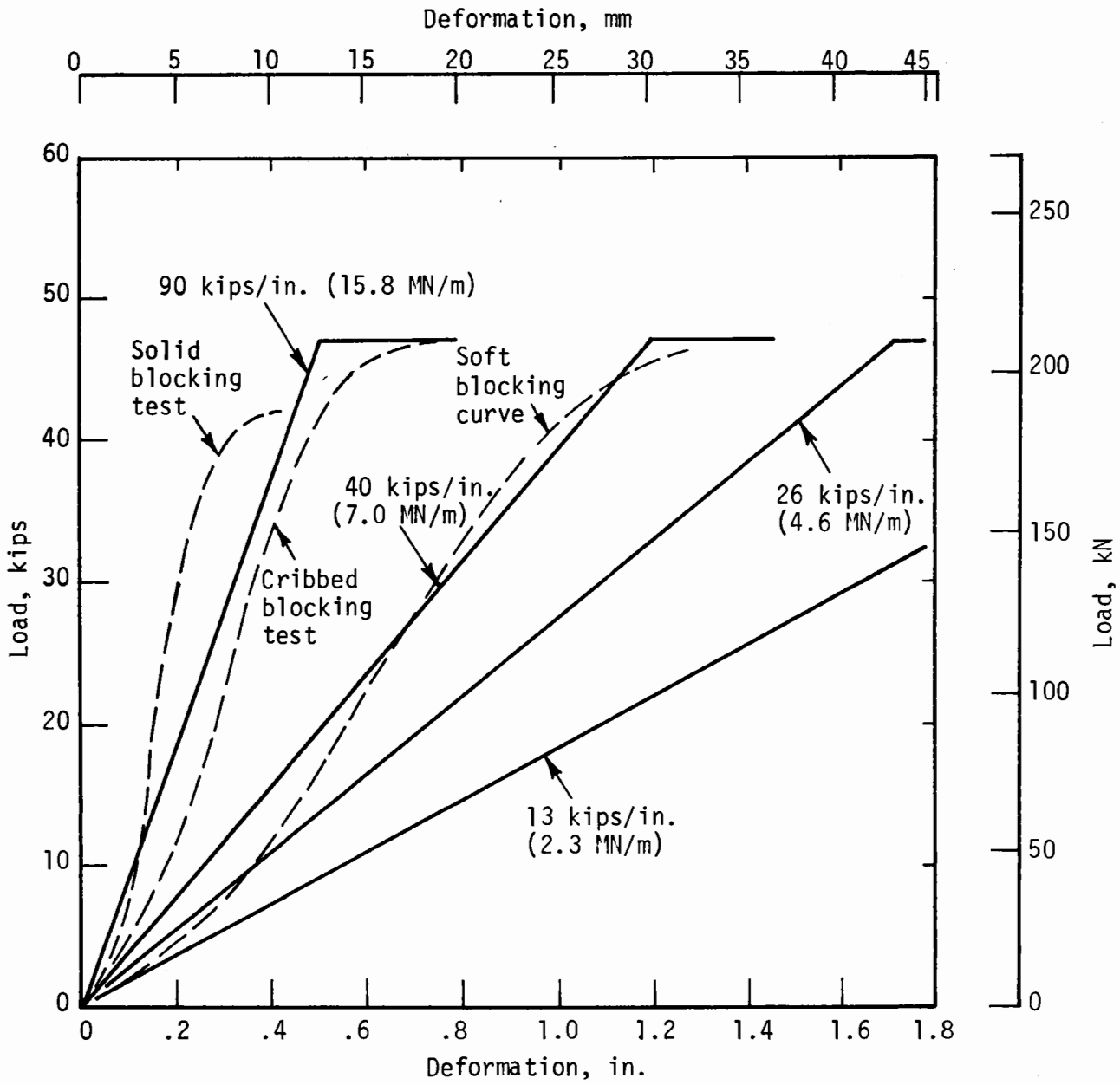

FIG. 5.8 LOAD-DEFORMATION FOR BLOCKING STIFFNESSES

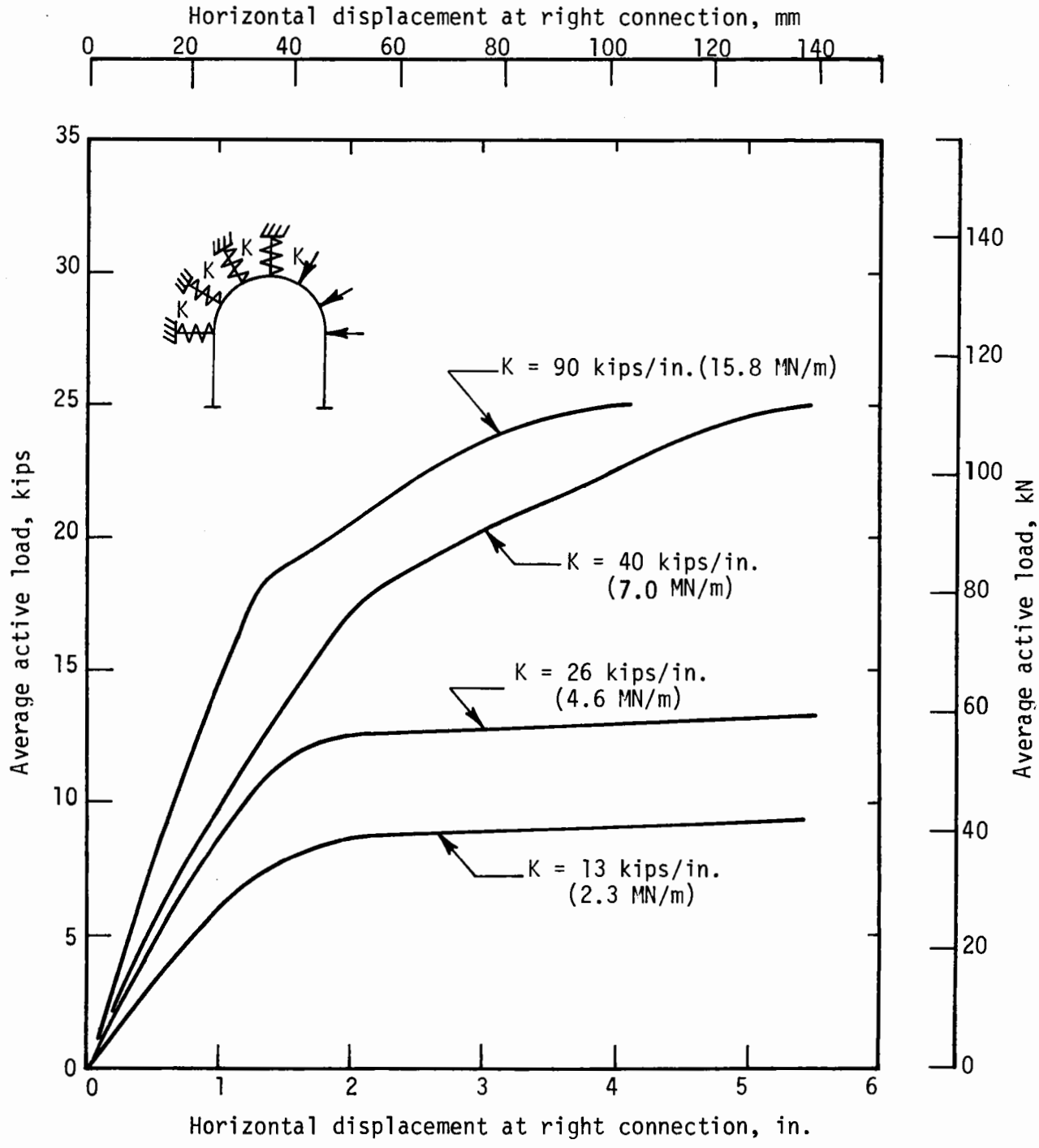

FIG. 5.9 EFFECT OF BLOCKING STIFFNESS ON LOAD-DISPLACEMENT OF THE SET

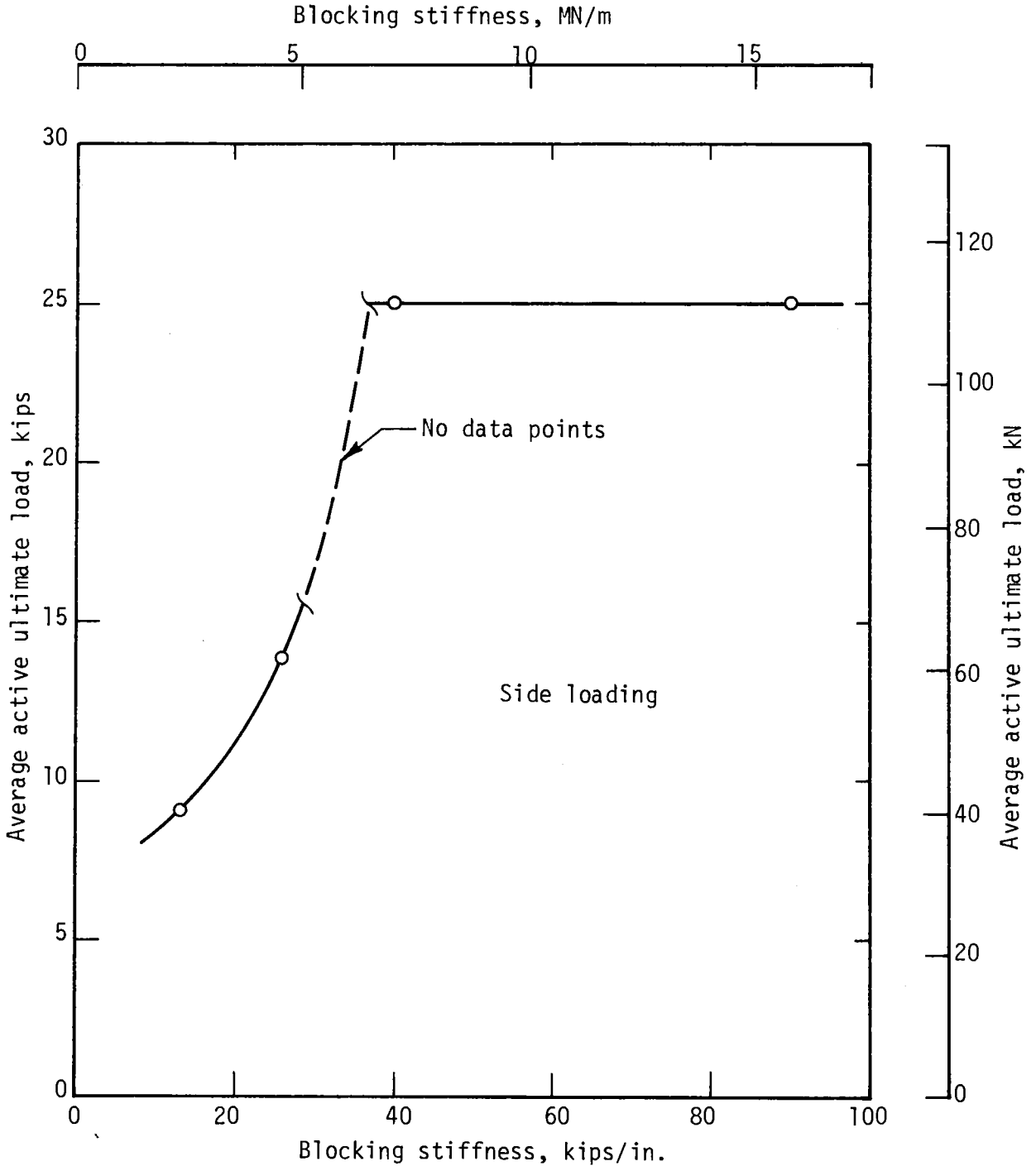

FIG. 5.10 EFFECT OF BLOCKING STIFFNESS ON ULTIMATE LOAD OF THE SET

for the four values used. The curve is approximate since only four points were obtained. At the lowest range of blocking stiffness the slope of the curve indicates that the ultimate load will be between 5 and 10 kips (22 and 44 kN) for zero blocking stiffness. This represents the ultimate load for the rib acting as a free-standing unbraced frame. At blocking stiffnesses higher than 40 kips/in. (7.0 MN/m), the ultimate load remains at about 25 kips (111 kN). Here, the failure mechanism becomes independent of the blocking stiffness because the blocking points are essentially rigid supports, which is the limiting case. There is one primary difference in the failure mechanisms. For low blocking stiffnesses the crown connection yields, and so becomes a hinge. With high blocking stiffnesses this does not occur. Evidence of this change in the mechanism is the rather sharp knee in the curve of ultimate load vs. blocking stiffness (Fig. 5.10).

It is significant that blocking stiffnesses higher than about 40 kips/in. (7.0 MN/m) do not increase the ultimate strength of the rib for this unsymmetrical loading case. In a test of a cribbed wood blocking configuration (Paul, et al., 1974) consisting of a stack of blocks 10-1/2 in. (267 mm) high, the stiffness was twice this value. Thus, 40 kips/in. (7.0 MN/m) is about one-half the stiffness of a neatly stacked crib, but a rib with such blocking has an ultimate strength about equal to that of one with rigid blocking. It can be concluded that, for this loading condition, ordinary wood blocking that is placed very tight and has small stress concentration that causes local deformations has sufficient stiffness. In addition it is reasonable to expect this to be true for symmetrical loading, though no

analyses have been performed for this to date. The bending stresses and displacements are lower for symmetrical than for a comparable unsymmetrical load, so the blocking stiffness is less critical. This conclusion remains to be verified by analysis.

ABSENCE OF BLOCKING

The NASTRAN analysis can be used to investigate the effect on ultimate strengths of the absence or loss of blocking at one or more positions on the rib. Only the side loaded case was considered, and only blocking which provides passive resistance was considered to be removed. The absence of blocking through which active loads are applied to the structure will also affect its strength. If the weight of a soil or rock mass is to be carried by a rib, it is evident that the structure will withstand the load better if it is well distributed. Precisely how much this affects the ultimate strength has not been investigated.

Figure 5.11 shows the load-displacement curves for three blocking arrangements, all with blocking stiffnesses of 90 kips/in. (15.8 MN/m), and with standard connections. One rib had all the blocking in place (representing set M1b). Another had the crown blocking removed and a third had the blocking removed immediately to the left of the crown. The severe effect of removing the crown blocking is apparent. Ultimate strength of the rib changed from 25 kips (111 kN) to 14 kips (62 kN), a reduction of over 40 percent. Removal of the blocking to the left of the crown also lowered the ultimate strength, but only to about 22 kips (98 kN). Thus, the critical location of the passive blocking for the side loaded case appeared to

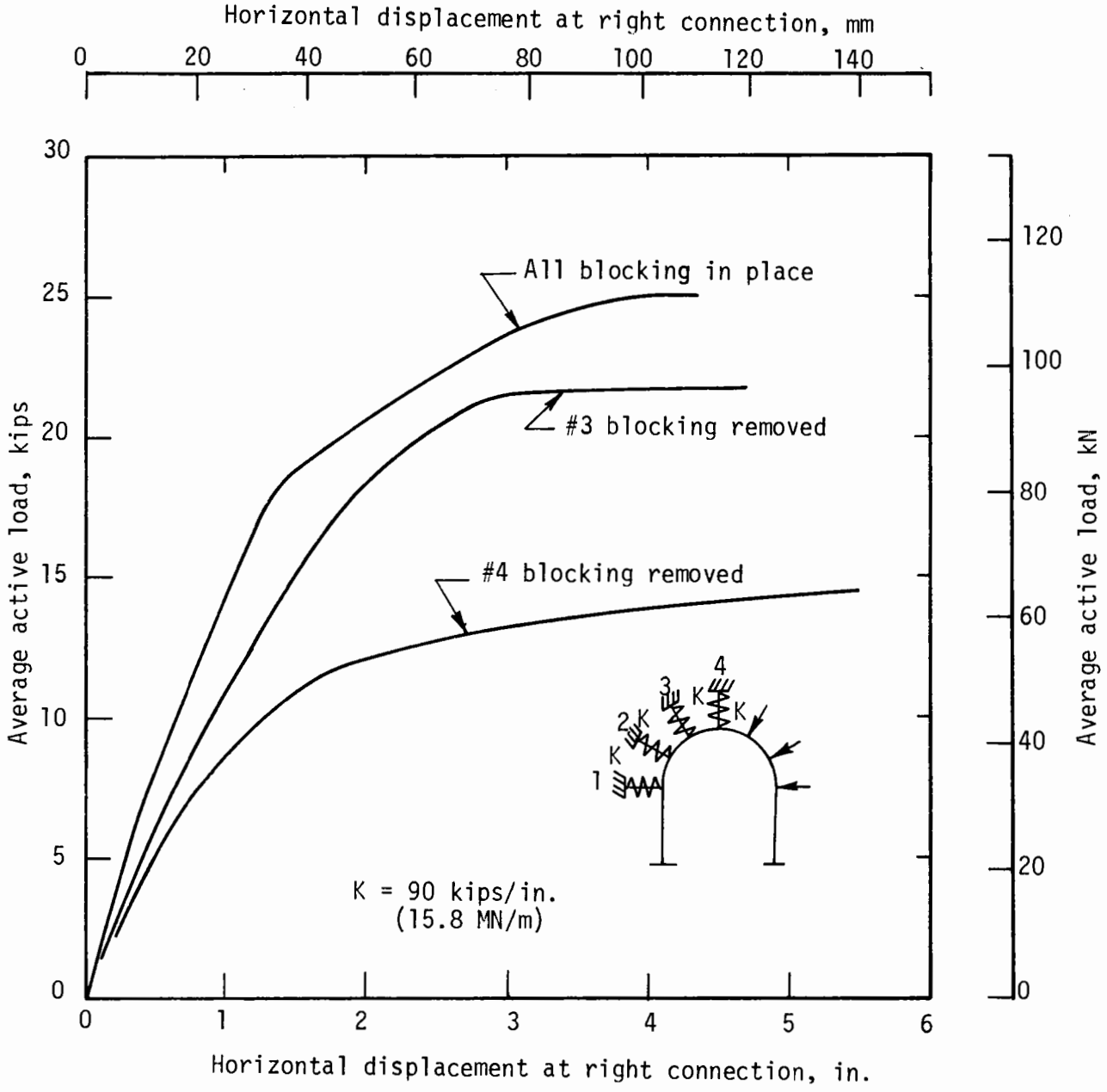

FIG. 5.11 EFFECT OF BLOCKING ABSENCE ON ULTIMATE LOAD OF THE SET

be at or near the crown, since removal of the blocking near the left connection will obviously affect the strength less.

5.2.3 EFFECT OF CONNECTION STRENGTH

The influence of connections on behavior of the rib was reported by Paul, et al. (1974), but the loading was limited to the elastic range. With the NASTRAN analysis the investigation was extended to the ultimate strength. For this study a blocking of 90 kips/in. (15.8 MN/m) was considered.

Three connection models were used in analyzing the effect of connection strength. These were the standard connection, the moment-resistant connection, and a weak standard connection. Figure 5.6 shows the moment capacities of these connections for various eccentricities of applied load. The models are discussed in greater detail in Section 5.1.2.

Curves of applied load vs. horizontal displacement at the right connection in Fig. 5.12 illustrate the effect of these connections on the stiffness and ultimate strength of the structure. As would be expected, the weaker connections decreased the stiffness of the rib. In the NASTRAN model this difference in stiffness in the elastic range is not significant, but at higher loads deflections with standard connections were considerably greater than deflections with moment-resistant conditions. However, deflections of the computer model at high loads were somewhat greater than those in the test rib (Fig. 5.7), so they should be studied relative to one another rather than with respect to the test.

A comparison of ultimate strengths indicates that moment-resistant

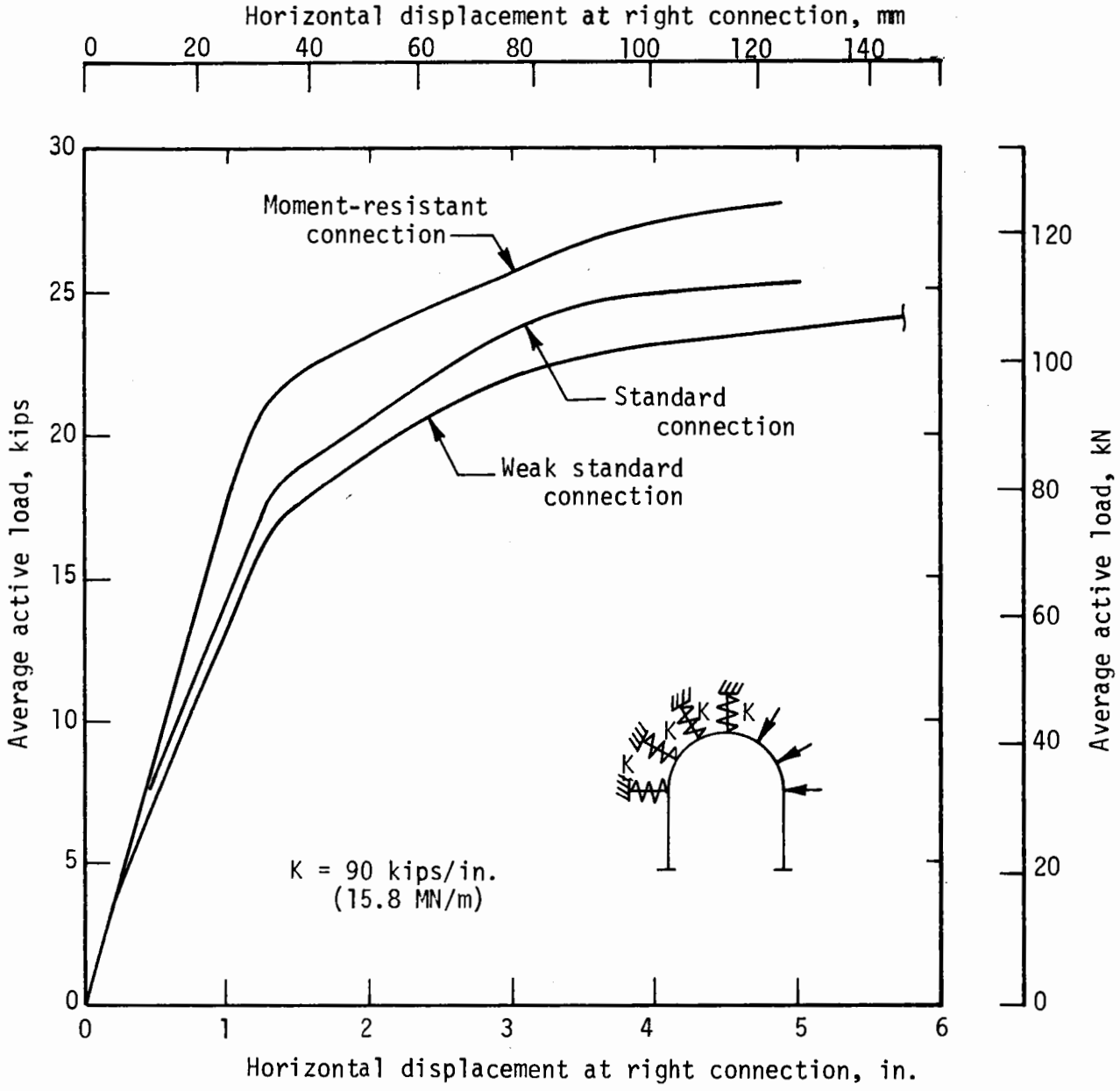

FIG. 5.12 EFFECT OF CONNECTION STRENGTH ON LOAD-DISPLACEMENT OF THE SET

connections, compared with standard connections, do not substantially increase the strength of the rib. The rib with moment-resistant connections reaches an ultimate load only about 15 percent higher than the one with standard connections. Furthermore, the weak connection (with a moment capacity less than half that of the standard connection) did not considerably lower the strength of the rib; in fact, the load converges to the same value if the rib is allowed to deflect far enough. However, this is not a realistic behavior.

In general, the ultimate strength of the rib was insensitive to connection strength. Therefore, the additional strength of the rib with moment-resistant connections probably does not warrant the extra expense involved. However, this is a tentative conclusion that needs further study, particularly with reference to other load configurations.

5.3 SUMMARY

The computer program NASTRAN was used to study the effect of connections and blocking on the behavior of horseshoe-shaped steel ribs. Results of connection tests on moment-resistant and standard connections were used to develop the connection model. The tests showed that the moment capacity of a two-bolt standard connection decreased with higher eccentricities of applied load while the moment capacity of a four-bolt moment-resistant connection increased with higher eccentricities. This behavior was modeled by adjusting the stress-strain relationship of elements in the model. Though the connection behavior was not modeled exactly, the correct type of behavior was obtained. This was considered

more important since the precise connection behavior depends on bolt pretension, bolt strength, butt-plate thickness, and other factors that may change from one connection to another.

Blocking was also represented in the computer model by elements that could be given nonlinear stress-strain properties. In this way the load-displacement behavior at blocking points in the large-scale test could be input for the model.

A comparison of the load-displacement behavior of the model with that of a large-scale rib test was made for active loads applied from one side. The difference was insignificant up to a load of about 80 percent of the ultimate load of the actual rib. At higher loads deflections in the computer model were larger than in the rib, and the ultimate load of the model was about 10 percent higher. An average blocking stiffness was then used for studying blocking and connection parameters.

Computer analyses were made on ribs using four blocking stiffnesses. For the unsymmetrical loading configuration used, there was no increase in ultimate strength of the rib when blocking stiffnesses were increased beyond 40 kips/in. (70 MN/m).

The absence or loss of blocking which resists deformations in the rib (passive blocking) was studied for side loading. It was found that the blocking locations which most affects the ultimate strength for the unsymmetrical loading case is near the crown.

A rib with active loads applied from the side was used for all parameter studies in this chapter. Since this loading produces higher

bending moments for a given load than symmetrical loading, it should be relatively severe. However, conclusions for symmetrical loading remain to be verified by analysis.

CHAPTER 6

COMPARISON OF TEST RESULTS WITH APPROXIMATE ANALYSIS

A procedure for the determination of loads on steel ribs and the analysis of the ribs is described in Proctor and White's "Rock Tunneling with Steel Supports," published by Commercial Shearing, Inc. (1968). The procedure, which has become the standard for the industry, is described briefly in this chapter, and the allowable loads it gives for the test sets discussed in Chapter 2 are compared with the results of the tests. The analysis is not intended to predict the ultimate strength of the ribs, but the comparison is of value because it gives a good idea of the factor of safety involved.

6.1 PROCTOR AND WHITE RIB-DESIGN PROCEDURE

The wood blocking, which is wedged between a steel rib and the tunnel opening,develops interactive forces between the rib and the opening at the blocking points. These forces are assumed to be radially directed since the blocking cannot transmit tangential forces of appreciable magnitude. In Proctor and White's terminology, the set exerts an active force F_r on the surface of the opening, while the rock exerts an equal and opposite passive force F_p on the rib (Fig. 6.1a). In the initial stages the weight of the rock is carried principally by arch action in the rock itself. However, as the tunneling progresses loosened rock begins to exert its weight on the rib and equilibrium of forces at a blocking point requires a change in the direction and magnitude of the passive force (Fig. 6.1b);

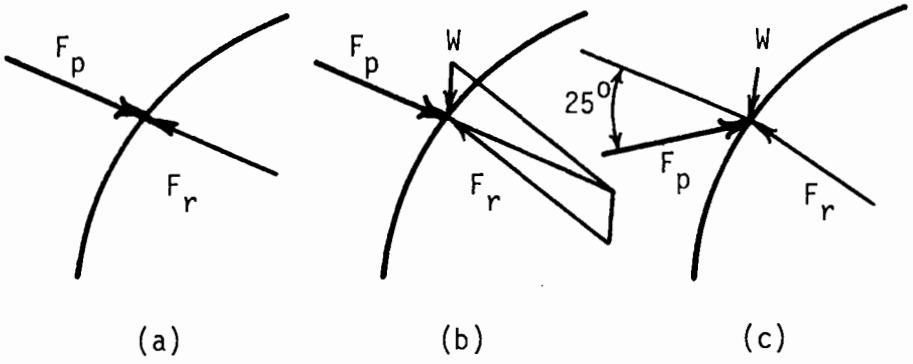

FIGURE 6.1 LOADS EXERTED BY THE GROUND ON THE RIB

which is now the resultant of forces exerted on the disturbed rock element by the adjacent ones. The vertical component of passive forces is assumed to be the result of friction. The angle of friction is assumed to be 25 deg, which is taken to be the maximum inclination of F_p (Fig. 6.1c).

The radial forces F_r at the various blocking points are assumed to be of such a magnitude as to produce a thrust line in the rib which passes through the intersections of F_r with the rib centerline. According to this assumption, the rib moments at the blocking points are zero. The maximum moment between blocking points is then Th, where T is the thrust and h the rise of the rib between blocking points (Fig. 6.2). However, since the rib is continuous there is a moment at each blocking point. According to Proctor and White's analysis, this blocking-point moment is larger than the maximum moment between blocking points, and equals 0.67Th if the rib is continuous and fixed at both ends and 0.86Th if it is hinged at the crown or at the crown and both ends.

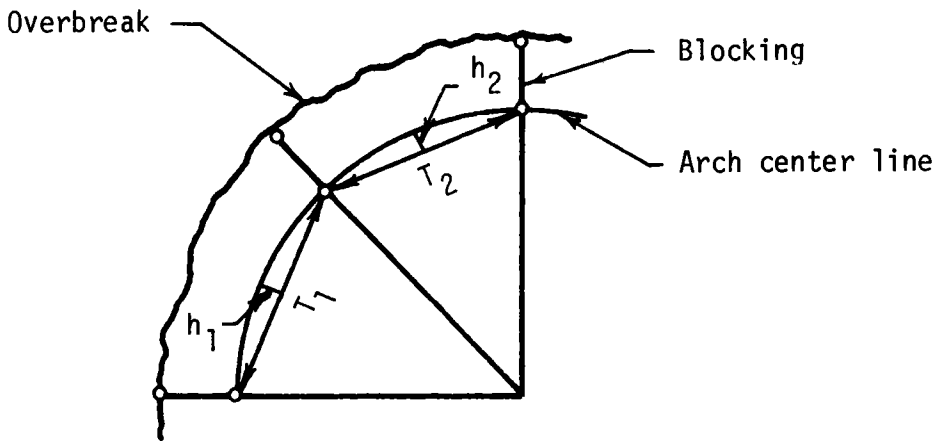

FIGURE 6.2 ASSUMED THRUST LINE OF THE ARCH

6.2 ANALYSIS OF RIB

The Proctor and White rib analysis is carried out as follows:

1. Assume the blocking-point spacing and an upper boundary of the rock which is to be carried by the rib (Fig. 6.3a). The weight W of each rock element tributary to each blocking point is then computed and resolved at the overbreak blocking point into a radial component F and a tangential component F_t if the tangent is inclined less than 25 deg to the horizontal, or into a radial component F and a component 25 deg with the horizontal if the inclination of the tangent exceeds 25 deg.
2. Draw the rays of a force polygon (Fig. 6.3b) with rays

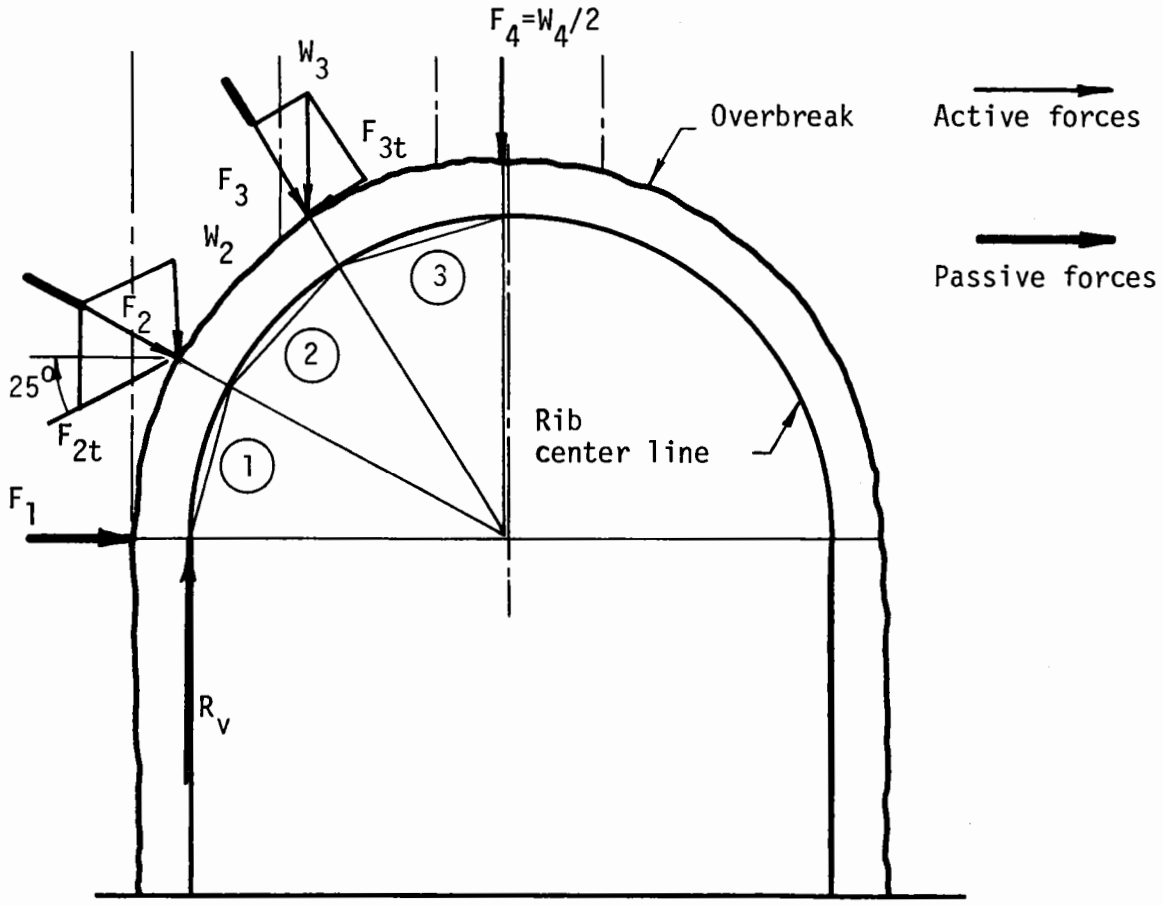

(a) Loading on ideal overbreak line

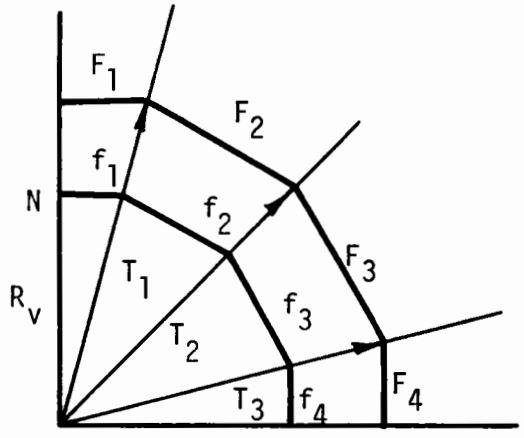

(b) Force polygon

FIGURE 6.3 ANALYSIS OF A RIB WITH ROCK LOADING

parallel to R_v, the thrust lines 1, 2, and 3, and the crown load F_4 of Fig. 6.3a.

3. Construct a trial force polygon f_1, f_2, f_3, f_4 (Fig. 6.3b). Proctor and White suggest that this be started at a point N on R_v corresponding to $R_v = 0.8\Sigma W$, where ΣW is the sum of the loads W on half the arch.

4. Compare each force f with the corresponding force F in Fig. 6.3a. Then construct a new force polygon F_1, . . ., F_4 based on the value of F in Fig. 6.3a for which the ratio F_n/f_n is largest. This is assumed to be the correct force polygon.

5. Compute the maximum rib moment M = 0.67Th or M = 0.86Th, as noted above.

6. Compute f = T/A + M/S for the largest thrust T where

   f = maximum stress in rib

   A = area of rib

   S = section modulus

   M = moment

   The resulting stress f must be equal to or less than the prescribed allowable value.

It will be noted that the values of F obtained in step 4 are all greater than those in Fig. 6.3a except for the one that determines the force polygon. Proctor and White assume that the difference is a passive resistance of the rock against a tendency of the rib to advance toward it.

6.3 ALLOWABLE LOADS FOR TEST RIBS

The outline of a test rib and positions of blocking points are shown in Fig. 6.4a. For the symmetrical loading, F_3, F_4, and F_3' were taken to be active loads while F_1, F_2, F_2', and F_1' were passive. For the unsymmetrical loading F_2 and F_3 were taken to be active loads with all others passive. The assumptions of the Proctor and White analysis lead to identical force polygons for these two cases (Fig. 6.4b), from which

$$2f_1 = f_2 = f_3 = 2f_4 = F \quad \text{and} \quad T_2 = T_3 = T_4$$

From the triangle $T_2T_3f_2$,

$$T_3 \sin 15° = \frac{f_2}{2} \qquad T_3 = 1.932f_2 = T_2 = T_4$$

$$T_1 \tan 15° = f_1 \qquad T_1 = 2.73f_1 = T_5 = 1.37T_3$$

The bases of the test ribs were hinged. Assuming the two-bolt butt-plate connection at the crown to be hinged, the stress f is given by

$$f = \frac{T}{A} + \frac{0.86Th}{S}$$

The arch-segment rise h is given by $h = R(1 - \cos 15°) = 1.98$ in. (50.2 mm). For the M section $A = 2.81$ in.^{2} (18.1 cm^2) and $S = 5.24$ in.^{3} (85.9 cm^3), which gives

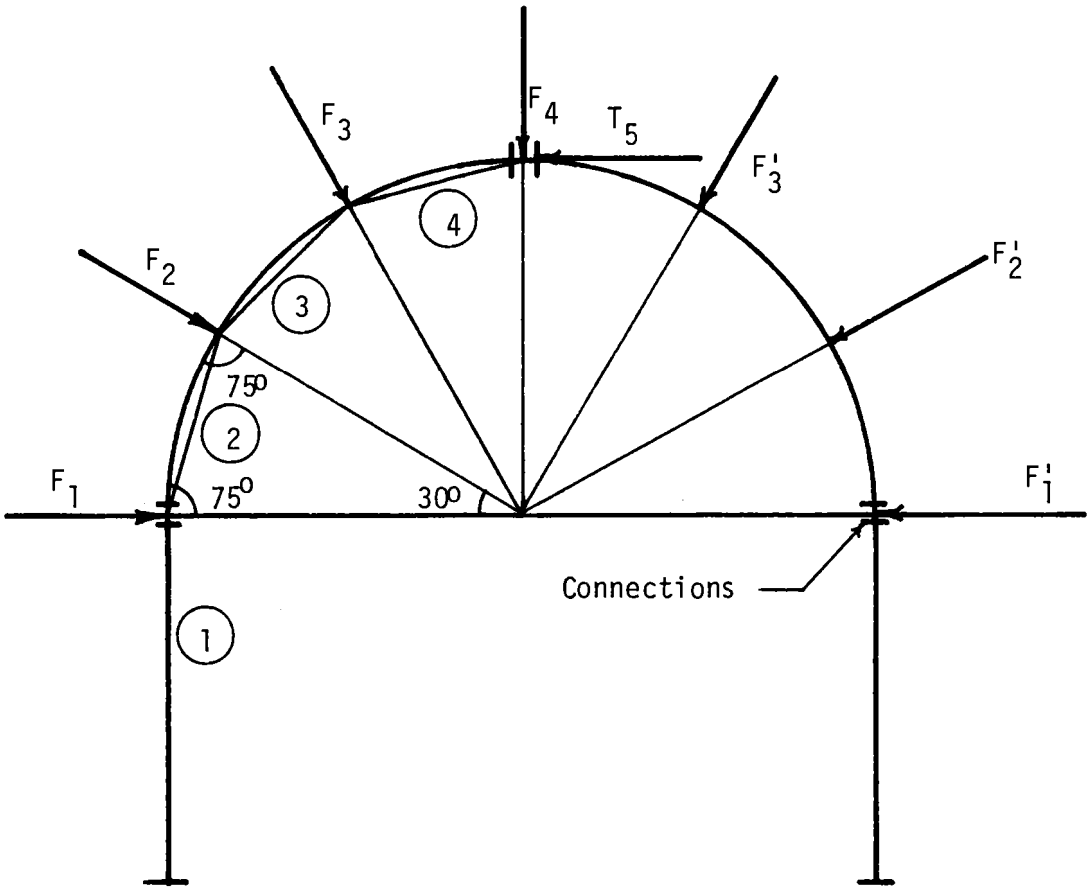

(a)

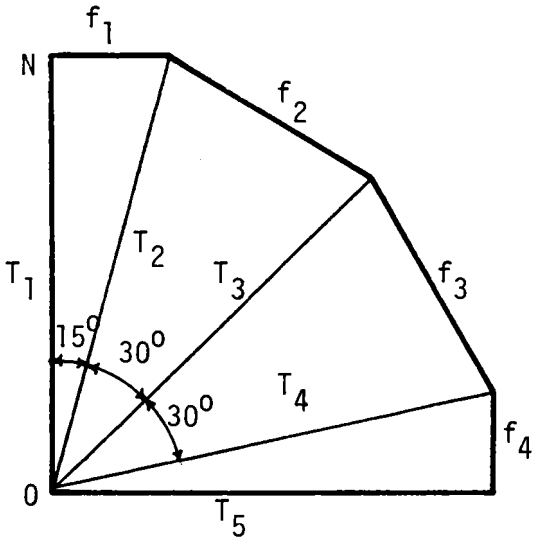

(b)

$$2f_1 = f_2 = f_3 = 2f_4 = F$$

FIG. 6.4 LOAD DIAGRAM AND FORCE POLYGON FOR THE TEST RIBS WITH SYMMETRICAL LOADING

$$F = 0.882\ f$$

For the square structural tube A = 3.54 in.^{2} (22.8 cm^2) and S = 4.0 in.^{3} (66 cm^3), which gives

$$F = 0.732\ f$$

6.4 COMPARISON OF TESTS WITH ANALYSIS

The allowable stress suggested by Proctor and White for temporary steel supports is f = 0.75 f_y, where f_y is the yield stress. The average yield stress from the test coupons was about 40 ksi (276 MPa), although there is considerable variation between the legs and the arch as discussed by Paul, et al. (1974). The actual yield stresses for various tests are discussed in Section 2.1.1. The allowable stress was taken at 0.75x40 = 30 ksi (207 MPa) for all the ribs tested. The comparison is made on the basis of the factor of safety against collapse, determined by dividing the maximum total active load in the test by the corresponding allowable load by the analysis.

The Group I entries in Table 6.1 give the results for ribs loaded in their plane. Two are of M section and two of TS section. One of each is loaded symmetrically and one of each unsymmetrically. The ratio of test load to working load varies from 1.32 to 1.49. It does not show a trend with regard to section or loading geometry and so probably results from variability among tests. It is of interest to note that the lower ratios are very nearly the reciprocal of the Proctor and White suggested

TABLE 6.1

COMPARISON OF TESTS WITH PROCTOR AND WHITE ANALYSIS

Group	Test specimen	Section	Loading geometry	Loading eccentric	No. 2 blocking omitted	Total active load in test, kips (kN)	Calculated total active load, kips (kN)	Factor of safety
I	M1	M	S	No	No	119.5 (531.5)	80 (355.8)	1.49
	B2	TS	S	No	No	109.7 (487.9)	83 (369.2)	1.32
	M6	M	U	No	No	71.8 (319.4)	53 (235.7)	1.35
	B5	TS	U	No	No	80.1 (356.3)	55 (244.6)	1.47
II	M10	M	S	Yes	No	56.4 (250.9)	80 (355.8)	0.71
	B13	TS	S	Yes	No	106.5 (473.7)	83 (369.2)	1.28
	M7	M	U	Yes	No	42.8 (190.4)	53 (235.7)	0.81
	B9	TS	U	Yes	No	77.4 (344.3)	55 (244.6)	1.41
III	M3	M	S	No	Yes	66.6 (296.2)	80 (355.8)	0.83
	B4	TS	S	No	Yes	68.4 (304.2)	83 (369.2)	0.82
	M8	M	U	No	Yes	55.9 (248.6)	53 (235.7)	1.05
IV	M3	M	S	No	Yes	66.6 (296.2)	32 (142.3)	2.08
	B4	TS	S	No	Yes	68.4 (304.2)	31 (137.9)	2.21
	M8	M	U	No	Yes	55.9 (248.6)	18 (80.1)	3.11

ratio 0.75 of allowable stress to yield stress. It is also of interest that the results appear to support the Proctor and White assumption that the set-rock (passive) interaction in the region of undisplaced rock takes on values that, together with the active loads from loosened, displaced rock, tend to hold the thrust line of the arch rib close to the neutral axis.

The Group II entries in Table 6.1 compare the test results for out-of-plane loading (2-in. (51 mm) eccentricity) with the Proctor and White analysis for in-plane loads. The cross sections and load geometries are the same as for the Group I tests. It will be noted that the M-sections fall considerably short of carrying the predicted load while the TS ribs have virtually the same factor of safety as for in-plane loadings of Group I. This is a dramatic demonstration of the superiority of the box section under nonideal loading conditions.

The Group III entries in Table 6.1 compare the results of tests on ribs with blocking at one haunch blocking point omitted with the Proctor and White analysis for the rib with blocking at all blocking points. The factors of safety range from 0.82 to 1.05. Compared with the corresponding tests in Group I the strength of the set with one blocking point unblocked is reduced by 46 and 38 percent for the two symmetrically loaded ribs and by 18 percent for the unsymmetrical loaded rib.

In order to determine whether the Proctor and White analysis can be used to predict the sensitivity of a rib to loss or absence of blocking, an analysis was made for the tests of Group III. The predicted active loads were reduced considerably. The test results are also lower, but

the factors of safety with respect to the analysis now range from 2.08 to 3.11. This suggests that the Proctor and White analysis may be somewhat sensitive to the number and distribution of blocking points assumed.

6.5 EVALUATION OF PROCTOR AND WHITE ANALYSIS

The Proctor and White analysis for rib forces is approximate and the structural design is based on a working stress. Therefore, it will not necessarily give a consistent factor of safety against collapse. At best, it would give a consistent factor of safety against yield. However, it is reasonable to evaluate the procedure on the basis of factor of safety at ultimate load because collapse is what the designer wishes to avoid.[1]

Maximum load depends on the mechanism that forms in the fully plastic condition of the set. Loading geometry, set geometry, blocking stiffness, etc. determine the failure mechanism. Thus, an "exact" analysis for ultimate load must be based on a mechanism approach as discussed in Chapter 5 of the report by Paul, et al. (1974). In the Proctor and White analysis the maximum moments are at the load points so plastic hinges will form there. This was not the case in the ribs that were tested, as is shown in the photograph of Fig. 2.13 where the yield regions are about midway between the load points.

A nonlinear ultimate-load analysis that follows the rib to the fully plastic condition is described in Chapter 5. It is shown in that

---

[1]Deflection might also be taken as a measure of failure. Thus, if a rib that deflects 3 in. (75 mm) is felt to be unsafe, and is replaced (or jump sets are installed), the rib has "failed".

chapter that rib capacity is not influenced by stiffness of the passive blocking, within limits, but once the stiffness reaches a lower limit the sensitivity becomes great. The passive-blocking stiffness of 20 kips/in. (3.5 MN/m) which was used in these tests is in the sensitive range, and is believed to be reasonable for most tunnels. The main reason for the sensitivity is the resulting relatively large deformation of the rib. In the tests, maximum load occurred at active-load deflections of 3 to 5 in. (76 to 127 mm). It was obvious when watching the test that the load-carrying mechanism changed under large deflections, because the active load region became quite flat and this part of the arch began to act more like a fixed-fixed beam with plastic hinges at the ends, with very little arch action. This effect would be reduced with stiffer blocking that would reduce the deflections. Although this discussion is based on a limited number of tests on small-scale ribs with a fixed geometry, it is believed that the comparisons are valid for large tunnel situations, since the blocking stiffness is approximately scalable to the larger tunnels and the blocking spacing would remain about the same.

There is a difference in basic philosophy between the Proctor and White loading mechanism and that used in selecting the loads for the large-scale tests. Proctor and White select a height of rock above and across the entire width of the opening and distribute the weight of that rock to the blocking points. Thus there are active vertical loads on the rib at every point but the springlines. Passive load occurs only if additional force is needed over and above the active load to satisfy equilibrium. In selecting loads for the large-scale tests only certain loads, in an

assumed region of loosening rock, were considered active and the passive blocking took load only when the rib moved into it. The Proctor and White loading is more uniform. Loosening rock over a portion of the opening is a more severe condition because more bending is involved, even though less total load is applied. Movement of rock blocks or wedges in a region of the opening appears to be more consistent with the observations of Cording and Mahar (1974).

Despite the above mentioned approximations involved in the Proctor and White analysis, it gives reasonably consistent factors of safety under the two quite different active-load conditions used in the tests.

CHAPTER 7

SUMMARY

Tests to failure of 18 steel tunnel supports were carried out. The horseshoe-shaped specimens spanned 10 ft (3 m) and were 12 ft (3.6 m) high. Square box sections, concrete-filled box sections, and pipe were used, as well as the standard I-shaped section, to determine their relative advantages. Results of the Proctor and White procedure for the design of steel supports are compared with the test results and the use of the NASA structural analysis computer program to predict the ultimate strengths is described.

The practicability of several new types of connections was studied and one support with sleeve connectors was tested to failure. The feasibility of using telescoping ribs to speed up erection was also investigated.

7.1 CROSS SECTION SHAPE

In respect to cross section shape the tests showed little or no advantage of one shape over another so long as the loads were in the plane of the set. However, the box section was definitely superior when the loads were eccentric, as might be the case, for example, with blocking driven from one side. Even with the loads applied at the edge of the 4 x 4 box and the 4 x 4 I-shaped section (eccentricity 2 in. (51 mm)) the box-section rib strength was reduced only 4 percent compared to in-plane loads, but the I-shaped set strength was reduced 40 percent or more (Table 2.2). Behavior

of the I-shape was also less desirable than the box, under eccentric loading, in that it exhibited very low ductility (Fig. 2.28). Thus, the box section would seem to be a good choice for rock tunnels and for tunnels in soft ground where lagging can be supported on the outer flange. If lagging is required and cannot be supported on the outer flange, the box could not compete with the I-shape since it does not provide a shelf for lower placement as does the inner flange of the I. However, lagging on both sides of the inner flange of an I delivers a load that is essentially concentric, and since the lagging is usually supported on wood bearing strips freedom to twist is reduced so that the box loses much of its advantage in this situation.

Concrete-filled box ribs were 16 to 18 percent stronger than the unfilled box and had essentially the same ductility (Table 2.4 and Fig. 2.38). Such an increase in strength does not justify the use of concrete fill. The 4 x 4 x 1/4 box weighs 12 lb/ft (17.9 kg/m) and the concrete-filled box 24 lb/ft (35.8 kg/m). The next larger 4 x 4 section (5/16 in. (8 mm) thick) would give a larger increase in strength and weighs only 14.5 lb/ft (21.6 kg/m). Considering the cost of placing a concrete fill compared to the extra cost of the larger box it seems clear that the concrete fill would be much more expensive.

7.2 CONNECTIONS

Two types of sleeve connections, a split sleeve (Fig. 4.18) and a solid sleeve, were investigated. The split sleeve can be drawn up tight

on the rib to offset the looseness necessitated by allowances for manufacturing and fabricating tolerances. A major manufacturer of cold-formed products who was consulted thinks this connection could be produced in volume at costs commensurate with the cost of welding plates to the ends of rib members for the standard butt-plate connection. However, this connection might be bulky for large members because of the limitations on cold-bending radii. A similar connection, fabricated by welding, was tested but no tests of a set with split-sleeve connection were made.

A simpler sleeve connector consists of a solid sleeve. It has the advantage of being in one piece but the disadvantage of looseness of fit in order to provide for tolerances in the connected members. Solid sleeve connections and one set with this type of connection were tested. The sleeve for the 4 x 4 x 1/4 box set was only 1/8 in. (3 mm) thick. Results of the rib test suggest that the sleeve connector has possibilities that warrant further investigation (Section 2.3.6).

7.3 TELESCOPING RIBS

A telescoping steel pole that has been developed for electric power transmission lines suggests the possibility of adapting the idea to steel tunnel sets. This is discussed in Chapter 3, where it is concluded that manufacturing and fabricating tolerances, possible damage in shipping and handling, and variation in rib strength due to reduced cross section of the telescoping elements make this idea impracticable for use in tunnels.

7.4 COMPUTER ANALYSIS

The computer program NASTRAN gave a fair prediction of the

behavior of a steel set tested to failure (Fig. 5.7). The modeling of the set cross section could probably be improved with further study. The program was used to investigate the effect of blocking stiffness and connection stiffness on set strength. Results of these studies are discussed in Chapter 5.

This phase of the project suggests that the computer analysis, possibly with some improvement in the simulation of the cross section, could take the place of laboratory testing in any further investigations of sets. However, it is not likely to be of value in routine design of sets since the Proctor and White analysis appears to give good results.

7.5 PROCTOR AND WHITE ANALYSIS

The Proctor and White procedure for the design of steel ribs, which is described in Chapter 6, is a standard for the industry. Comparisons of the results of sets tested to failure with their predicted working loads show consistent factors of safety for in-plane symmetrical (crown) loading and in-plane side loading (Table 6.1, Group 1). The factors of safety for Groups II and III in the table are given to show the effect of eccentricity of load and local loss or absence of blocking. It is significant that the I-shaped cross section with a 2-in. (51 mm) eccentricity of load failed at loads less than the Proctor and White working load (Group II) while, as was mentioned earlier, the box cross section is practically immune to the effect of an eccentricity of this magnitude.

REFERENCES

Cording, E. J., J. W. Mahar (1974). "The Effect of Natural Geological Discontinuities on Behavior of Rock in Tunnels," *Proceedings, North America Rapid Excavation and Tunneling Conference,* American Institute of Mining, Metallurgical, and Petroleum Engineers, San Francisco, Vol. 1, Chapter 12, pp. 107-138.

Parker, H. W., D. U. Deere, R. B. Peck, P. C. Birkemoe, R. N. Semple (1973). *Testing and Evaluation of Prototype Tunnel Support Systems,* Report No. FRA-ORDD 74-11, Federal Railroad Administration, Department of Transportation (order No. PB-231-112/AS from NTIS).

Paul, S. L., E. H. Gaylord, A. J. Hendron, C. E. Kesler, B. Mohraz, R. B. Peck (1974). *Research to Improve Tunnel Support Systems,* Report No. FRA-ORD & D 74-51, Federal Railroad Administration, Department of Transportation (Order No. PB-235-762/AS from NTIS, Springfield, Va. 22151).

Peck, R. B. (1969). "Deep Excavations and Tunneling in Soft Ground," *Proceedings,* 7th International Conference on Soil Mechanics and Foundation Engineering, State-of-the-art Volume, pp. 225-90.

Proctor, R. V., T. L. White (1968), "Rock Tunneling with Steel Supports," Commercial Shearing, Inc., Youngstown Printing Company, Youngstown, Ohio.

☆U.S. GOVERNMENT PRINTING OFFICE: 1976-211-173/483